FILOPODIAL DYNAMICS AND SYNAPSE SPECIFICATION IN THE *DROSOPHILA* VISUAL SYSTEM

APPROVED BY THE SUPERVISORY COMMITTEE

Peter Robin Hiesinger, Ph.D. (Mentor) ……..

Jonathan Terman, Ph.D. (Chair) ……..

Julian Meeks, Ph.D. ……..

Gaudenz Danuser, Ph.D. ……..

Kimberly Huber, Ph.D. ……..

DEDICATION

For the greater good…

FILOPODIAL DYNAMICS AND SYNAPSE SPECIFICATION IN THE *DROSOPHILA* VISUAL SYSTEM

by

Mehmet Neset Ozel

DISSERTATION

Presented to the Faculty of the Graduate School of Biomedical Sciences

The University of Texas Southwestern Medical Center at Dallas

In Partial Fulfillment of the Requirements

For the Degree of

DOCTOR OF PHILOSOPHY

The University of Texas Southwestern Medical Center at Dallas

Dallas, Texas

December, 2017

ACKNOWLEDGEMENTS

I would like to thank my mentor Peter Robin Hiesinger for his guidance and support every step of the way, for giving me the opportunity to pursue my ideas and providing the necessary tools. I am particularly grateful to him for his patience as he helped me (slowly) understand how to survive in academia and form professional relationships. Lastly, I would like to thank him for doing his very best during our move to Berlin in order to make it as smooth as possible for all us.

I would like to thank my past and present committee members: Adrian Rothenfluh, Jonathan Terman, Julian Meeks, Gaudenz Danuser, Ege Kavalali and Kimberly Huber for their time.

I am grateful to all of my past and present lab mates for their support; but particularly Egemen Agi and Jennifer Jin, who were always there for me from the very first day I landed in Dallas to this day in Berlin. I would like to thank Marion Langen for her help with the data analysis in Chapter 2, Abhishek Kulkarni for his contributions to data and my collaborators in Zuse Institut Berlin, Josephine Schallau and Vincent Dercksen, for developing the analysis tools for Chapter 3.

From my Dallas days, I would like to thank Kacey Rajkovich, Vural Tagal, Melodi Tastemel, Basar&Bercin Cenik and Gizem Yesilyurt for their friendship and support. I am particularly thankful to Stephanie Hernandez for always being there for me despite the distance.

Finally, I would like to thank my family for their 27 years of continuous love and support.

FILOPODIAL DYNAMICS AND SYNAPSE SPECIFICATION IN THE *DROSOPHILA* VISUAL SYSTEM

MEHMET NESET OZEL, Ph.D.

The University of Texas Southwestern Medical Center at Dallas, 2017

PETER ROBIN HIESINGER, Ph.D.

PREFACE

How is the synaptic specificity achieved in neural circuits comprised of hundreds of different types of neurons? My dissertation aims to advance our knowledge on this overarching question using the complex visual processing circuitry of *D. melanogaster*. This system not only provides excellent genetic amenability but also a model where almost all connectivity can be built without environmental input, i.e. it is genetically hardwired. Nearly three decades of research has identified a vast array of genes required for various steps of synapse specification. However, it remained unclear how these genes implement the developmental rules that result in the final connectivity and we understand very little of what actually goes wrong between a particular genetic

perturbation and the resulting miswired circuit. To that end, I focused on the actual subcellular substrate of connectivity: axonal growth cones. To gain access to the details of their dynamic behavior during development, I developed an imaging technique which allows the monitoring of intact, developing fly brains over long periods in high temporal and spatial resolution.

Using live imaging and the axonal terminals of R7 photoreceptor as a model, I performed a detailed analysis of growth cone dynamics during various steps of synaptic specification, in wild-type and perturbed conditions. Interestingly, I found that none of the perturbations that were previously tied to ‘layer specific targeting’ of R7 axons were actually required for the recognition of or targeting to a specific layer; instead, all displayed a loss of stabilization with various timings of onset. High speed live analysis revealed the stochastic filopodial dynamics of these axons as crucial mediators of this stabilization. First, as the substrate of attachment to the target layer during early development (Chapter 2); second, as the searching agents for postsynaptic partners during synapse formation (Chapter 3).

In brief, my research provided a valuable bridge between the genetic factors that instruct the synapse specific wiring of the brain and how they regulate the dynamic properties of axonal growth cones and synaptic terminals in distinct ways to achieve that final outcome.

TABLE OF CONTENTS

PUBLICATIONS

Özel, M.N., and Hiesinger, P.R. (2017). Live Imaging of Connectivity in Developing Neural Circuits in Drosophila. In Decoding Neural Circuit Structure and Function: Cellular Dissection Using Genetic Model Organisms, A. Çelik, and M.F. Wernet, eds. (Cham: Springer International Publishing), pp. 149-167.

Ozel, M.N., Langen, M., Hassan, B.A., and Hiesinger, P.R. (2015). Filopodial dynamics and growth cone stabilization in *Drosophila* visual circuit development. Elife *4*.

Doldur-Balli, F., **Ozel, M.N.**, Gulsuner, S., Tekinay, A.B., Ozcelik, T., Konu, O., and Adams, M.M. (2015). Characterization of a novel zebrafish (Danio rerio) gene, wdr81, associated with cerebellar ataxia, mental retardation and dysequilibrium syndrome (CAMRQ). BMC Neurosci *16*, 96.

Zschatzsch, M., Oliva, C., Langen, M., De Geest, N., **Ozel, M.N.**, Williamson, W.R., Lemon, W.C., Soldano, A., Munck, S., Hiesinger, P.R.*, et al.* (2014). Regulation of branching dynamics by axon-intrinsic asymmetries in Tyrosine Kinase Receptor signaling. Elife *3*, e01699.

Cherry, S., Jin, E.J., **Ozel, M.N**., Lu, Z., Agi, E., Wang, D., Jung, W.H., Epstein, D., Meinertzhagen, I.A., Chan, C.C.*, et al.* (2013). Charcot-Marie-Tooth 2B mutations in rab7 cause dosage-dependent neurodegeneration due to partial loss of function. Elife *2*, e01064

LIST OF FIGURES

CHAPTER TWO FIGURES

CHAPTER TWO SUPPLEMENTARY FIGURES

CHAPTER THREE FIGURES

CHAPTER THREE SUPPLEMENTARY FIGURES

CHAPTER ONE

Parts of this chapter were previously published in:

Özel, M.N., and Hiesinger, P.R. (2017). Live Imaging of Connectivity in Developing Neural Circuits in Drosophila. In Decoding Neural Circuit Structure and Function: Cellular Dissection Using Genetic Model Organisms, A. Çelik, and M.F. Wernet, eds. (Cham: Springer International Publishing), pp. 149-167.

Background

1.1 The developmental context: From dynamics to synaptic specificity

Key questions in modern neuroscience include "*how do neural circuits work?*" and "*how do neural circuits form?*". Approaches to answer these questions require overlapping information concerning neuronal morphology and connectivity. When Roger Sperry referred to an "unadaptable rigidity" of mechanisms that drive the development of visuomotor connectivity (Sperry, 1943), he provided a theory that was to define developmental neuroscience for decades to come. The chemoaffinity theory has evolved to include the idea of wiring codes that neurons use to make connections with their targets based on specific molecular markers.

The search for guidance molecules and the elucidation of their molecular mechanisms have been hugely successful, especially during the last 20 years (for review see (Kolodkin and Tessier-Lavigne, 2011; Raper and Mason, 2010; Yogev and Shen, 2014)). As more molecules and mechanisms were discovered, the ideas of how guidance cues and codes function became more nuanced. Numerous molecules have been shown to function repeatedly at different places and times, in combinations and in gradients (Sanes and Zipursky, 2010; Yogev and Shen, 2014). Importantly, not all

molecules that exhibit attractive or repulsive binding function as guidance cues; for example, thousands of isoforms of the repulsive, homophilic cell adhesion molecule Dscam ensure self-avoidance of dendritic branches from the same neuron, but provide no specific directional cue for any neuronal extension where to grow or make synapses. Instead of functioning as cues, Dscam isoforms (similar to vertebrate Protocadherins) execute a simple pattern formation process based on self-avoidance (Kise and Schmucker, 2013). In another example, the widely expressed cell adhesion molecule N-Cadherin is not required as a targeting cue in *Drosophila* photoreceptors, but can function in the stabilization of growth cones (Chapter 2). Hence, attractive and repulsive molecules can play important roles in neural circuit assembly without specifying target areas or cells.

The two examples above highlight another important extension of the original chemoaffinity theory: both Dscam-mediated self-avoidance and N-Cadherin-mediated stabilization contribute to wiring specificity using dynamic and stochastic processes. Apart from the random Dscam isoform choice of individual neurons, self-avoidance leads to spreading of dendritic branches only if individual branches non-deterministically grow such that self-avoidance can act on them. As a consequence, every neuron, like every snow flake and every apple tree, has a uniquely different branching pattern. Similarly, every growth cone has a unique branching pattern of dynamically extending and retracting filopodia. In the case of Drosophila R7 photoreceptor axons, this random pattern of extensions of retractions seems to be required for N-Cadherin-mediated growth cone stabilization (Chapter 2). These cases exemplify how dynamic and stochastic growth is in fact necessary for the molecules to execute their function. This

observation significantly extends on the early versions of the chemoaffinity theory based on molecular matchmaking cues. The idea of matchmaking is more deterministic: from the perspective of a specific cue a stochastic process is more likely to represent noise that the system would try to minimize, rather than a necessary part of the molecular mechanism. Neural circuit assembly is likely to employ both mechanisms: pattern formation based on stochastic growth as well as molecular specification through matchmaking; examples for both have been firmly established (Hassan and Hiesinger, 2015; Kolodkin and Tessier-Lavigne, 2011; Yogev and Shen, 2014).

To understand the role of dynamic and stochastic processes as part of neural circuit assembly, our lab have recently proposed a rules-based framework to help incorporate the mechanisms and roles of molecules like Dscam and N-Cadherin as part of developmental algorithms underlying brain wiring (Hassan and Hiesinger, 2015). In the example of Dscam, in this framework, the focus is on the level of the rule ‘self-avoidance’ as part of a larger developmental program, rather than the molecular mechanism of homophilic, repulsive binding that executes that rule (or the molecule itself for that matter: the same rule can be carried out by different molecules, as exemplified by Protocadherins in vertebrates). In this case, the rule can be formulated as: (1) grow stochastic filopodial extension and branches, (2) stop individual filopodia from growing further when contacting other filopodia from the same neuron. This rule is not sufficient without additional constraints, e.g. probability of branching, inter-branch spacing, etc., but it captures the essence of the developmental process executed by the homophilic repulsion function of Dscam.

To understand the interplay of stochastic growth and molecular mechanisms in executing a rule like self-avoidance, it is beneficial to think of neurons and neuronal processes as individual entities that explore the environment, advance to targets and compete with each other. Lichtman and Fraser proposed the analogy between such a setting and a football (or similar sports) game (Lichtman and Fraser, 2001). Each player has its abilities, restrictions as well as his or her own agenda. If the players each follow the rules, these games will create an ordered structure without any external supervision; however, the exact outcome is not scripted. Referees and game plans can help structure the game, but are not strictly required: even a backyard football game with variable numbers of players and imprecise playing field can work out wonderfully.

How do we figure out the rules of the game called ‘brain wiring’, which is arguably much more complicated than any sports we have ever invented? An established approach is to disrupt specific genes, in particular those encoding presumptive guidance cues, and study the end results of the effects on the circuit. *Drosophila* has been a particularly useful system using this approach, in part due to the development of a technique to render individual neurons mutant in an otherwise wild-type animal (Lee and Luo, 1999). If the disrupted gene is indeed a molecular matchmaking cue, then loss or gain in individual neurons predictively rewire connectivity, as has been shown in several examples, e.g. the teneurins in Drosophila (Hong et al., 2012) or type II Cadherins in the vertebrate retina (Duan et al., 2014). In many cases, however, loss and gain of function studies for single genes led to surprising, less instructive outcomes. Following up with the soccer analogy, a perturbation may, for example, restrict the usage of hands for each player one-by-one,

revealing that only in the case of the goalie this causes the eventual score to change. Here, the analogy highlights what gene perturbations may indirectly provide: insight into the rules of the game. Many rules have been discovered through carefully conducted gene perturbation experiments, including the discovery of self-avoidance through mutant analyses of Dscams. If the goal is the characterization of the rule, however, it is not *a priori* clear that a gene perturbation experiment is the shortest path to uncover the rule. For example, the rule on usage of hands in a soccer game may also be deduced from observation of the unperturbed game. Comparing static pictures from different points of different games would not easily reveal this rule. Static pictures can provide important information on the game but will fail to capture stochastic and dynamic actions that do not stereotypically happen at an exact time point for every single member of a "player" type. Since stochastic and dynamic actions are key to pattern formation rules like self-avoidance, live observation is of particular importance to the discovery of rules underlying brain wiring. Ultimately, a combination of gene and cell perturbation experiments with live observation yields the highest likelihood of uncovering principles underlying the development of connectivity.

During the past 15 years our ability to image live neurons forming circuits in their natural environments has significantly improved, especially in the model organisms worm, fly, zebrafish and mouse. Yet, we have only begun to characterize the dynamic properties of developing neural circuits. In the early parts of brain development, live imaging has already been very useful for the study of neural stem cell migration (Lerit et al., 2014; Ortega and Costa, 2016). When it comes to studying the development of circuit connectivity, we need to look at neurons that develop two types of dynamic

structures: axonal growth cones and dendritic extensions. In both cases stochastic extension and retraction dynamics of filopodia underlie what appear to be robust choices in the adult connectivity. The next subsections will address our current state of knowledge about the role these subcellular filopodial structures *in vivo* and how they might relate to the establishment of synaptic specificity.

1.1.1 Growth cone guidance and early filopodia

When Cajal studied chick embryos to show that axons grow out of neurons, he discovered what he called a “cone-like lump with a peripheral base” with thorny processes at the tips of commissural axons (Cajal, 1890). This description came to define the features of the ‘textbook growth cone’: a widened terminal with filopodia and lamellipodia at its tip**.** The growth cone has received plenty of attention over the decades as the presumptive structure that detects guidance cues and actively advances to the target (for review see (Raper and Mason, 2010; Vitriol and Zheng, 2012). Filopodia have been suggested as agents for the detection of guidance cues (Rajnicek et al., 2006; Zheng et al., 1996) and *in vitro* evidence was provided in favor of filopodia forming a clutch mechanism for growth cone movement by acting as ‘sticky fingers’ (Chan and Odde, 2008; Heidemann et al., 1990). It has largely remained unclear, why and how stochastic extension and retraction dynamics execute these processes.

Most of our understanding of the dynamics of growth cones is based on *in vitro* systems. However, some *in vivo* live imaging data has already provided glimpses into the functions of filopodia that do not easily fall into the categories ‘searching agents’ or

‘sticky fingers’. Some of the first live imaging studies in intact tissue revealed that growth cones tend to adapt simple, streamlined forms while extending and more complex forms (like the classical growth cone) when they pause or reach their targets, e.g. in mammalian retina preparations (Godement et al., 1994) and intact zebrafish embryos (Jontes et al., 2000; Kaethner and Stuermer, 1994). These observations have been interpreted as growth cones adapting to complex, high filopodial activity forms at ‘decision regions’, where there are multiple cues and the axon needs to make a decision on which direction to go; then it quickly advances towards that direction without many filopodia (Mason and Erskine, 2000). On the other hand, it has been shown that filopodia are at least partially dispensable for axon navigation but essential for terminal arborization of retinal axons (Dwivedy et al., 2007). My recent findings on developing R7 photoreceptor growth cones in intact *Drosophila* eye-brain complexes revealed a similar pattern (Chapter 2). These axons exhibit streamlined structures while extending but expand into more complicated filopodial structures once they stabilize at the target layer. Interestingly, when their attachment to that layer was genetically impaired, these growth cones went, at unpredictable time points, through a gradual filopodial collapse followed by regaining of motility by the axon tip. The close temporal link between filopodia formation and axon stabilization suggests that in this case filopodia might function as an adhesion surface for stabilization, rather than being important for guidance or extension. However, a direct causal link between the two processes is yet to be established.

Finally, rather than directing the growth cone to the target, filopodia can also function in guidance by extending to a target, expanding and becoming the new axon

terminal/growth cone. This was observed *in vitro* (O'Connor et al., 1990) and in intact *Drosophila* embryo (Murray et al., 1998). A similar behavior is observed for developing R8 photoreceptor growth cones in *Drosophila* as they relocated from their temporary position to the medulla layer M3 at mid-pupal development (Chapter 2). These growth cones extend a single filopodium to deeper layers, which is initially very dynamic with almost complete retractions and re-extensions but eventually stabilized its tip in the correct target layer, expands and ultimately forms the adult R8 axonal terminal prior to synaptogenesis.

The few selected examples discussed here highlight the origin of an important aspect of adult circuit connectivity: The precise axon positions, dendritic branch points and their contacts in the adult may not only be slightly imprecise due to biological noise, but be the result of necessary stochastic processes based on filopodial dynamics during growth cone guidance, stabilization and synaptic partner identification. Especially on this latter aspect, important insight comes from filopodia on axons and dendrites at later developmental stages, as discussed in the following section.

1.1.2 Synapse specification and late axonal and dendritic filopodia

After a growth cones reaches its target area, the main body of the axon no longer advances; therefore, it may be more accurate to classify the filopodia at this stage as ‘axonal filopodia’. These are not limited to the tip of the axon and have been linked to axonal branching (reviewed in (Gallo, 2011). Dendrites also form filopodia, and these

perhaps constitute the class of filopodia that has so far been most closely linked to the establishment of synaptic connectivity.

Work by Stephen Smith and colleagues has provided pioneering insights into the roles of axonal and dendritic filopodia during brain wiring. Live imaging of tectal neuron dendritic arbors in intact developing zebrafish revealed that young arbors create many transient filopodia, some of which become the sites of *de novo* synapse formation. In turn, formation of these synapses directly stabilizes the respective filopodia, turning it into a stable branch (Niell et al., 2004). Live observation helped to establish a link between the processes of synapse formation and filopodial stabilization without perturbation experiments. Filopodia without a synapse never persisted longer than an hour and the stabilized filopodia only retracted if its synapses were eliminated. Similarly at the presynaptic partners of these cells (retinal axons), new branches extend preferentially from newly formed synaptic sites and no branch is stabilized over an hour without a synaptic site present (Meyer and Smith, 2006). Together, these observations support the synaptotropic model (Vaughn, 1989), whereby stabilization through synapse formation guides axonal and dendritic extension. Importantly, this process can only work if axonal and dendritic arbors provide initially stochastically extended filopodial processes to select from. A process based on the rule of selection and stabilization precludes precise positioning of pre- and postsynaptic partners, but not synaptic specificity, in adult circuit connectivity.

These data showcase links between synapse formation and filopodial dynamics and how the former can direct the latter to bias axonal and dendritic arbors towards stabilized connection sites. However, they are only our first glimpses into the roles of

filopodial dynamics in brain wiring in intact, developing brains - and they have largely been limited to wild type. Important questions remain, for example: How are some synapses selected to stabilize while others are lost? What are the rules and mechanisms underlying synapse-mediated branch stabilization? Watching the dynamics of axonal and dendritic dynamics in wild-type and mutant neurons are necessary approaches to answer these questions and understand the rules that establish adult connectivity.

1.2 The model system: *Drosophila* visual circuit and photoreceptors

The fly visual system consists of retina and the optic lobe which is subdivided into four distinct neuropils: lamina, medulla, lobula and lobula plate (Meinertzhagen and Hanson, 1993). Retina is made of approximately 800 ommatidia, each containing 8 photoreceptor neurons (R-cells). R1-6 subtypes express the broad spectrum rhodopsin 1 (Rh1) and are primarily important for motion vision; while R7 and R8 subtypes are required for color vision and express blue (Rh5) or green (Rh6) rhodopsins (R8) or UV (Rh3 or Rh4) rhodopsins (R7) (Morante et al., 2007).

Unlike vertebrate photoreceptors, *Drosophila* R-cells are proper neurons i.e. they send axonal projections to the optic lobe and connect directly to the visual circuitry. They do so in a retinotopically ordered fashion and this organization is tightly coupled to the birth order of photoreceptors in the eye imaginal disks during the third-instar larval stage; and the resulting differential expression in the posterior-anterior axis of transcription factors such Sequoia as well as cell-surface proteins (Kulkarni et al., 2016; Petrovic and Hummel, 2008). R1-6 axons target to the first neuropil lamina and terminate by a glia-derived signal (Poeck et al., 2001). They in turn induce the differentiation of their postsynaptic targets, lamina monopolar cells (L-cells), using Hedgehog in a glia-signaling dependent mechanism (Fernandes et al., 2017; Huang and Kunes, 1996). During the early pupal development, R1-6 axons are sorted with L-cells into cylindrical synaptic units called cartridges in a manner that ensures the axons of the photoreceptors that see the same point in space in retina are sorted into the same cartridge. This intricate process is known as *neural superposition* and its mechanisms are reviewed in detail elsewhere (Agi et al., 2014).

My dissertation is primarily focused on the connectivity of R7 cells, which along with R8 axons pass through the lamina and instead terminate in the second and largest neuropil: the medulla. There are over 50 different neuronal cell types in the medulla that process the information coming from R7-8 axons as well as from the L-cell axons which relay the information from R1-6 axons in the lamina (Fischbach and Dittrich, 1989). Medulla is organized as a layered structure with specific synaptic organization in each layer M1-10; both R7-8 as well as L-cell axons terminate within the specific layers of the distal medulla M1-6. Medulla is also organized as a columnar structure which preserves the retinotopic organization of the retina and lamina. Recently, electron microscopy (EM) reconstruction from multiple medulla columns have been used to decipher the specific synaptic organization within the each layer of medulla (Takemura et al., 2013; Takemura et al., 2015); giving us a very detailed understanding of the underlying connectivity.

1.2.1 Layer specific targeting in the medulla

During development R8 axons arrive to the medulla first and terminate in a superficial position (sometimes referred as M0). This is a temporary position for R8 axons and they are subsequently sorted to their final layer, M3, in mid-pupal stages (Ting et al., 2005). Stopping at the temporary layer and preserving the retinotopic columnar organization appears to require two cell-surface proteins: Flamingo (Senti et al., 2003), and Golden Goal (Gogo) (Tomasi et al., 2008). Around P+45%, R8 axons regain motility and relocate to the M3 layer. Initially, another cell-surface protein Capricious (Caps) has been implicated in this process as the potential factor that leads to the recognition of M3 layer by R8 axons (Shinza-Kameda et al., 2006). However,

further studies indicated that this requirement was not absolute (Berger-Muller et al., 2013) and strong loss-of-function phenotypes observed previously were likely due to a sensitized background. Later, it has been shown that Netrin derived from the terminals of L3 axons (which reach to M3 layer before R8 axons) was necessary for proper targeting of R8 axons to the M3 layer through the receptor Frazzled signaling (Timofeev et al., 2012). Further studies with intravital live imaging have found that even though Netrin/Frazzled is required for the stabilization of R8 terminals in M3 layer, R8 axons lacking Frazzled are still able to reach down to their target and able to track it till their eventual destabilization (Akin and Zipursky, 2016). These findings ruled out any Netrin based attraction to the M3 layer and it remains unclear what (if any) molecular factors are required for the initial recognition of their final target layer by R8 axons.

R7 photoreceptors are last to be born in the eye-imaginal disk and their axons follow the pioneering R8 axons to the medulla and initially terminate right below their terminals in the superficial medulla (Ting et al., 2005). This interdependency allows the retinotopic columnar organization of R8 axons to be directly translated onto the R7 axons and ensures the photoreceptors that are within the same ommatidia in the retina and see the same point in space, are sorted into the same medulla column. N-Cadherin (CadN) emerged as a crucial factor regulating the layer specificity of R7 terminals (Lee et al., 2001); its loss causing R7 axons to sort into wrong layers starting from early pupal stages (Ting et al., 2005). Other factors including DLar (Clandinin et al., 2001), Liprin-α (Hofmeyer et al., 2006) and PTP69D (Hofmeyer and Treisman, 2009) are also required for correct layer targeting of R7 axons; but these defects only start to manifest after the mid-pupal stages. These observations led to the widespread interpretation that

R7 axons, similar to R8s, would employ a two-stage targeting mechanism in the medulla (Hadjieconomou et al., 2011; Melnattur and Lee, 2011). According to this model, R7 axons target to a temporary layer (future M3) in a CadN-dependent manner and the initial separation of R7 and R8 terminals during the early pupal stages happens through the intercalation of L-cell axons between the two temporary layers (Ting et al., 2005). Later, presumably at the same time with R8 axons, R7 axons would regain motility and target to their final layer. CadN is required for this step too (Nern et al., 2005) as well as the other factors listed above. Nevertheless, despite being taken as a common assumption in the field for over a decade, this model had never been properly tested; and it remained unknown whether R7 axons actually regain motility during the 'second-stage targeting' and actively extend to another layer as R8 axons do.

Another perplexing aspect of R7 layer specificity is the clearly crucial role of CadN. It is expressed widespread in all layers of the medulla and it is also required for the layer specificity of the most L-cell axons (Nern et al., 2008) in the same brain region as R7 cells (distal medulla). It was suggested that tight temporal regulation of expression levels in different cell types could help ensure specificity; yet it remains difficult to imagine CadN as a mediator of layer specific recognition.

All of these underscore the importance of placing the genetic perturbations of synaptic specificity into the context of developmental dynamics as discussed in the first section of this chapter. For example, despite the plethora of genetic manipulations we have at our disposal to disrupt the layer specificity of R7 cells; it remained essentially unclear how these axons choose their target layer and how all of these molecular factors affect the underlying growth cone mechanics to cause the defects observed in

their absence. This crucial gap in our understanding is essentially what my dissertation research aimed to fill by live imaging of the distinct processes that underlie synaptic specificity.

1.2.2 Synaptic partner matching during development

Much less is known regarding the selection of synaptic partners in the optic lobe after all of the layer- and column-specific sorting of the axons and dendrites is completed at the mid-pupal stages. EM reconstructions in adult stages revealed that neurites in the medulla are in close proximity with many different cell types in each layer and column but form synapses with only a limited selection (Takemura et al., 2015). These lead to the idea that pre- and postsynaptic cells must employ specific cell-surface molecules to ensure selective contacts to the correct partners.

One such group of molecules proposed to function in this way in the *Drosophila* optic lobe are Dpr family of immunoglobulin (Ig)-domain containing proteins and their binding partners DIPs (Dpr interacting proteins). It was shown that specific binding partners may be specifically expressed in corresponding synaptic partners (Tan et al., 2015); and that dpr11 which is expressed in a subgroup of R7 cells (yR7s) may be important for proper connectivity to their postsynaptic partner Dm8s, which express the binding partner DIP-γ (Carrillo et al., 2015). However, further research has revealed that Dpr11 - DIP-γ interaction functions primarily in modulating the survival of Dm8 cells (thus ensuring the right amount of synaptic partner cells are generated in the first place), but are dispensable for eventual synapse formation in R7 cells (Claude Desplan and Lawrence Zipursky, personal communication).

Finally, it is also important to consider that final positions at the adult stage may not necessarily reflect the level of overlap between potential synaptic partners during development, as well as the fact that synaptic specificity is not absolute. It is easily conceivable that additional restrictions on the connectivity could be achieved by spatial sequestering of correct partners together during certain crucial periods. In the end, a combination of spatial proximity as stated by Peters' rule (Braitenberg and Schüz, 1991) and probabilistic biasing of the contacts by cell-surface proteins is likely to underlie final synaptic specificity (Hassan and Hiesinger, 2015).

CHAPTER TWO

This chapter was previously published in *eLife 2015;4:e10721 DOI: 10.7554/eLife.10721*

Filopodial Dynamics and Growth Cone Stabilization in *Drosophila* Visual Circuit Development

M. Neset Özel[1,2,3], Marion Langen[1,*], Bassem A. Hassan[4,5], P. Robin Hiesinger[1,2,3,#]

1: Department of Physiology, UT Southwestern Medical Center, Dallas, TX 75390, USA

2: Division of Neurobiology, Institute for Biology, Freie Universität Berlin, 14195 Berlin, Germany

3: NeuroCure Cluster of Excellence, Charite Universitätsmedizin Berlin, 10117 Berlin, Germany

4: Center for the Biology of Disease, VIB, Leuven, Belgium

5: Center for Human Genetics, University of Leuven School of Medicine, Leuven, Belgium

* Current address: Department of Pharmaceutical Chemistry, University of California San Francisco, San Francisco, CA 94158, USA

2.1 Abstract

Filopodial dynamics are thought to control growth cone guidance, but the types and roles of growth cone dynamics underlying neural circuit assembly in a living brain are largely unknown. To address this issue, we have developed long-term, continuous, fast and high-resolution imaging of growth cone dynamics from axon growth to synapse formation in cultured Drosophila brains. Using R7 photoreceptor neurons as a model we show that >90% of the growth cone filopodia exhibit fast, stochastic dynamics that persist despite ongoing stepwise layer formation. Correspondingly, R7 growth cones stabilize early and change their final position by passive dislocation. N-Cadherin

controls both fast filopodial dynamics and growth cone stabilization. Surprisingly, loss of N-Cadherin causes no primary targeting defects, but destabilizes R7 growth cones to jump between correct and incorrect layers. Hence, growth cone dynamics can influence wiring specificity without a direct role in target recognition and implement simple rules during circuit assembly.

2.2 Introduction

Live dynamics data in intact nervous systems are critical to understand developmental processes and mutant phenotypes during the establishment of synaptic connectivity. However, most analyses of molecular perturbation experiments are based on fixed tissue and most live data are obtained in cell culture. Dynamics measurements have been difficult to obtain in intact developing brains at the resolution of growth cone filopodia, especially over long developmental time periods, in any organism (Langen et al., 2015; Mason and Erskine, 2000).

Growth cone filopodia have been shown to follow guidance cue gradients (Gallo and Letourneau, 2004; Zheng et al., 1996) and provide physical support for growth cone migration (Chan and Odde, 2008; Heidemann et al., 1990). They have also been associated with dendritic spine formation (Sekino et al., 2007). However, filopodia may exhibit very different and changing roles during the lifetime of a growth cone (Kolodkin and Tessier-Lavigne, 2011; Mason and Erskine, 2000; Mason and Wang, 1997). The types and roles of filopodial dynamics that control specific growth cone behaviors during neural circuit assembly in developing brains are largely unknown.

Amongst genetic model organisms with a complex brain, *Drosophila* provides a unique combination of small size, rapid development and the ability to culture developing eye-brain complexes (Ayaz et al., 2008; Gibbs and Truman, 1998). The fly visual system provides a well-studied model for axon outgrowth, targeting, layer formation, and quantitative synapse formation (Clandinin and Feldheim, 2009; Hadjieconomou et al., 2011; Melnattur and Lee, 2011). The fly's compound eye is an

assembly of ~750 ommatidia. Each ommatidium contains six outer photoreceptors (R1–R6) that terminate in the first optic neuropil, the lamina; the axons of the central photoreceptors R7 and R8 establish a retinotopic array of terminals in two separate layers of the second optic neuropil, the medulla. In particular, the development of the deepest projecting photoreceptor neuron, subtype R7, has been analyzed in great detail from axon outgrowth to layer-specific targeting and synapse formation (Hadjieconomou et al., 2011; Melnattur and Lee, 2011; Ting et al., 2007; Ting et al., 2005). However, to our knowledge, these steps have not yet been shown in the living, developing brain and the underlying types and roles of growth cone dynamics are unknown.

We have recently performed a slow time-lapse intravital imaging study of photoreceptor R1-R6 growth cone dynamics in intact pupae (Langen et al., 2015). However, intravital imaging has reduced resolution in deeper brain regions and is limited to early pupal stages. Previous imaging in cultured brains established high-resolution imaging in short developmental time windows (Medioni et al., 2015; Zschatzsch et al., 2014) and over long periods at low resolution and with slow time lapse (Rabinovich et al., 2015), thus preventing in depth analysis of the role of filopodial dynamics during an entire neural circuit assembly process. Here we present the development of an *ex vivo* imaging method for *Drosophila* eye-brain development using 2-photon microscopy that allows widely applicable continuous, fast, high-resolution 4D live imaging anywhere in the fly brain throughout pupal development.

We present R7 growth cone imaging at single filopodium resolution for both long periods (up to 24 hours per session) and at high temporal resolution (< 1 min), without deleterious effects on normal development. Our measurements show that R7 growth

cones do not actively extend after initial target recognition. Concurrently, the vast majority of R7 filopodia are motile and function in growth cone stabilization during layer formation. Loss of the cell adhesion molecule N-Cadherin (Lee et al., 2001; Nern et al., 2008; Ting et al., 2005) reduces filopodial dynamics and causes destabilization of R7 growth cones, resulting in active growth cone 'jumping' between layers even days after targeting has been concluded in wild type. These findings reveal an unexpected role for growth cone filopodia during layer formation and highlight the importance of assessing subcellular dynamics in relation to long-term neuronal development during brain wiring.

2.3 Results

2.3.1 Development of *ex vivo* brain culture in an imaging chamber

In preparation for fast and high-resolution imaging of growth cone dynamics through different phases of brain development (**Fig. 1a**) we systematically tested and adapted culture methods of developing *Drosophila* brains (Ayaz et al., 2008; Gibbs and Truman, 1998) in an imaging chamber (**Fig. 1b**; detailed description in Online Methods and **Fig. 1-supplement 1**). A pupal eye-brain complex dissected at P+24% exhibited only minor overall shape changes after 24h culture in the imaging chamber (**Figure 1c-d)**. Eye pigmentation became apparent at the end of this time period, indicating developmental progress. In contrast, a parallel control in which the brain developed normally in the pupae during the same time period exhibited a more pronounced expansion of the eye discs, but not yet any obvious eye pigmentation (**Fig. 1e**). Similarly, an eye-brain complex dissected at P+50% and cultured for 24h exhibited increasing eye pigmentation, but less overall shape changes than a brain developed inside the fly (**Fig. 1f-h**).

To analyze development at the level of axon targeting, we expressed a membrane-tagged GFP (CD4-tdGFP) (Han et al., 2011) in all photoreceptor neurons. We again compared the development of a brain in culture (from now on referred to as *ex vivo*), at different time points with brains that developed normally inside the fly (from now on referred to as *in vivo)*. As shown in **Figure 1i-l** and **Movie 1**, the distance between the terminals of R7 and R8 axons increase significantly after 19 hours *ex vivo* and *in vivo* (blue and green arrows). In contrast, a prominent rearrangement of

neuropils, where the lamina repositions itself around the medulla, appeared to occur only partially *ex vivo* (red arrows **Fig. 1k-l**). We next compared 18 hours *ex vivo* and *in vivo* development of photoreceptor axon projections starting at P+40%. We observed increases of both lamina and distal medulla thickness (between arrowheads) that occurred both *ex vivo* and *in vivo*, suggesting similar developmental progress (**Fig. 1m-p** and **Movie 1**). These observations suggest that large-scale morphological rearrangement may require factors outside of the eye-brain complex but may have no obvious effects on axon targeting inside the brain.

2.3.2 Culture and continuous laser scanning do not adversely affect developmental outcome

Next, we sought to determine (1) to what extent the rate of development is affected in culture and (2) the effect of continuous laser scanning during development. To measure developmental speed we compared stage-matched brains *ex vivo* and *in vivo*. To assess the effect of uninterrupted laser scanning, we compared a continuously imaged optic lobe (scanned every 30 minutes for approximately 15 minutes) with an unscanned control optic lobe of the same brain *ex vivo*. For brains dissected at P+22% and cultured for 20 hours we found no difference in distal medulla expansion between the optic lobes subjected to continuous laser scanning and the control optic lobes within the same brains (**Fig. 2a-b**). However, this expansion in the *ex vivo* brains was more rapid than in brains kept *in vivo*; the latter required 10 hours extra to achieve the same distal medulla size (**Fig. 2a-b)**. Importantly, the final thickness of the distal medulla was identical and did not increase further in both cases.

Next, we analyzed the development of brains dissected at P+41% and cultured for 19 hours. Similar to the earlier time point, we found no differences in the levels of distal medulla expansion between the continuously scanned and unscanned optic lobes. In addition, we found no quantitative differences for medulla expansion at this later stage (**Fig. 2d-f**). In sum, at this resolution the developmental outcomes appear normal in culture, and are not affected by continuous 2-photon imaging.

2.3.3 Imaging at high spatial resolution: Distinct growth cone shapes and filopodia types accompany different developmental stages

We next set out to image R7 growth cone dynamics at high resolution. To visualize individual growth cones we sparsely labeled ~10% of R7 cells, the deepest projecting photoreceptor axons in the *Drosophila* brain (Fischbach and Dittrich, 1989), through MARCM (Lee and Luo, 1999) using GMR-FLP. The development of R7 axons, particularly with regards to their layer specificity (Clandinin et al., 2001; Lee et al., 2001; Ting et al., 2005) and columnar restriction (Ting et al., 2007; Ting et al., 2014) has been studied extensively in fixed preparations.

As before, we compared brains *ex vivo* and *in vivo,* which were staged in parallel. We compared cultures starting at P+20% (**Fig. 3a**), P+40% (**Fig. 3b**) and P+55% (**Fig. 3c**) that were imaged continuously for up to 20 hours each (**Movie 2**); together these time intervals cover the development from layer selection to synapse formation over a 50 hour time period. As expected, live imaging deep in the brain leads to significant loss of fine structure; it was difficult to ascertain many faintly labeled filopodia and as a

result we consistently counted only about half as many filopodia *ex vivo* compared to *in vivo* fixed controls (**Fig. 3a-d**). However, this undercount affected filopodia of different lengths equally, resulting in the same mean lengths (**Fig. 3e**). Amongst live preparations, a P+20% preparation after additional 20 hours in culture looked qualitatively and quantitatively identical to fresh preparation at P+40%; similarly a P+40% preparation after additional 15 hours in culture looked like a fresh preparation at P+55%. We conclude that changes in the R7 growth cone structure occur similarly *ex vivo* and *in vivo* at this resolution.

The high-resolution structure of R7 growth cones revealed two distinct filopodial 'signatures' before and after P+50%. Prior to P+50%, we observed that each R7 growth cone had numerous filopodia that invaded several neighboring columns. During this period R7 growth cones slowly became restricted to their individual columns (**Fig. 3a, lower panel; Fig.3 supplement 1a**). Around P+40% R7 growth cones underwent extensive loss of filopodia (**Fig. 3d-e; Fig.3 supplement 1a**). Initial high filopodial activity coincides with the beginning of layer separation (**Fig. 3a, upper panel**) as lamina neuron axons intercalate between R7 and R8 terminals (Ting et al., 2005). Afterwards, R7 terminals have significantly fewer and shorter filopodia during the remainder of R7/R8 layer selection (P+45-55%; **Fig. 3b; Fig.3 supplement 1a**).

Surprisingly, longer filopodia reemerge after P+55% (**Fig. 3c, e**). These are fewer in number per growth cone compared to the early-stage filopodia. In addition, the late-stage filopodia often develop bulbous-like tips (**Fig. 3c**, arrows) unlike any of the earlier filopodia. These observations suggest previously undescribed filopodial dynamics that start after P+55%. During and after this time the R7 terminal undergoes a transition from

a morphologically distinct growth cone to an elongated structure with a branched axon shaft, reminiscent of previously observed axonal filopodia in spinal cord culture (Spillane et al., 2012; Spillane et al., 2011) . However, we only observed filopodia within the medulla neuropil where active layer formation and synapse formation occurs, and not on the main axon leading to the medulla neuropil (**Fig.3 supplement 1a-c**). In summary, distinct growth cone structures accompany separate developmental events and suggest different roles of filopodia during columnar restriction, layer separation and synaptogenesis.

2.3.4 Imaging at high speed: Most R7 filopodial dynamics are fast, transient and continuous throughout layer formation

To correlate fast filopodial dynamics with developmental events that are hours apart, we applied an imaging protocol that alternated between slow time-lapse imaging of the overall structure and high-resolution fast time-lapse imaging (every 1 minute) for 1 hour periods. We focused on critical periods of three major developmental events: the first stage of layer separation until P+40%, the separation or R7/R8 terminals in what will become the M3 and M6 medulla layers in the adult, and the onset of synaptogenesis.

We found distinct signatures of filopodial dynamics for each of these three processes (**Fig. 4a**). Specifically, at P+28% (during the first stage of layer separation), many transient filopodia (<8 minutes lifetime) as well as stable filopodia (lifetime >60 min) are apparent (**Fig. 4b-c**; **Movie 3**). In contrast, at P+50%, a reduced number of

transient filopodia (with the same kinetic characteristics) are present, but no stable filopodia (**Movies 3, 4**). At P+60% (onset of synaptogenesis), transient filopodia are dramatically reduced and a new type of stable filopodia has emerged that are less active than those during the first stage of layer separation (**Movie 4**). The culture and imaging conditions had little or no deleterious effects, as we observed very similar dynamics for different growth cones that had been in culture for different times at the same developmental timepoints (**Fig. 4a; Fig. 4-supplement 1**).

What is the role of transient and stable filopodia during development? Transient filopodia constitute more than 90% of all filopodia at P+28% and more than 70% of all filopodia at P+60% (**Fig. 4b**). Remarkably, these filopodia exhibit indistinguishable dynamics throughout pupation. We measured no significant changes in their mean lengths (**Fig. 4d**), average speed of extension and retraction (**Fig. 4e**), levels of inactivity (**Fig. 4f**) and the variance of these measurements (blue traces in **Fig. 4d-f**). Hence, these dynamics do not correlate with any particular developmental time period or event. Instead, the transient filopodial extensions suggest a continuous function for the even spatial distribution of the columnar and layer structure throughout early developmental stages. The number of transient filopodia reduces increasingly with time (**Fig. 4a**) while more cellular processes solidify the adult anatomy.

In contrast to transient filopodia, stable filopodia exhibit a bimodal distribution. A first type of stable filopodia exists up to P+35% and then rapidly vanishes before P+50%. These filopodia are significantly longer than transient filopodia, with some exploring up to two columns (**Fig 4b, d**). Surprisingly, their average speed and inactivity (i.e. intervals with no significant extension or retraction) are not significantly different

from transient filopodia at this stage (**Fig. 4e-f**; **Fig. 4-supplement 2**). This indicates that at early stages some filopodia appear stable only because they are longer. Unlike the earlier stable filopodia, those that emerge after P+55% exhibit a significantly greater inactivity compared to both the transient filopodia at this stage as well as the filopodia in earlier stages (**Fig. 4f**; **Fig. 4-supplement 2**). Combined with their peculiar bulbous tips (**Fig. 3c**), they define a distinct class of filopodia in both structure and dynamics. The two types of stable filopodia correlate with different developmental subprograms: The first type accompanies columnar stabilization and restriction of the growth cone, while more layers are being formed. In contrast, the second type of stable filopodia emerges after layers are defined and interactions with presumptive synaptic partners commence. The time period around P+50% where stable filopodia are absent matches precisely the moment when the final R7 and R8 layers are defined.

In summary, measurements of fast filopodial dynamics reveal that the majority of R7 filopodia are transient and may function during continuous column and layer stabilization; in contrast, distinct classes of stable filopodia may be substrates for the specific types of neurite interactions underlying the developmental events they accompany.

2.3.5 Single growth cone tracking reveals continuous R7 growth cone stabilization during layer formation

The temporary absence of stable filopodia around P+50% marks a critical developmental period when the final R7 and R8 layers are determined (Ting et al.,

2005). In this well-studied model for layer formation the R8 growth cone is known to actively extend (Timofeev et al., 2012). In contrast, how R7 reaches its final target layer is less clear. R7 ends up in the deepest layer of the distal medulla through one of two processes: it may extend away from a temporary layer to a new, more proximal layer (active model) (Hadjieconomou et al., 2011; Mast et al., 2006; Melnattur and Lee, 2011); alternatively, more layers are intercalated by other neurons while R7 remains in the same layer throughout (Ting et al., 2005) (passive model) (**Fig. 5a**). The recent finding that R7 is in close proximity with its Dm8 target dendrites as early as P+17% (Ting et al., 2014) supports the passive model (Ting et al., 2005); however, it remains unclear whether R7 growth cones actively participate in any part of the layer formation process. Live imaging of the entire process of layer formation can provide an unequivocal answer to the question whether R7 growth cones exhibit any extension activity by following the same growth cones over time.

We used a time-lapse interval of 30 minutes to track individual growth cones and their shape changes (**Movie 5)**. At P+30% the R7 growth cone exhibits a cone-shape that expands towards the terminal ending from its thin axonal process (triangle in **Fig. 5b**, t=0). Over the next 18 hours we observed a gradual change of this shape, but no extension away from it (**Fig. 5b**). How does the R7 axon accommodate new layer formation in the expanding distal medulla without extension? As shown in **Figure 5b**, a new varicosity emerges distally on the axon shaft of the cone-shaped growth cone (t=5 hours, arrow). This varicosity expands to give the entire terminal a bipartite structure (t=5-14 hours); these observations suggest the intercalation of a new layer and support the passive model. Importantly, the continuous observation of the same growth cone

and its dynamics (**Movie 5, Fig. 5-supplement 1**) unequivocally reveals the lack of active extension without the need for a stationary landmark that is necessary in fixed images to verify movement.

In contrast to R7, the growth cones of R8 extend a single filopodium towards their final layer (**Fig. 5c**, arrow); this filopodium is initially highly dynamic and exhibits almost complete retractions and re-extensions. It is finally stabilized in a deeper layer and gradually becomes thicker to form the new R8 terminal in the same layer as the distal end of the intercalated R7 varicosity (**Fig. 5c**, arrowhead).The formation of the bipartite R7 growth cone and its intercalating varicosity precedes the stabilization of the dynamically extending and retracting R8 process. This observation suggests that some other cell type first defines the layer where first the R7 growth cone forms its expanding varicosity and finally R8 targets.

In summary, our live data demonstrate that R7 terminals do not actively extend after P+30%. Instead, R7 growth cones arrive directly to their final layer and are only passively dislocated by the intercalation of other axons and dendrites (**Fig. 5d**). This process requires their continuous stabilization.

2.3.6 N-Cadherin is required for growth cone stabilization, but not for layer-specific targeting

The idea of passive retention implies that R7 growth cones do not engage in any active targeting process after P+30% and is consistent with the continuous transient filopodial dynamics shown above (**Fig. 4**). However, previous mutant analyses

described R7 targeting defects into layers that form after P+30%. For example, the homophilic adhesion molecule N-Cadherin (CadN) (Hatta et al., 1985) has emerged as a major regulator of synaptic layer specificity and its loss of function causes R7 mistargeting to the R8 layer (Lee et al., 2001; Ting et al., 2005). Previous studies focused on structure-function analyses of CadN (Nern et al., 2005) and its molecular interactions with other proteins (Prakash et al., 2009) and found that the penetrance of the mistargeting defect increased over time, suggesting retractions (Ting et al., 2005). However, how loss of *CadN* causes mistargeting or retractions is still unclear. In particular, it is unknown what changes in the growth cone dynamics cause this phenotype.

To investigate these aspects we performed live imaging of *CadN* mutant R7 axons (positively labeled using MARCM) in an otherwise wild-type brain **(Movie 6)**. We observed that almost all R7 terminals arborized correctly in a layer right below R8 terminals upon arrival at the medulla prior to P+20%. At P+23%, some of the 'oldest' mutant terminals that first arrived at the medulla were mislocalized (17% of all R7 terminals, n=54). As predicted (Ting et al., 2005), this increase is due to the retraction of R7 terminals which were initially in the correct position (**Fig. 6a, d**). These retractions were always preceded by a gradual collapse of their filopodial structure that could predict the remobilization of the growth cone at least 2 and up to 10 hours prior to retraction.

The fraction of mislocalized terminals increased to 33% (n=85) by P+40% and 56% (n=62) by P+52%. In addition, these numbers are underestimates since some of the mutant terminals retract completely from the medulla (**Fig. 6-supplement 1**).

Retractions continued even after the wild-type neurons formed their final layers (**Fig. 6b, d**), resulting in the previously observed penetrance of 70% in adult brains (Lee et al., 2001). These late retractions could be the consequence of dying back axons, or, alternatively, *CadN* deficiency is sufficient for R7 axons to regain active mobility days after their targeting is concluded.

Live observations of growth cone dynamics provided a clear distinction of these two possibilities: we observed that 52% (n=23) of retracted axons at P+40% APF actually *re-extended* towards more proximal layers within the next 8 hours. These axons often re-arborize in both correct and incorrect layers (**Fig. 6c, d**), but again fail to stabilize those arborizations (**Movie 6**). This phenotype was previously impossible to recognize in fixed preparations and masked by the overall increase in mistargeting penetrance. These data show that *CadN* mutant axons regain motility for days after their targeting should have been concluded. We conclude that CadN is not required for targeting *per se*, but for the stabilization of R7 growth cones after initial targeting.

2.3.7 N-Cadherin is required for fast filopodial dynamics

What is the role of filopodia in growth cone stabilization? Our R7 filopodial dynamics measurements revealed that >90% of all filopodia were transient and exhibit continuous, stochastic extension/retraction dynamics that did not correlate with any specific developmental processes (**Fig. 4**). These dynamics are consistent with continuous stabilization of the passively retained R7 growth cones throughout

development (**Fig. 5**). If filopodia control growth cone stabilization, then CadN growth cones should exhibit reduced filopodial dynamics.

CadN R7 growth cones do not appear obviously disrupted as long as they remain in their initial, correct arrival layer (**Fig. 6**) and filopodia numbers are not significantly affected at P+28% (**Fig. 7a**). However, both transient and stable filopodia of mutant growth cones exhibit reduced average speed of extension/retraction (**Fig. 7b, Movie 7**). As a consequence, both types of filopodia are on average also significantly shorter than wild-type (**Fig. 7c, d**). These findings point to a general slow-down of the filopodial dynamics in *CadN* growth cones and suggest that N-Cadherin mediated adhesion(Hatta et al., 1985) is important for the stabilization of R7 growth cones through filopodial interactions at the target layer.

In summary, we find that filopodial dynamics predict growth cone stabilization in a specific layer. This attachment of the growth cone in a specific layer is a continued requirement long after initial targeting is completed and it is further reflected in the majority of transient filopodial extension/retraction dynamics. Loss of *CadN* reduces these dynamics and increases the likelihood of layer destabilization even days after targeting is concluded.

2.4 Discussion

Fast filopodial movements of growth cones are thought to play important roles during brain development, but their types and roles remain largely unknown. In this study we developed a brain culture live imaging system that is applicable for all developmental stages of *Drosophila* brain development across a wide range of temporal and spatial scales. We used this system to investigate the role of R7 growth cone dynamics during layer formation throughout a 3-day developmental period. Our findings provide new insights into a major role of filopodia during column- and layer-specific growth cone stabilization. In addition, these observations indicate that growth cone dynamics can influence wiring specificity without a direct role in target recognition and more generally may implement simple rules during circuit assembly.

2.4.1 *Ex vivo* live imaging of *Drosophila* brain development at the resolution of filopodial dynamics

Our *ex vivo* brain development system in a closed imaging chamber allows continuous laser scanning during development for at least 20 hours per session. For longer imaging periods, the system can be modified to a semi-open state with perfusion (Williamson and Hiesinger, 2010). However, the ease of the closed chamber outweighed the advantage of longer imaging periods in our hands. Our key goal was to follow subcellular dynamics at the resolution limit of conventional light microscopy with fast enough time-lapse to quantitatively describe subcellular dynamic properties in developing brains over many hours. Important advances in *Drosophila ex vivo* brain

imaging have recently established high-resolution imaging in short developmental time windows (Medioni et al., 2015; Zschatzsch et al., 2014) and over long periods at low resolution and with slow time lapse (Rabinovich et al., 2015). We identify phototoxicity and drift as key problems to obtain high spatial and temporal resolution 3D dynamics data over long developmental time periods, for which the imaging system presented here provides a successful approach.

We have tested our system for developmental processes ranging from L3 brain development (cell migration, data not shown) and throughout pupal development (growth cone dynamics). We further provide the calibration of developmental progress in this culture system under imaging conditions. For example, morphological changes of the eye and 'lamina rotation' occur only incompletely outside of the fly's head **(Fig. 2c and Fig. 2-supplement 1)**. In contrast, early layer formation of photoreceptor axonal projections are accelerated with normal outcome; development after P+40% occurs with identical speed in our *ex vivo* system and *in vivo*. These findings indicate that layer and synapse formation are not directly dependent on distal tissue morphogenesis. However, different developmental processes must be calibrated for their *ex vivo* progress compared to *in vivo* development in the fly. Based on our quantitative analyses of layer formation in the distal medulla, we anticipate that the developmental progress of more proximal brain regions will be similar to the calibrated optic lobe development.

We show that conventional 2-photon microscopy can safely be used over long periods with virtually no drift and at high resolution in our imaging chamber when following a simple 'no bleaching' rule. In some cases we even observed mild photobleaching (e.g. **Fig. 2d**) without adverse effects on developmental progress. We

conclude that as long as there is no significant decrease in the signal intensity over time, 2-photon imaging *per se* does not negatively affect the development. In addition, *ex vivo* imaging has the advantage that the culture media allow pharmacological manipulations which are not easily possible *in vivo* or with intravital imaging.

In summary, the *ex vivo* imaging system and conditions developed here allow to observe live the formation of neural circuits anywhere in the *Drosophila* brain. Importantly, imaging at different spatial and temporal scales allows relating fast, high-resolution filopodial dynamics to much slower, long-term developmental processes.

2.4.2 Linking fast dynamics to long-term development: The role of filopodia

Growth cone behavior is highly dynamic and context-dependent (Mason and Erskine, 2000). Understanding the role of growth cone dynamics as part of a longer developmental process requires observation in their normal environment. Growth cone filopodia have traditionally been interpreted as probes that detect guidance cue gradients (Gallo and Letourneau, 2004; Zheng et al., 1996) or as ‘sticky fingers’ that provide the traction required for growth cone migration (Chan and Odde, 2008; Heidemann et al., 1990). Our characterization of the R7 growth cones revealed a different role for the vast majority of its filopodia during layer formation in the distal medulla: Surprisingly, more than 90% of R7 filopodia exhibit apparently stochastic extension/retraction dynamics that do not correlate with any major structural change during layer formation in the distal medulla. Instead, these movements are fast,

transient and only slowly reduce over the period of days during brain development, while new neurons innervate and new layers form.

What is the role of these filopodia? Our imaging data revealed that R7 growth cones do not actively extend after their initial target recognition, in contrast to some of the earlier models (Clandinin and Feldheim, 2009; Hadjieconomou et al., 2011; Ting and Lee, 2007). Instead, other axons and dendrites intercalate while R7 growth cones define the most proximal boundary of the distal medulla. Hence, R7 must stably maintain their position while active intercalation of other neurons, e.g. R8 extension, pushes the R7 layer proximally (**Fig. 5d**). This stabilization is consistent with continued filopodial extension/retraction dynamics that are decreasingly required as the final adult column and layer organization solidifies. However, we note that our imaging data do not establish a causal relationship between the observed dynamic behaviors.

The stabilizing function is reminiscent of zebrafish retinotectal axons which display a broadened structure while resting but are more streamlined during extension (Kaethner and Stuermer, 1992); stabilization through filopodial dynamics is further supported by the observation of ‘jumping’ growth cones in CadN mutants, as discussed below. Finally, we also observed a previously undescribed kind of filopodia that emerge at later stages. These are more stable, appear to coincide with the timing of synaptogenesis and are reminiscent of densities observed in hippocampal cultures using VAMP-GFP (Ahmari et al., 2000). However, adult R7 synapses are restricted to the main axonal trunk of the R7 terminal and the precise roles of these late, stable filopodia away from the main axonal trunk remain to be investigated.

Our observation of growth cones from initial arrival through layer formation and synaptogenesis reveals a remarkable transitioning of the R7 terminal shape from a more classical growth cone to an elongated structure with branched axon shaft (**Fig. 3-supplement 1a**). Filopodia on this extended R7 axon are reminiscent of axonal filopodia observed in spinal cord culture (Spillane et al., 2012; Spillane et al., 2011), but restricted to the axon shaft inside the medulla neuropil where layer formation and synaptogenesis occur (**Fig. 3-supplement 1b-c)**. Before P+40%, we only observe filopodia at the axon tips as in classical growth cones. Therefore, we suggest these structures are still growth cones although they appear to use filopodia as a means to stabilize rather than as a substrate for migration. We think that the subsequent transition morphologies could reasonably be interpreted as an extended growth cone or a distinct and short part of the proximal axon that got recruited to new active functions during layer formation **(Fig. 3-supplement 1a)**.

2.4.3 The role of N-Cadherin: Stabilizing the targeting decision, rather than making it

Our findings support a model in which continuous stabilization of R7 growth cones in a column/layer grid depends on the levels of N-Cadherin (CadN). The observation of mistargeted photoreceptor axons (Lee et al., 2001) as well as its classical role in axon guidance (Matsunaga et al., 1988) have previously led to the interpretation of CadN as a guidance cue. The interpretation as a part of a specificity code is complicated by the observation that CadN is expressed in all presynaptic and postsynaptic neurons during distal medulla development; however, temporal regulation

(Petrovic and Hummel, 2008) as well fine-tuning of expression levels (Schwabe et al., 2014) have been proposed as solutions.

Our live imaging data reveal that CadN-deficient R7 axons have no initial targeting defects and CadN does not function as a target layer-specific cue. Instead, growth cones fail to stabilize and engage in an aberrant process of ‘jumping’ between incorrect and correct layers. Remarkably, CadN-deficient R7 growth cones retain the ability to jump between distal medulla layers for days after their normal targeting should have been concluded and stabilized, presumably through the filopodial dynamics described here. CadN has been shown to localize to the filopodia of R1-6 photoreceptor axons in the lamina neuropil (Schwabe et al., 2013); we speculate that R7 growth cones could use the surface area of their filopodia to form stabilizing adhesions through CadN. Consistent with this interpretation, loss of CadN reduces filopodial extension/retraction dynamics and ‘jumps’ between medulla layers are preceded by a slow, several hours-long filopodial retraction process.

CadN mediated adhesive interactions were shown to be essential for growth cone migration in primary neuronal cultures (Bard et al., 2008). We observed decreased filopodial lengths in CadN growth cones, consistent with the longer neurite lengths observed with increased CadN mediated adhesions. While such interactions were previously correlated with growth cone velocity, our observations provide a link to their stability in a different context.

CadN-mediated adhesion with other medulla cells is required for R7 terminals to end up in the correct layer independent of its signaling function (Yonekura et al., 2007). This finding is consistent with a growth cone stabilization function via interactions with

many different medulla cells, independent of the eventual synaptic partners. This idea is further consistent with the widespread expression of CadN in many cell types. In sum, our data together with previous observations support a ‘non-guidance cue’ function for CadN in stabilizing the positions and contacts of neurites once the targeting is complete. Indeed, several cell adhesion molecules previously thought to function as guidance cues have recently been shown to exert ‘non-cue’ functions cell-autonomously (Petrovic and Schmucker, 2015) and through implementing simple developmental rules (Hassan and Hiesinger, 2015). Initial R7 targeting to the correct layer could be achieved by other molecules or by a developmental rule such as “stop at the first target layer encountered past the pioneer R8 axon, and then stabilize”. It is possible that such a rule could result in the correct initial targeting of R7 and L-cell axons simply by their arrival order (**Fig. 5d**), requiring no layer-specific molecular code(Hassan and Hiesinger, 2015).

2.5 Materials and Methods

2.5.1 Genetics

Pan-photoreceptor labeling was done by GMR-Gal4 expressing the membrane tethered CD4-tdGFP (Han et al., 2011). Sparse R7 labeling as well as the generation of *CadN* mutant R7 neurons were achieved through MARCM (Mosaic analysis with a repressible cell marker)(Lee and Luo, 1999) using GMRFLP. GMR-myr-RFP or GMR-myr-tdTomato was used to label all photoreceptors in the background.

Fly stocks: i) *;;GMR-Gal4, UAS-CD4-tdGFP* ii) *GMR-FLP; GMR-Gal4; FRT80B, UAS-CDR-tdGFP* iii) *GMR-myr-RFP;; FRT80B, tub-Gal80* iv) *GMRFLP; FRT40A, tub-Gal80; GMR-Gal4, UAS-CD4-tdGFP, GMR-myr-RFP* v) *;FRT40A, CadN*^{405}; vi) *hs-FLP; GMR-FRT-w*$^{+}$*-FRT-Gal4; UAS-CD4-tdGFP* vii) *GMR-myr-tdTomato; FRT80B, tub-Gal80*.

2.5.2 Histology and Fixed Imaging

Eye-brain complexes were dissected in PBS, fixed in 3.7% paraformaldehyde (PFA) in PBS for 40 minutes, washed in PBST (0.4% Triton-X) and mounted in Vectashield (Vector Laboratories, CA). Images were collected using a Leica TCS SP5 confocal microscope with a 63X glycerol objective (NA=1.3).

2.5.3 Brain Culture

The culture chambers were built inside 60x15 mm petri dish lids with a layer of Sylgard 184 (Dow Corning) at the center (2 cm in diameter). 200 μm thick X-ray films

cut in 1x1 mm pieces were used as spacers to prevent the coverslip from crushing the tissue. 2% low melting point agarose was prepared in water and dialyzed in pure water for 48 hours with changing the water every 12 hours at room temperature, then stored at 4^{o}C.

The culture media was modified from a previous recipe (Ayaz et al., 2008). It was prepared with 1:10 fetal bovine serum (FBS), 10 µg/ml human insulin recombinant zinc (Stock: 4 mg/ml), 1:100 Penicillin/streptomycin (Stock: 10000 IU/ml penicillin, 10 mg/ml streptomycin), 1 µg/ml 20-Hydroxyecdysone (Stock: 1 mg/ml in ethanol) in Schneider's Drosophila Medium. All were acquired from Life Technologies. Brains were dissected in chilled Schneider's Medium and mounted in 0.4% dialyzed low-melting agarose diluted in the culture media. Step-by-step chamber assembly (**Fig. 1-supplement 1**):

1) Oxygenize culture medium at room temperature.
2) Melt a piece of 2% dialyzed agarose. Mix with culture media preheated to 42 ^{o}C at 1:4 ratio (to the final concentration of 0.4%). Keep the mixture at 32 ^{o}C.
3) Dissect brains in chilled Schneider's Drosophila Medium. Keep them in chilled culture medium until mounting.
4) Place the brain (with a pipette) at the center of Sylgard layer in a 30-40 µl drop of the diluted agarose (**Supplement 1a (ii-iii)**).
5) After correctly positioning the brain, place a coverslip (circular, 4 cm diameter) on the drop (**Supplement 1a (iv)**).
6) Glue the coverslip to the petri dish at 4 points using rubber cement.

7) After the polymerization of agarose (15-20 minutes), fill the rest of the space between coverslip and the petri dish with culture media (**Supplement 1a (v)**).
8) Seal the chamber completely with rubber cement (**Supplement 1a (vi)**).

The final imaging chamber (**Supplement 1b, c**) provides sufficient oxygen and nutrients through diffusion for at least 24 hours. 20-Hydroxyecdysone is excluded from the cultures that start after 50% APF. This is due to previously measured physiological titers(Paul Bainbridge and Bownes, 1988) as well as our experimental data (**Methods-figure supplement 1**).

2.5.4 Live Imaging

Live imaging was performed at room temperature using a Zeiss LSM 780 multiphoton microscope with a 40X LD water objective (NA=1.1) or a Leica SP8 MP microscope with a 40X IRAPO water objective (NA=1.1) with a Chameleon Ti:Sapphire laser (Coherent). For single-channel CD4-tdGFP imaging, excitation was done at 900 nm. For double-channel CD4-tdGFP and myr-RFP imaging, excitation was done at 800 nm.

Our chamber can be imaged in conjunction with both water and glycerol objectives with both upright and inverted microscopes. We compared the images of R7 growth cones of a P+27% brain acquired by above setup with those acquired by a conventional Leica TCS SP5 confocal microscope with a resonant scanner, using a 63X Glycerol objective (NA=1.3). A resonant scanner provides superior scan speeds compared to standard two-photon systems. However, we observed a rapid decrease in

signal level with the confocal microscope at tissue deeper than 60 μm from the coverslip (**Methods-figure supplement 2**). Even at moderately deep tissue, the laser power required on the confocal system to acquire images with comparable quality to the two-photon system is too high to take advantage of the superior scan speeds for extended periods (data not shown). Nevertheless, the resonant scanner would still be the preferred option for imaging superficial tissues when speed is the most important factor.

2.5.5 Data Analysis

Imaging data were analyzed and presented with Imaris (Bitplane). Deconvolved data were used in Figures 4, 5 and 6 and supplementary movies. 3D deconvolution was done with Autoquant X3 using adaptive PSF (blind). For all datasets, 10 iterations were performed at medium noise level (noise value: 20) with recommended settings. Distance from the coverslip was set to 40 μm.

Filopodial analysis was done with the Filament module of Imaris. Each filopodium was manually segmented and tracked across time points. “Automatic placement” option was used while drawing to ensure that we measured the actual 3D length of each filopodium. We exported the “length over time” data for all of the filopodia of a growth cone to an Excel sheet and performed further analysis with MATLAB.

We used a custom MATLAB code to calculate the number of extension& retraction events, mean extension&retraction speeds, mean lengths and lifetimes for each TrackID. Heat maps of lengths versus time for all filopodia in a growth cone were also generated. In those, filopodia were sorted by the angle of their orientation at the

time of their initial formation. We did not find any overall, significant difference between the average speeds of extension and retraction on any growth cone; so they were combined to calculate a single average speed for all further analysis. We considered any changes in length less than 0.3 μm between consecutive time points as zero movement or “static” periods because manual segmentation cannot be precise enough to reliably account for such a small retraction or extension. Average speeds were therefore calculated only from the points that had a change in length greater than 0.3 μm. We used the ratio of static time points to the lifetime of a filopodium to calculate “inactivity”.

Further analysis, i.e. classification into transient and stable filopodia, statistical analysis, and the generation of graphs were done with GraphPad Prism. Where needed statistical differences were calculated with unpaired, parametric t-tests. Filopodia number percentages over time in **Figure 4c** were fitted with second order polynomials to generate curves. For inactivity measurements, we generated two different graphs. Due to their short lifetimes, many transient filopodia have zero inactivity by definition; resulting in drastically lower average inactivity for transient filopodia compared to other filopodia (**Fig. 4-supplement 2g-i**). This may unfairly imply an intrinsic difference of dynamics between transient and stable filopodia (**Fig. 4-supplement 2j**). Indeed, when the filopodia with ‘zero inactivity’ are excluded, their average inactivity is statistically identical with the early-stage stable filopodia (**Fig. 4-supplement 2k**). We therefore used these graphs in Figures 4 and 6.

2.6 Chapter Two Figures

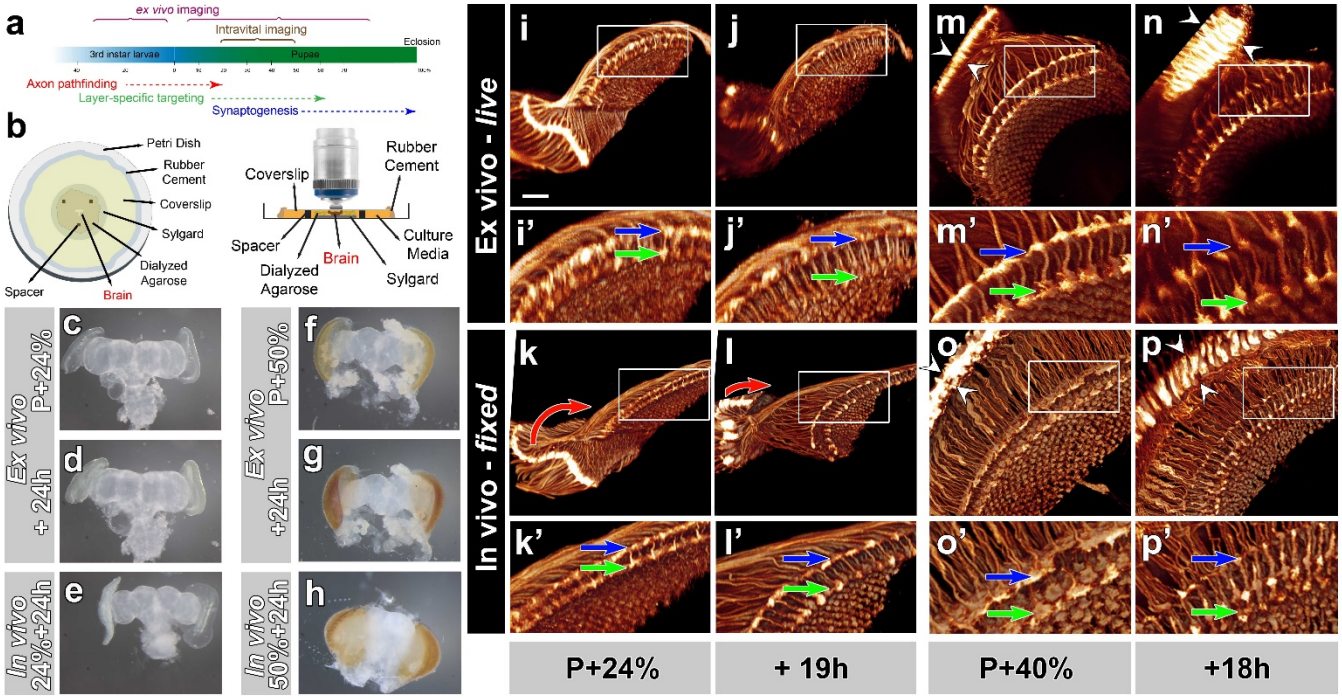

Figure 1: Development of Drosophila pupal brains in culture. a, Timeline of photoreceptor circuit formation during brain development and the periods accessible by live imaging. **b,** *Ex vivo* imaging chamber, top (left) and side (right) views (see **supplement 1** for step-by-step assembly). **c-h,** Changes in brain morphology during development *ex vivo* v. *in vivo*. **c,f,** Pupal brains dissected at P+24% and P+50%. **d,g,** The same brains after 24h of development *ex vivo*. **e,h,** Brains that were dissected from pupae collected at P+24% and P+50% and aged in parallel to the *ex vivo* brains. See **supplement 2** for comparison with free-floating cultures.

i-p, Optic lobe development *ex vivo* v. *in vivo* (**i'-p',** magnified details of **i-p**). All photoreceptors express CD4-tdGFP. Initial layer separation (P+24% + 19h) occurs *ex vivo* (**i',j'**) similarly to the *in vivo* controls (**k', l'**) aged in parallel (blue arrows: R8, green arrows: R7). Lamina rotation (red arrows) observed *in vivo* (**k, l**) is defective *ex vivo* (**i, j**). Final layer formation and lamina expansion (P+40% + 18h) occurs similarly *ex vivo* and *in vivo*, **m'-n'** v. **o'-p'** (arrows) and **m-n** v. **o-p** (between arrowheads), respectively. Note that for the *ex vivo* brains, images of the same specimens were taken at different time points, while for the *in vivo* controls different brains had to be fixed and imaged for the different time points. Scale bars, 20 µm.

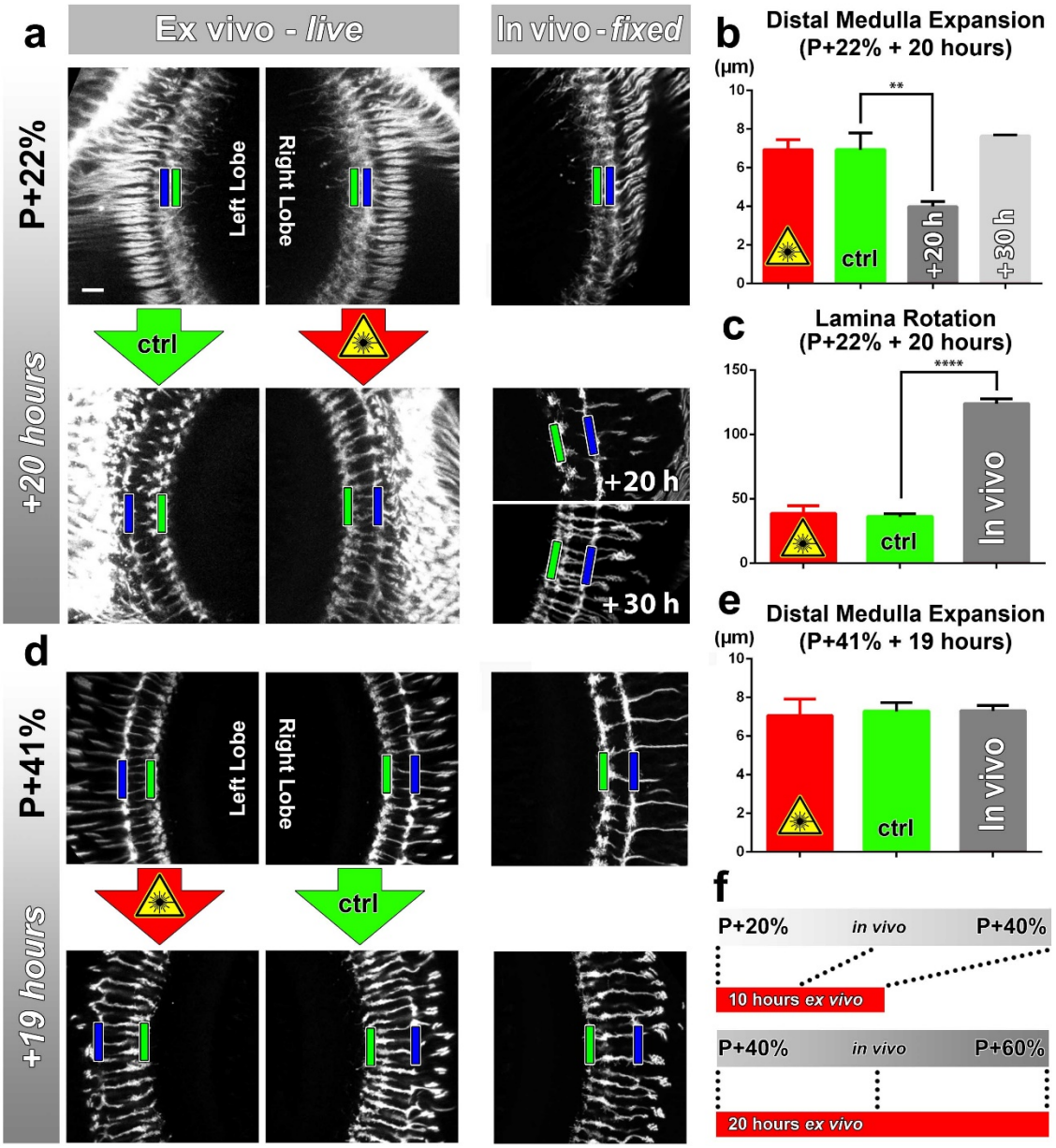
a
Ex vivo - live
In vivo - fixed
P+22%
+20 hours
Left Lobe
Right Lobe
ctrl
+20 h
+30 h
b
Distal Medulla Expansion
(P+22% + 20 hours)
(µm)
**
ctrl
+20 h
+30 h
c
Lamina Rotation
(P+22% + 20 hours)
****
ctrl
In vivo
d
P+41%
+19 hours
Left Lobe
Right Lobe
ctrl
e
Distal Medulla Expansion
(P+41% + 19 hours)
(µm)
ctrl
In vivo
f
P+20%
in vivo
P+40%
10 hours ex vivo
P+40%
in vivo
P+60%
20 hours ex vivo

Figure 2: Effects of culture conditions and laser scanning on the optic lobe development ex vivo. Two-photon imaging of the medulla was performed with brains cultured at P+22% for 20h (**a**), and P+41% for 19h (**d**), all photoreceptors express CD4-tdGFP. For each experiment one image stack was acquired containing both optic lobes of a brain. Next, only one of the lobes was scanned every 30 minutes. Finally, another stack was acquired with both lobes. Different brains aged in parallel in pupae have been dissected as *in vivo* controls. **b**, Quantification of the layer distance increase in P+22% cultures. The distance between R8 (green rectangles in **a,d**) and R7 (blue rectangles) layers increase identically in scanned and unscanned *ex vivo* lobes, but higher than the *in vivo* control ($p=0.0036$, $n=3$). **c**, Quantification of the change in the angle between the planes of posterior lamina and the anterior medulla. *Ex vivo* lobes rotate similarly but slower than *in vivo* controls ($p<0.0001$, $n=3$). **e**, Quantification of the layer distance increase in P+41% cultures. All groups show a similar increase in the distance between R8 temporary layer and R7 terminals. Error bars depict SEM. **f**, Calibration of the developmental speed in culture to *in vivo* development, based on distal medulla expansion. Scale bars, 10 μm.

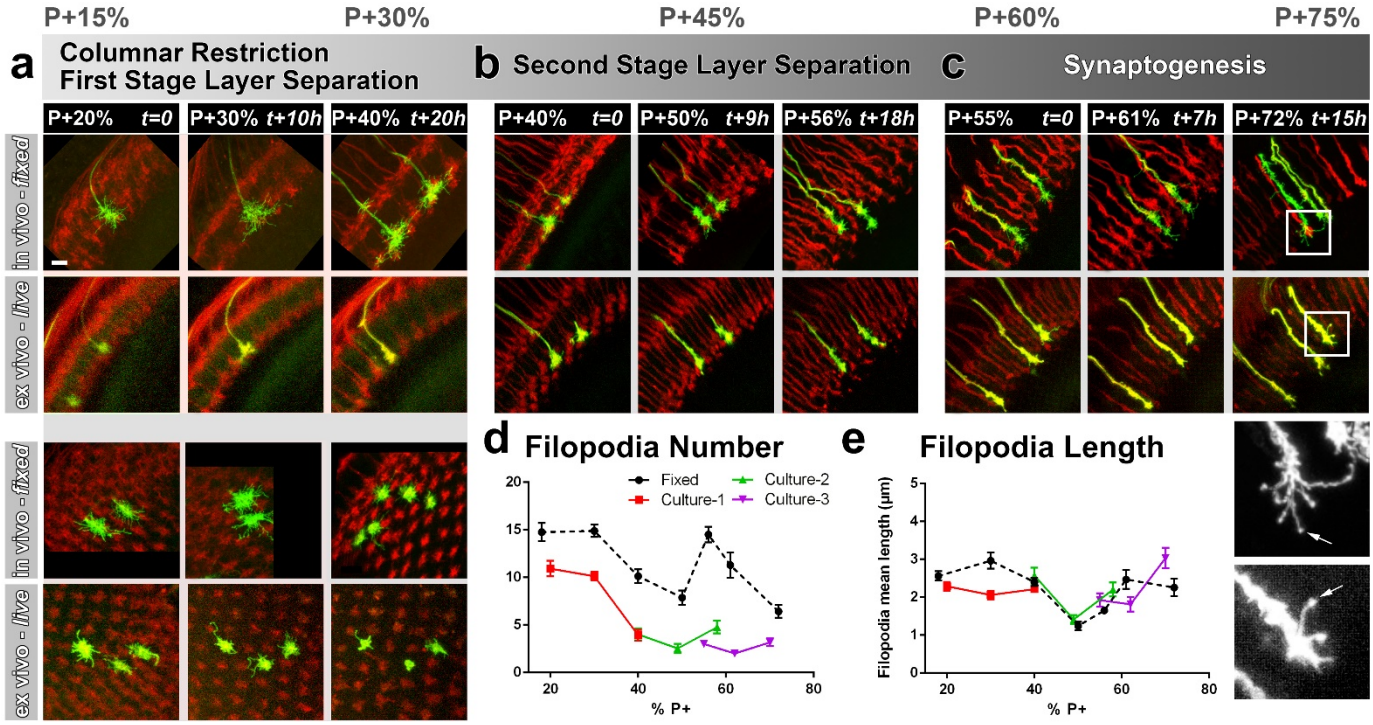
P+15%
P+30%
P+45%
P+60%
P+75%
a
Columnar Restriction
First Stage Layer Separation
b Second Stage Layer Separation
c Synaptogenesis
P+20% t=0
P+30% t+10h
P+40% t+20h
P+40% t=0
P+50% t+9h
P+56% t+18h
P+55% t=0
P+61% t+7h
P+72% t+15h
in vivo - fixed
ex vivo - live
in vivo - fixed
ex vivo - live
d Filopodia Number
Fixed
Culture-1
Culture-2
Culture-3
% P+
e Filopodia Length
Filopodia mean length (µm)
% P+

Figure 3: Different filopodial signatures accompany separate circuit formation steps. Slow (30 min interval) time-lapse imaging of pupal brains dissected at P+20% (**a**), P+40% (**b**) and P+55% (**c**) in comparison with *in vivo* fixed controls at the same stages. The same growth cones were analyzed for all live imaging experiments while different samples from parallel aged pupae had to be dissected for the *in vivo* controls. All photoreceptors were labeled with myr-mRFP and R7 cells were sparsely labeled with CD4-tdGFP using GMR-FLP through MARCM. **a**, As the R7 and R8 layers go through their initial separation (upper panel), R7 terminals have numerous filopodia that invade neighboring columns (lower panel), which are pruned around P+40% both *ex vivo* and *in vivo*. **b**, As the layers start to reach their final configuration, R7 terminals form a bipartite structure around P+50%. Filopodia numbers remain low. Around P+55%, more (shorter) filopodia are observed again as R7 axon assumes a brush-like look. **c**, After P+55% shorter filopodia are pruned and R7 growth cones form new, longer filopodia that are fewer in number and have bulbous tips (arrows). Quantifications of **d**, total number of filopodia per growth cone and **e**, mean length of filopodia through the *ex vivo* experiments **a-c** and respective *in vivo* controls. Error bars depict SEM. Scale bars, 5 μm.

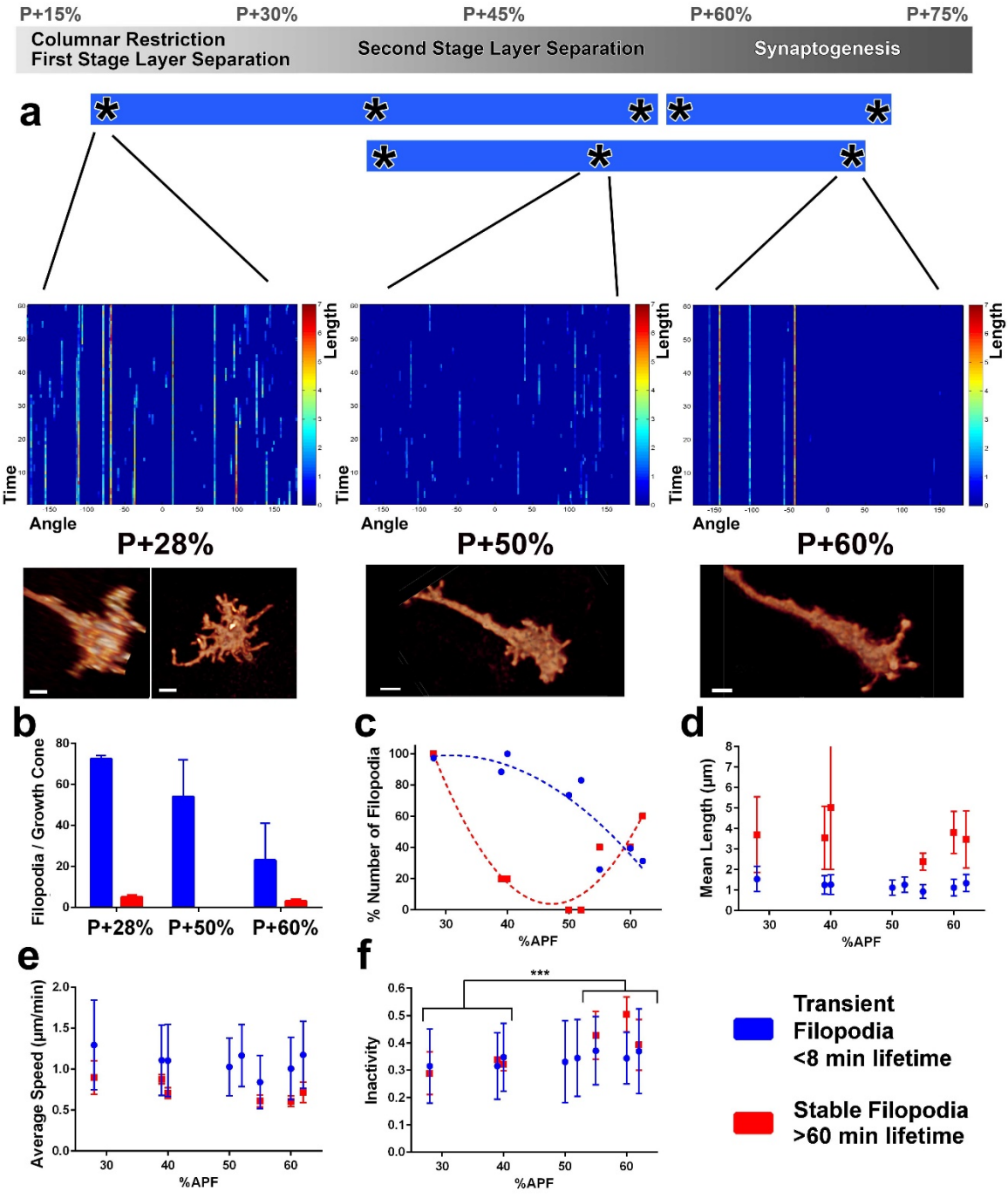
P+15%
P+30%
P+45%
P+60%
P+75%
Columnar Restriction
First Stage Layer Separation
Second Stage Layer Separation
Synaptogenesis
a
Time
Angle
Length
P+28%
P+50%
P+60%
b
Filopodia / Growth Cone
P+28%
P+50%
P+60%
c
% Number of Filopodia
%APF
d
Mean Length (µm)
%APF
e
Average Speed (µm/min)
%APF
f
Inactivity
***
%APF
Transient Filopodia <8 min lifetime
Stable Filopodia >60 min lifetime

Figure 4: Distinct classes of transient and stable filopodia underlie different developmental events. Fast (1 min interval) time-lapse imaging was performed at multiple points of three *ex vivo* experiments. **a,** Three time points are shown; during the first-stage (P+28%) and second-stage (P+50%) layer formation, and synaptogenesis (P+60%). 3D graphs (upper panel) show the dynamics of individual filopodia observed in a one hour period. In the heat maps on blue background, individual filopodia are shown as verticals lines. The filopodia were sorted by their initial orientation angle (x-axis). The length of the vertical lines represents the life time of the filopodia (time on the y-axis). The color map indicates the length (μm) for each filopodium through time. Representative images of the growth cones at the above time-points (lower panel). See **supplement 1** for heat maps and representative images at all time points. **b**, Numbers of filopodia per growth cone for the time-points shown in **a**; for filopodia with lifetime<8 min (transient) and lifetime>1 h (stable). **c**, Numbers of filopodia relative to the numbers at P+28% for all time-points imaged. Fitted curves: $y=28.17+4.597x-0.075x^2$ (transient) and $y=583.1-24.53x+0.26x^2$ (stable). **d**, Mean length (μm) **e**, Average speed (μm/min) and **f**, Inactivity (ratio of intervals with no significant extension or retraction) for transient and stable filopodia at all time-points. Stable filopodia observed after P+50% have significantly higher inactivity than those observed before (Means: 0.3002 v. 0.4346, p=0.0002, n=14 for each). See **supplement 2** for these parameters as a function of filopodia lifetime on the same growth cone. Error bars depict SD. Scale bars, 2 μm.

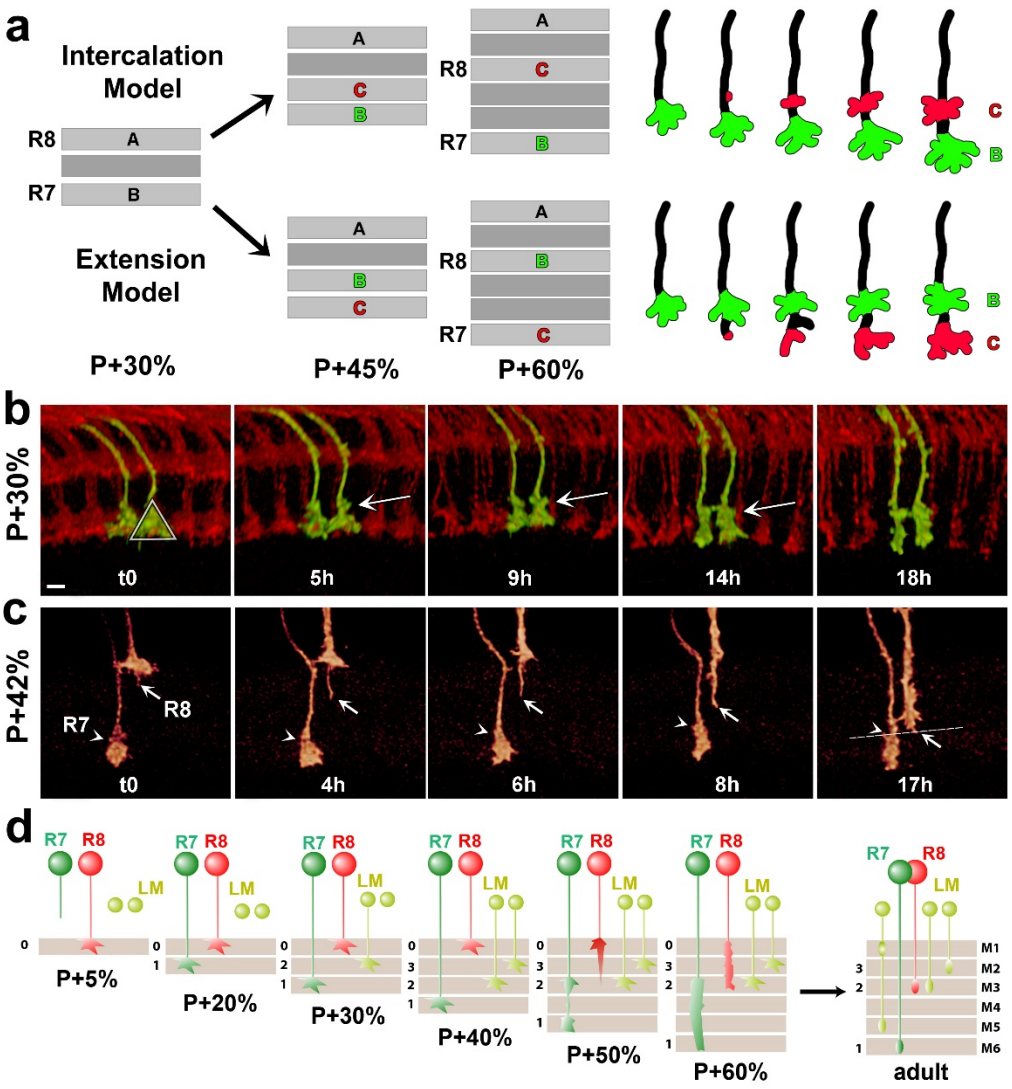
a
Intercalation Model
R8
A
R7
B
A
C
B
R8
A
C
R7
B
C
B
Extension Model
A
B
C
R8
A
B
R7
C
B
C
P+30%
P+45%
P+60%
b
P+30%
t0
5h
9h
14h
18h
c
P+42%
R7
R8
t0
4h
6h
8h
17h
d
R7
R8
LM
P+5%
P+20%
P+30%
P+40%
P+50%
P+60%
adult
M1
M2
M3
M4
M5
M6

Figure 5: R7 growth cones do not actively extend in the medulla. a, R7 may reach its final target layer through active extension or passive displacement and intercalation. **b,** Live imaging starting at P+30%. All photoreceptors were labeled with myr-mRFP and R7 cells were sparsely labeled with CD4-tdGFP using GMR-FLP through MARCM. R7 growth cone (triangle) initially has a cone structure. As the layer formation progresses, a new varicosity (arrow) is formed from the axon shaft. This structure expands further and by P+50% the entire terminal thickens. See **supplement 1** for all time points. (N=31). **c**, Live imaging starting at P+42%. Both R7 and R8 cells were sparsely labeled with CD4-tdGFP using hsFLP. R7 axon has already formed its distal varicosity (arrowhead); the R8 axon has extended a single filopodia proximally (arrow). Later, this filopodia reaches to the R8 final layer and forms the new terminal. R7 terminal shows no active extension activity. (N=17 for R7 and 15 for R8). **d**, Model of layer formation in the distal medulla. After their arrival to the medulla R7 and R8 terminals are initially separated by intercalation of lamina cell (LM) axons. After P+40%, R8 growth cones actively extend to new layer while R7s remain in their arrival layer throughout. Scale bars, 3 μm.

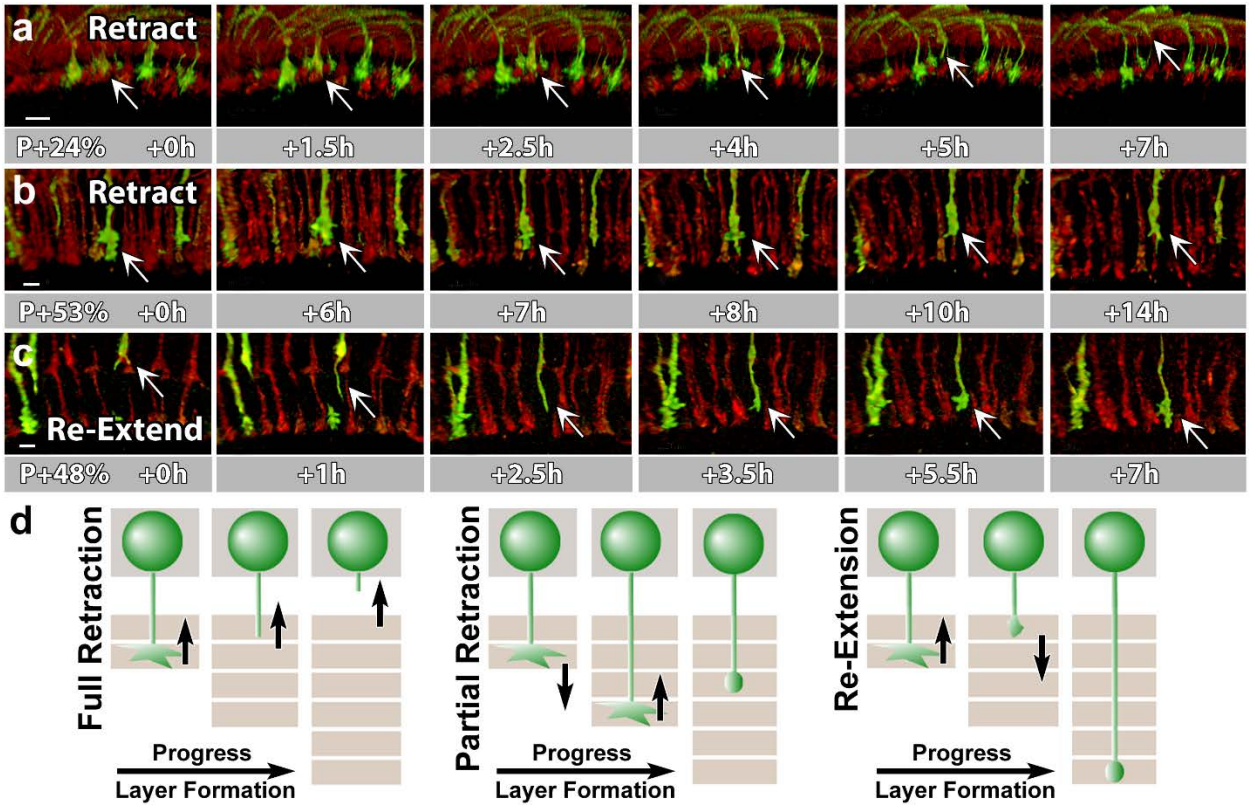
a
Retract
P+24%
+0h
+1.5h
+2.5h
+4h
+5h
+7h
b
Retract
P+53%
+0h
+6h
+7h
+8h
+10h
+14h
c
Re-Extend
P+48%
+0h
+1h
+2.5h
+3.5h
+5.5h
+7h
d
Full Retraction
Progress
Layer Formation
Partial Retraction
Progress
Layer Formation
Re-Extension
Progress
Layer Formation

Figure 6: N-Cadherin is required for the stabilization but not the layer specific targeting of R7 growth cones. All photoreceptors were labeled with myr-mRFP. *CadN*^{405} R7 cells were generated with MARCM, using GMR-FLP and positively labeled with CD4-tdGFP. **a**, Live imaging started at P+24% shows a mutant R7 growth cone (arrow) that retracts from its target layer over the course of 5 hours. **b**, Live imaging started at P+53% shows a mutant R7 growth cone (arrow) that retracts from its target layer over the course of 10 hours. Some mutant axons retract completely from the medulla (**supplement 1**) **c**, Live imaging started at P+48% shows an R7 axon (arrow) that has been retracted to the edge of distal medulla but re-extends and attempts to re-innervate both wrong (5.5h) and the right (7h) layers. **d,** Schematics of observed retraction and re-extensions events. Left and middle: Full Retraction leads to complete loss of the R7 axons from the medulla (left), while partial retraction (middle) leads to R7 terminals in an incorrect layer. Number of mislocalized terminals: 33% (n=85) at P+40% and 56% (n=62) at P+52%. Right: Previously retracted R7 axons can re-extend, even days after they would have been stabilized in wild type. 52% (n=23) of retracted axons at P+40% re-extended before P+50%Scale bars, 5 μm.

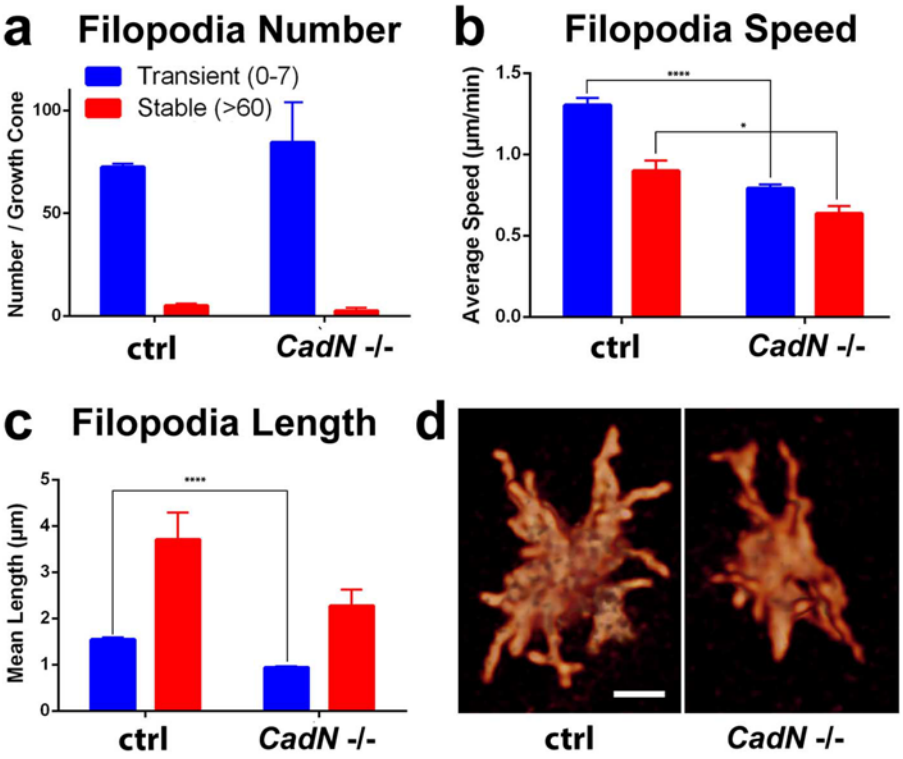

Figure 7: N-Cadherin is required for fast filopodial dynamics. *CadN*^{405} R7 cells were generated with MARCM, using GMR-FLP and positively labeled with CD4-tdGFP. Fast (1 min interval) time-lapse imaging was performed at P+28%. **a**, The average numbers of filopodia per growth cone are not significantly different between wt and *CadN*^{405}. **b**, Mutant filopodia are slower, (for transient, means wt: 1.303 (n=143), *CadN*^{405}: 0.791 (n=169), p<0.0001; for stable, means wt: 0.898 (n=10), *CadN*^{405}: 0.636 (n=5) p=0.0199) and **c**, shorter (for transient, means wt: 1.542 (n=143), *CadN*^{405}: 0.939 (n=169), p<0.0001; for stable: means wt: 3.707 (n=10), *CadN*^{405}: 2.275 (n=5), p=0.1257). **d**, *CadN*^{405} R7 growth cones at the correct layer. Scale bars, 5 µm.

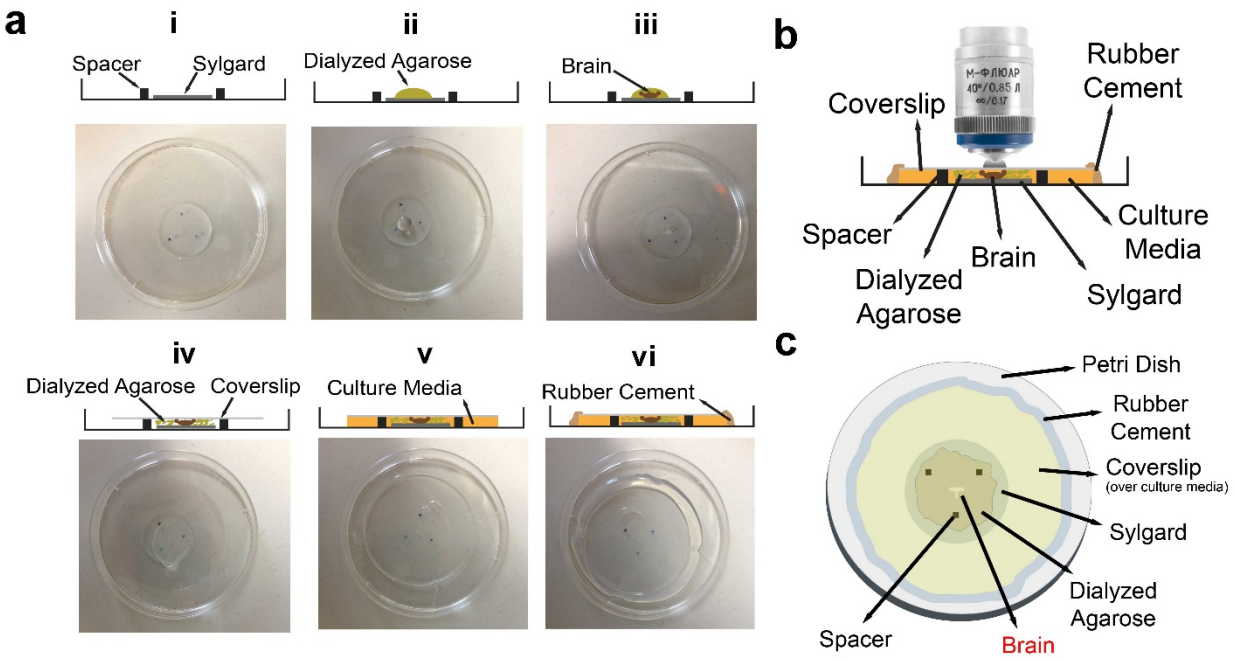

Figure 1-figure supplement 1: Culture imaging chamber. a, Step-by-step construction of the imaging chamber. (i) Spacers are placed on the Sylgard layer in a triangle formation. (ii) A drop of diluted dialyzed agarose is pipetted onto the Sylgard. (iii) Dissected eye-brain complex is placed into the agarose drop. (iv) The mix is covered with a coverslip. (v) After the agarose polymerization, remaining space under coverslip is filled with the culture media; (vi) and sealed completely with rubber cement. The schematic of the final chamber **b**, from the side **c**, and the top.

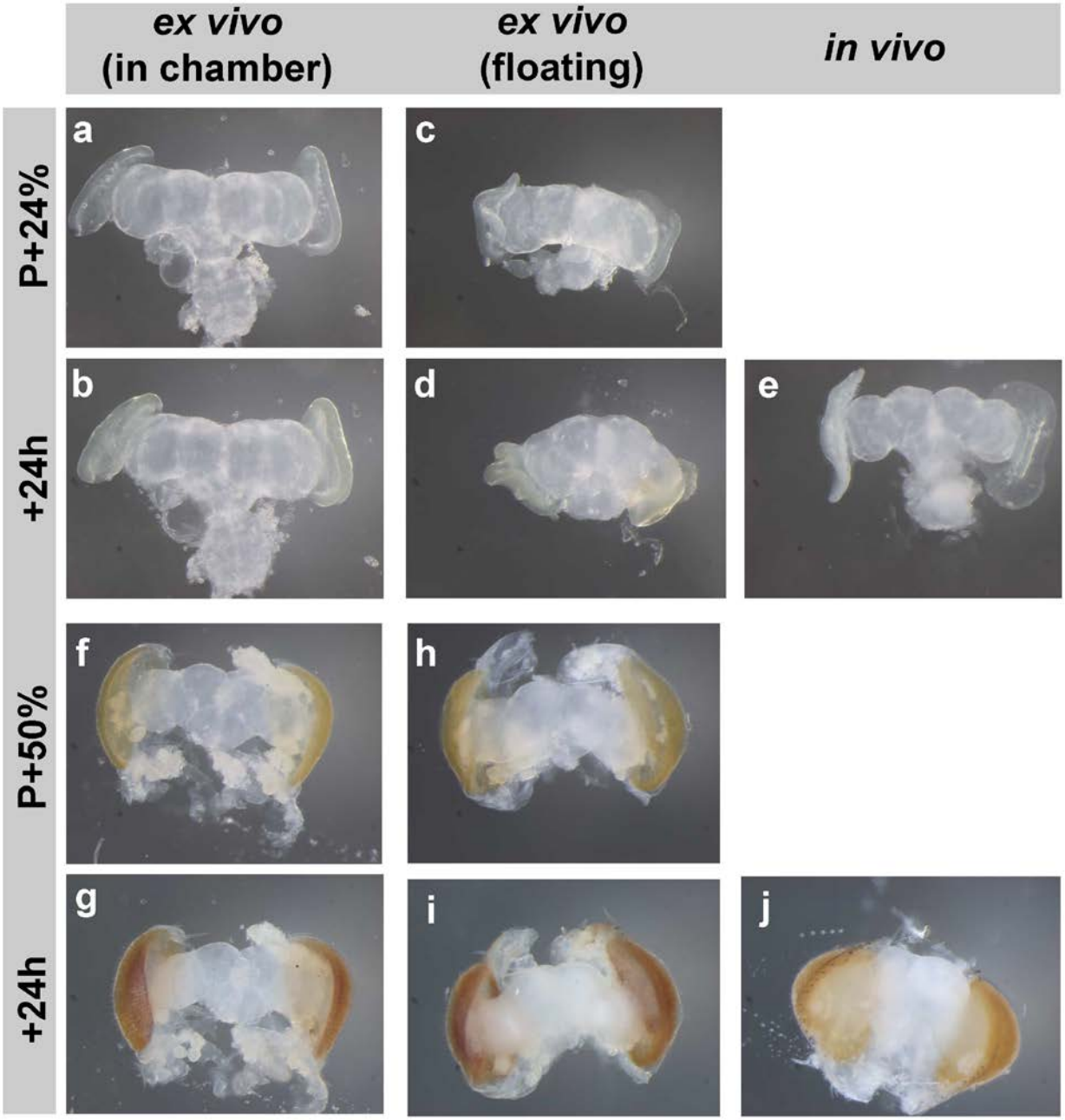
ex vivo
(in chamber)
ex vivo
(floating)
in vivo
P+24%
+24h
P+50%
+24h
a
b
c
d
e
f
g
h
i
j

Figure 1-figure supplement 2: Brain development in imaging chamber compared to liquid media. Changes in brain morphology during development *ex vivo* in chamber vs. *ex vivo* in liquid media (free floating) vs. *in vivo*; from brains dissected at P+24% (**a-d**), P+50% (**f-i**) and cultured for 24h. Parallel developed in vivo controls (**e, j**) were dissected at the end of cultures. At early stages, brains that developed in the imaging chamber (**b**) are more similar in morphology to the *in vivo* controls (**e**) than the brains that developed in fully liquid media (**d**).

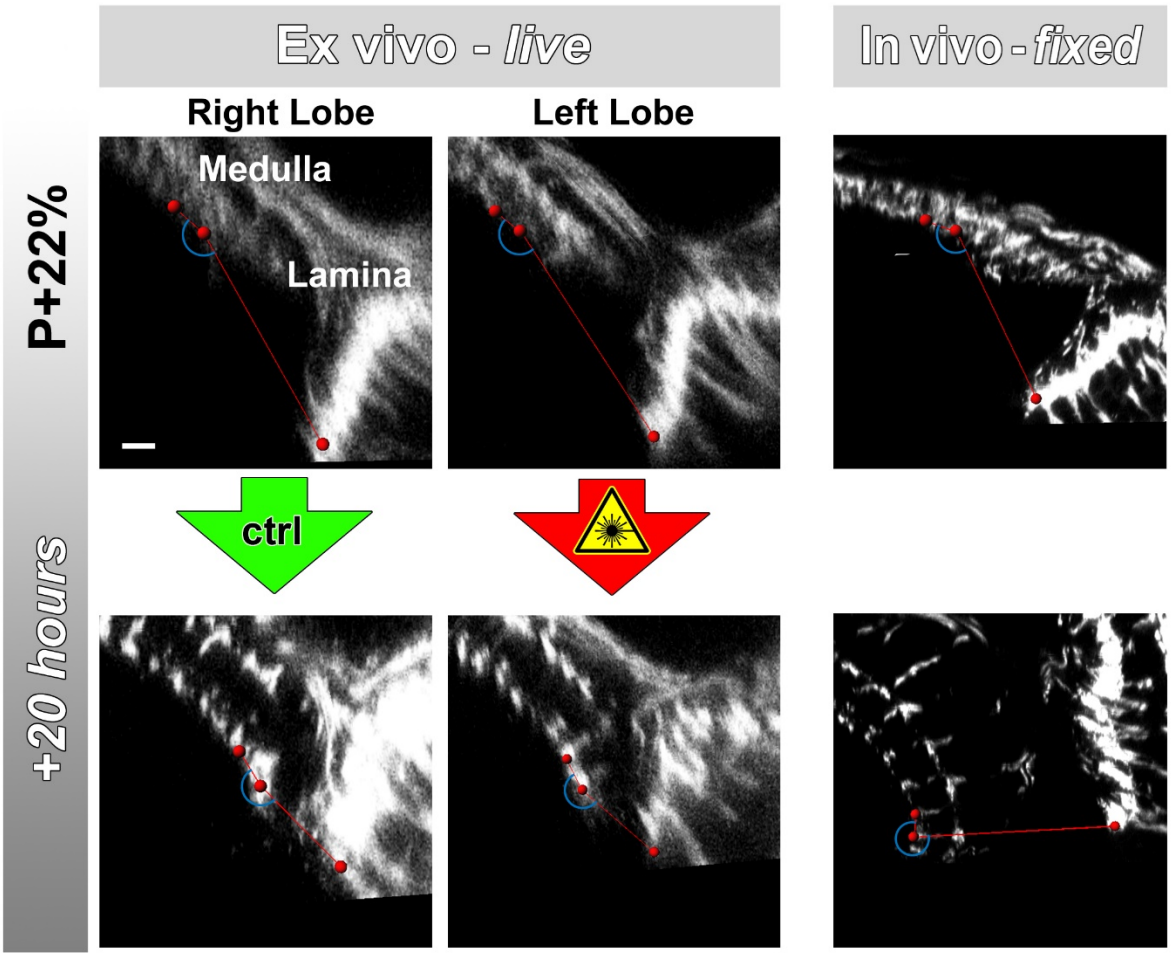

Figure 2-figure supplement 1: Lamina rotation is incomplete ex vivo. Two-photon imaging of the medulla was performed with brains cultured at P+22% for 20h, all photoreceptors express CD4-tdGFP. Continuously scanned *ex vivo* culture, unscanned control optic lobe and *in vivo* (fixed) control experiments were done as described in **Fig. 2**. The angles (blue arches) between the planes of posterior lamina and anterior medulla have been measured for the start and end points of each culture as well as the corresponding *in vivo* controls; and plotted in **Fig. 2c**. Scale bar, 10 μm.

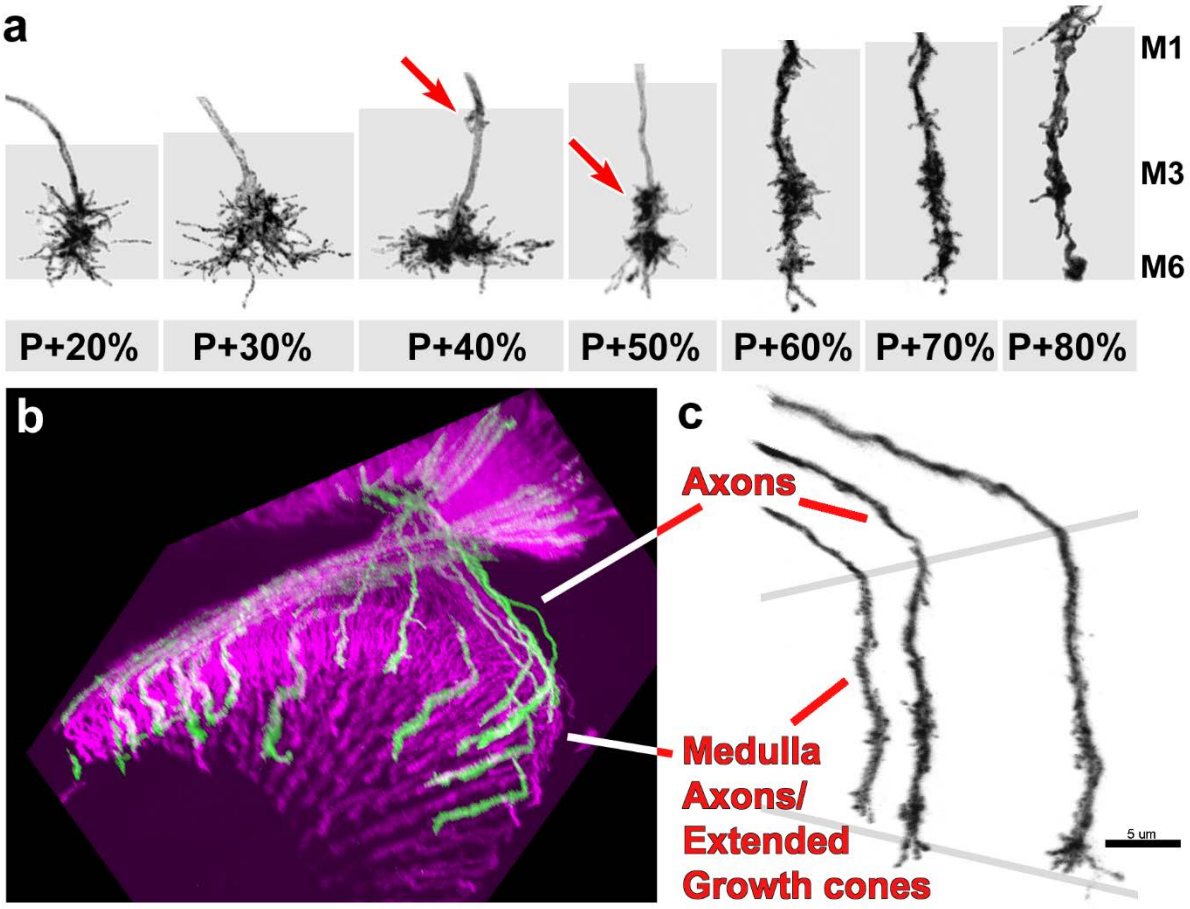

Figure 3-figure supplement 1: Filopodial dynamics are restricted to the growth cone and axon shaft inside the medulla neuropil. a, representative R7 terminal structures inside the medulla neuropil (grey background) reveal the transition of a more classical growth cone to a branched axonal structure. **b,** 3D visualization of individual R7 axons (green) on the background of all photoreceptors (magenta) at P+70%. c, analysis of R7 axons and extended growth cones/axon shafts in the medulla reveals that filopodia only occur within the medulla neuropil.

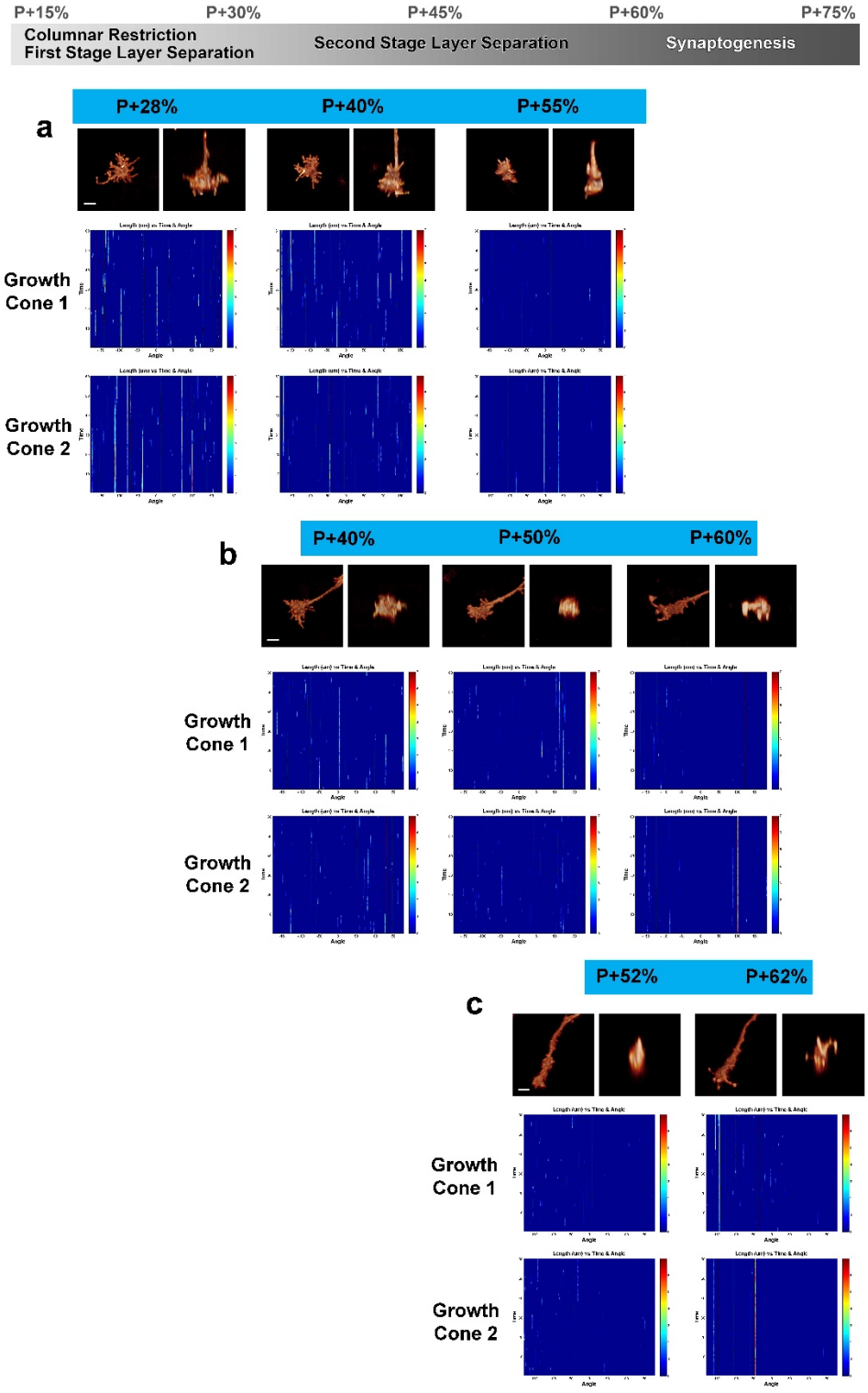
P+15%
P+30%
P+45%
P+60%
P+75%
Columnar Restriction
First Stage Layer Separation
Second Stage Layer Separation
Synaptogenesis
a
P+28%
P+40%
P+55%
Growth Cone 1
Growth Cone 2
b
P+40%
P+50%
P+60%
Growth Cone 1
Growth Cone 2
c
P+52%
P+62%
Growth Cone 1
Growth Cone 2

Figure 4-figure supplement 1: Fast filopodial dynamics throughout pupal development. Dynamics data from all 6 growth cones (2 independent growth cones for each time point) that were used in Figure 4.. The heat maps on blue background show individual filopodia as verticals lines. The filopodia were sorted by their initial orientation angle (x-axis). The length of the vertical lines represents the life time of the filopodia (time on the y-axis). The color map indicates the length (μm) for each filopodium through time. **a**, starting at P+28%, after 9h in culture and after 19h in culture. **b**, starting at P+40%, after 8h in culture and after 21h in culture. **c**, starting at P+52% and 8h in culture.. Scale bars, 3 μm.

Supplemental Figure 4

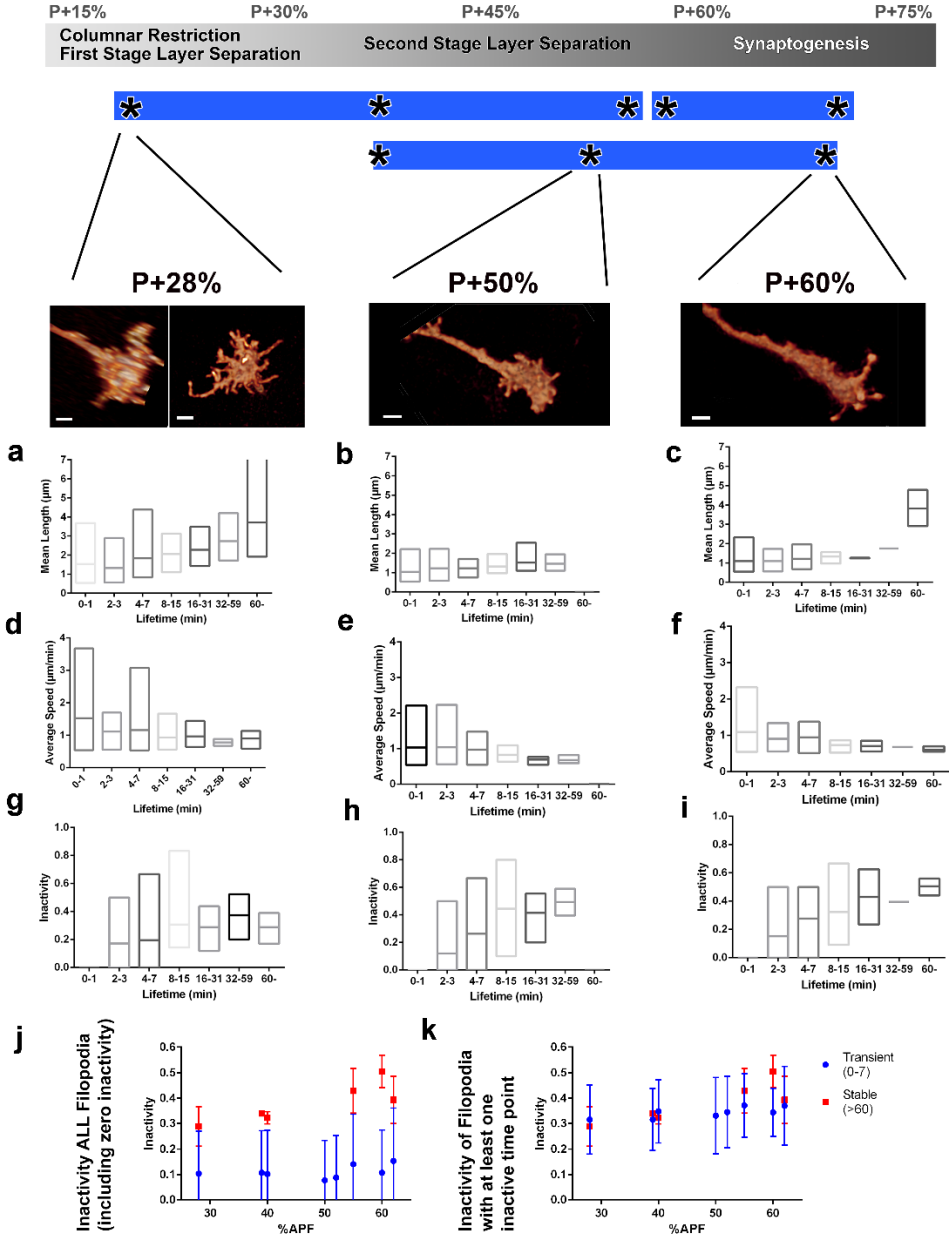

Figure 4-figure supplement 2: Filopodial dynamics as a function of lifetime. a-i, For the same growth cones depicted in Figure 4, every filopodia observed in a 1h period were binned into different lifetime classes: <1 min, 2-3 min, 4-7 min, 8-15 min, 16-31 min, 32-59 min or >60 min. Mean length (**a-c**), speed (**d-f**) and inactivity (**g-i**) were plotted for each group of the three growth cones. The boxes cover the entire range and horizontal lines show the mean. Scale bars, 2 μm. **j-k**, Mean inactivity (ratio of intervals with no significant extension or retraction) for transient (<8 min) and stable (>60 min) filopodia at all time-points. **j**, Inactivity: due to the high ratio of filopodia with 'zero' inactivity in transient filopodia (**g-i**), average inactivity appear much lower for transient filopodia. **k**, Inactivity of filopodia with at least one inactive time point: after the exclusion of 'zero inactivity' filopodia, inactivity of transient and early stage stable filopodia are identical. Error bars depict SD.

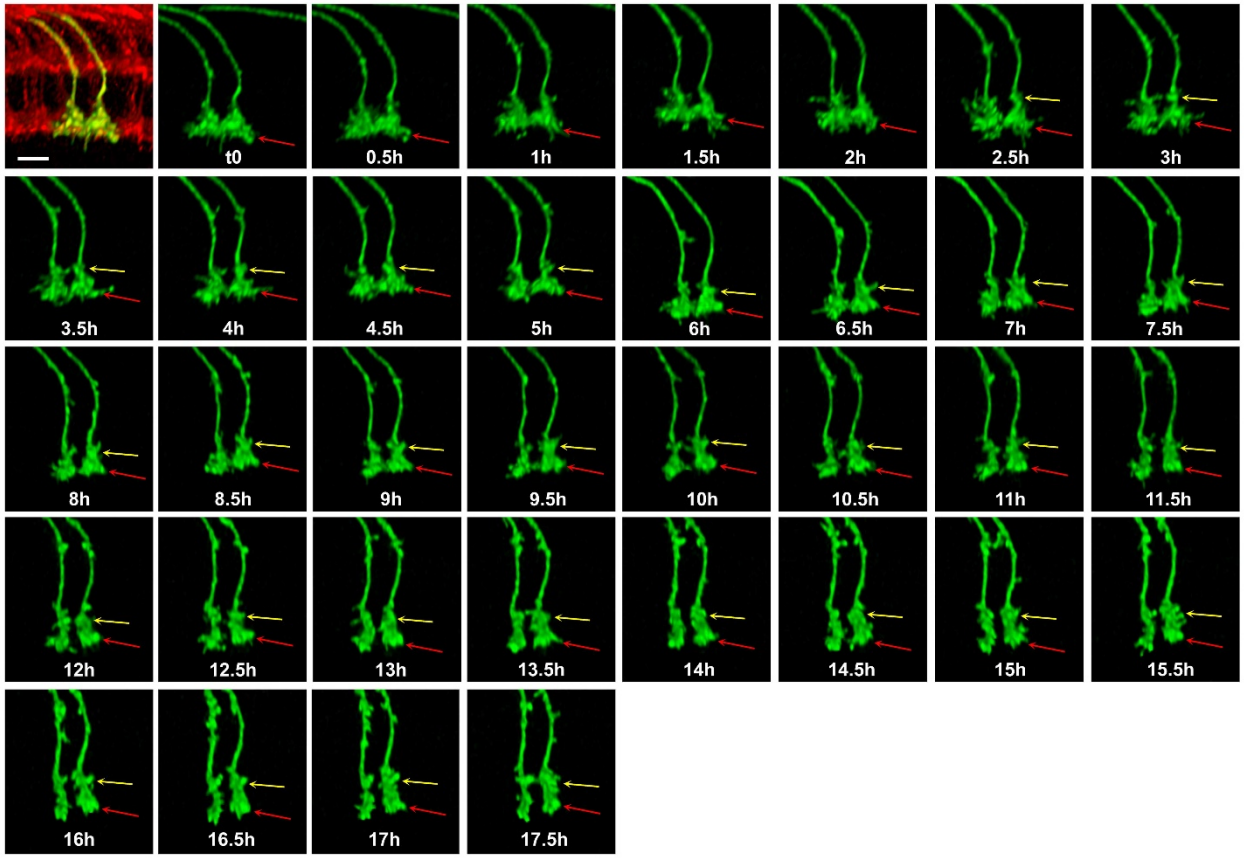

Figure 5-figure supplement 1: Single growth cone tracking demonstrates R7 terminals remain passive throughout layer formation without a stationary landmark. Live imaging starting at P+30%. All photoreceptors were labeled with myr-mRFP and R7 cells were sparsely labeled with CD4-tdGFP using GMR-FLP through MARCM. R7 terminal (red arrow) can be followed throughout 17.5h based on its specific filopodial morphology and dynamics. A new varicosity (yellow arrow) was formed from the axon shaft and expands over the course of 15h, pushing the terminal distally. No directed activity was observed at the growth cone tip throughout the imaging period. Scale bar, 5 μm.

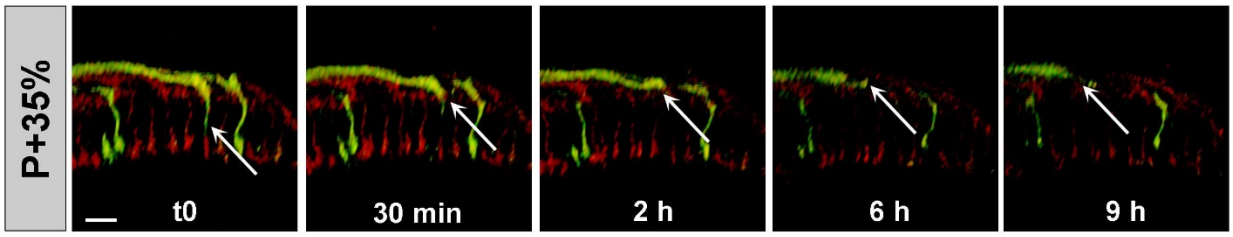

Figure 6-figure supplement 1: CadN mutant R7 axons may retract completely from the medulla. All photoreceptors were labeled with myr-mRFP. *CadN*^{405} R7 cells were generated with MARCM, using GMR-FLP and positively labeled with CD4-tdGFP. Live imaging starting at P+35% demonstrates an R7 axon which retracts from its target layer in the first 2h. During the remaining 7h, the axon retracts below the R8 temporary layer (upper red layer) and leaves the distal medulla completely. Scale bar, 4 μm.

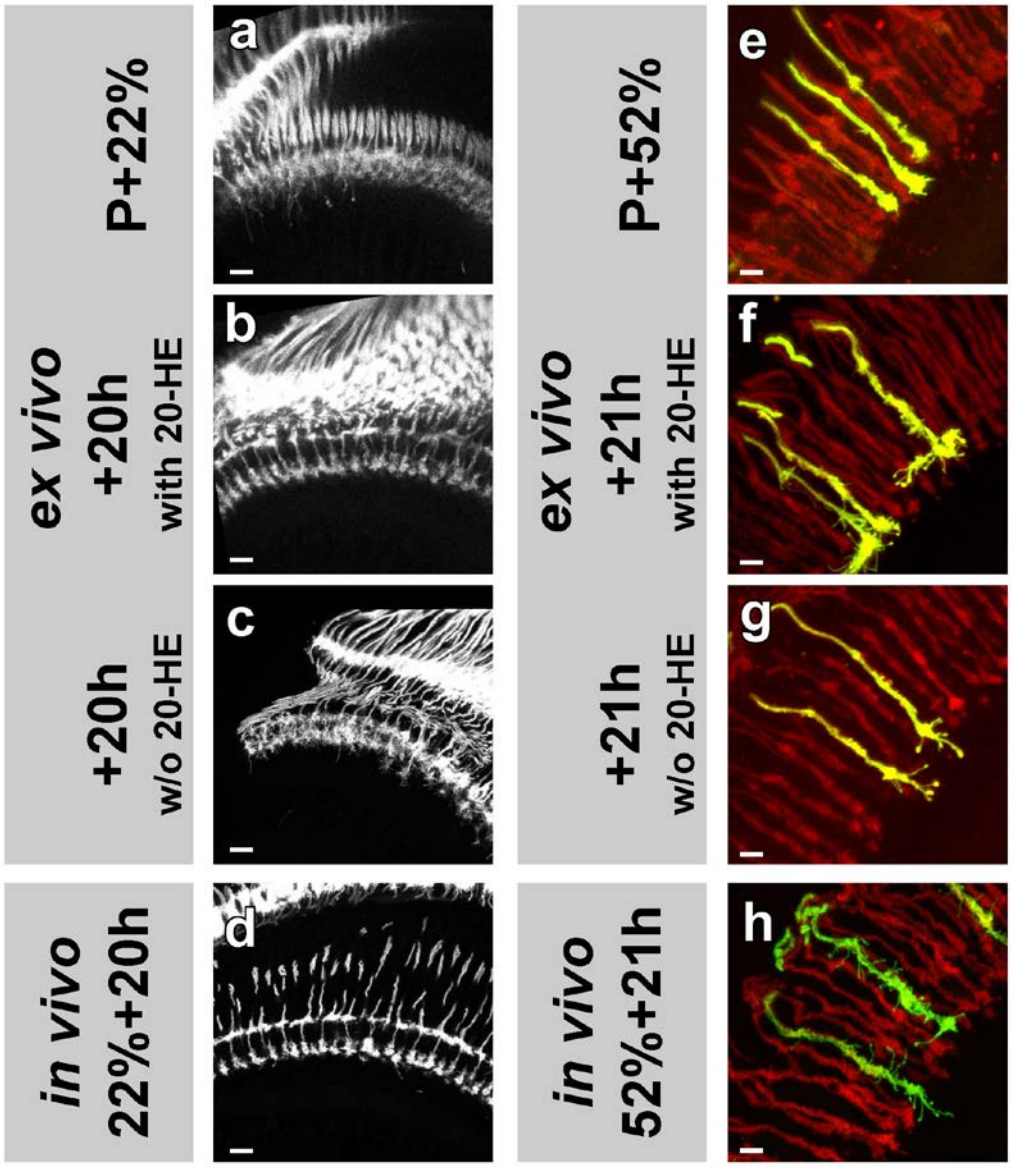
ex vivo
+20h
w/o 20-HE
ex vivo
+20h
with 20-HE
P+22%
in vivo
22%+20h
ex vivo
+21h
w/o 20-HE
ex vivo
+21h
with 20-HE
P+52%
in vivo
52%+21h
a
b
c
d
e
f
g
h

Methods-figure supplement 1: 20-Hydroxyecdysone is required for early but detrimental to late pupal development in the optic lobe. a-d, All photoreceptors were labeled with CD4-tdGFP. Cultures were set-up at P+22% (**a**), with (**b**) or without (**c**) 20-hydroxyecdysone (20-HE) in the culture media. Parallel developed pupae were dissected and imaged at the end of cultures as *in vivo* controls (**d**). R7-R8 layer separation in the medulla was impaired in cultures without 20-HE compared to *in vivo* controls or cultures with 20-HE. Scale bars, 10 μm. **e-h**, All photoreceptors were labeled with td-Tomato and R7 cells were sparsely labeled with CD4-tdGFP using GMR-FLP through MARCM. Cultures were set-up at P+22% (**e**), with (**f**) or without (**g**) 20-HE in the culture media. Parallel developed pupae were dissected and imaged at the end of cultures as *in vivo* controls (**h**). R7 axons that developed in the presence of 20-HE showed excessive filopodial formations on their terminals compared *in vivo* controls or the cultures without 20-HE. Scale bars, 4 μm.

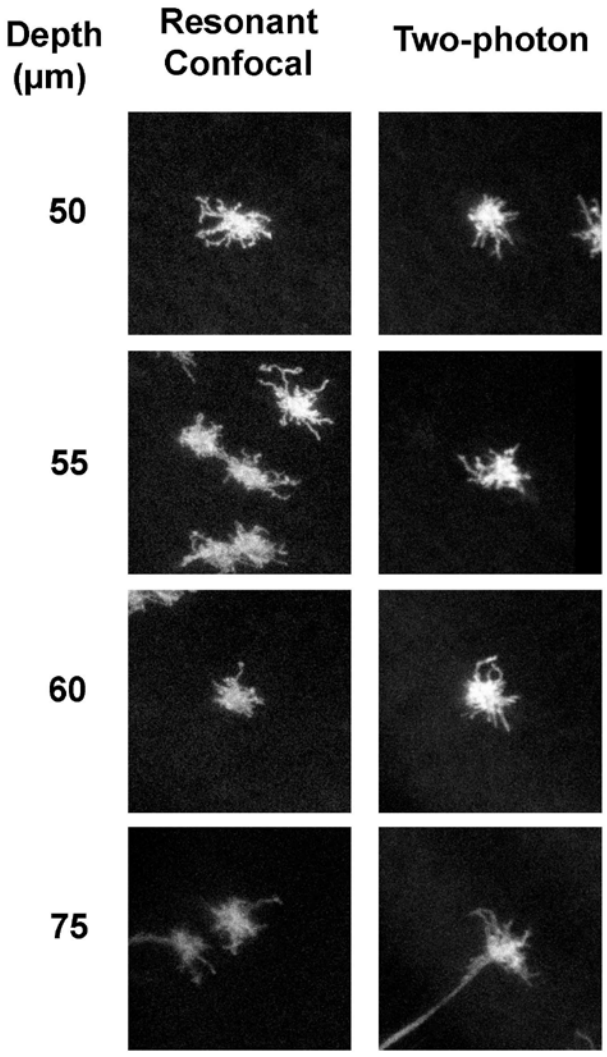

Methods-figure supplement 2: Image quality from live imaging with two-photon and confocal microscopes. R7 cells were sparsely labeled with CD4-tdGFP using GMR-FLP through MARCM. Individual R7 growth cones were imaged in the culture chamber at P+30%. Images were acquired with a Leica TCS SP5 confocal microscope with a resonant scanner or a Zeiss LSM 780 multiphoton microscope at various depths from the coverslip. Confocal signal reduces dramatically below 60 μm while the multiphoton signal holds.

2.7 Chapter Two Movies

All movies can be streamed from: https://doi.org/10.7554/eLife.10721.012

Movie 1: *Ex vivo* imaging of *Drosophila* brain development in culture. All photoreceptors are labeled with CD4-tdGFP. Two live imaging sessions (30min intervals) starting at P+24% (19h) and at P+40% (18h) are shown. Four developmental processes i) lamina rotation ii) lamina column expansion iii) first-stage separation of R7 and R8 terminals and iv) Final layer formation of R7 and R8 terminals, are shown.

Movie 2: Long-term ex vivo imaging of R7 photoreceptor growth cone filopodial dynamics. All photoreceptors are labeled with myr-tdTomato and R7 photoreceptors are sparsely labeled with CD4-tdGFP using GMR-FLP. Three live imaging sessions (30min intervals) starting at P+22% (21h), P+42% (19h) and P+55% (15h) are shown. The development of the filopodial structure of R7 growth cones are shown throughout layer and synapse formation.

Movie 3: *Ex vivo* imaging of fast filopodial dynamics-1. All photoreceptors are labeled with myr-mRFP and R7 photoreceptors are sparsely labeled with CD4-tdGFP using GMR-FLP. Live imaging started P+28% and continued for 20h. We used an alternating slow (30min intervals) imaging of the general structure and fast (1min interval) imaging of two growth cones at higher resolution at three different time points. Fast filopodial dynamics of the same two growth cones at P+28%, P+40% and P+55% are shown.

Movie 4: *Ex vivo* imaging of fast filopodial dynamics-2. All photoreceptors are labeled with myr-mRFP and R7 photoreceptors are sparsely labeled with CD4-tdGFP

using GMR-FLP. Two live imaging sessions starting at P+40% (22h) and P+52% (9h) are shown. We used an alternating slow (30min intervals) imaging of the general structure and fast (1min interval) imaging of two growth cones at higher resolution at different time points. Fast filopodial dynamics of the same two growth cones at P+40%, P+50% and P+60% and fast filopodial dynamics of another three growth cones at P+52% and P+62% are shown.

Movie 5: Second stage layer targeting of R7 and R8. Two live imaging experiments are shown. (1) All photoreceptors are labeled with myr-mRFP and R7 photoreceptors are sparsely labeled with CD4-tdGFP using GMR-FLP. Imaging started at P+30% and continued for 18h, with 30min intervals. Two R7 growth cone tips (red arrow) were followed. At the 2.5h mark a varicosity starts to develop from the axon shaft and expands over the next 15h, contributing to the elongation of the R7 axon. Note that being able to follow the same growth cone tip based on its unique filopodial structure allows us to verify lack of active extension without a stationary landmark. (2) R7 and R8 photoreceptors were sparsely labeled with CD4-tdGP using hs-FLP. Imaging started at P42% and continued for 21h. We used an alternating slow (30min intervals) imaging of the general structure and fast (1min interval) imaging of two neighboring R7 and R8 growth cones at higher resolution at different time points. R8 axon relocates to its final layer by sending a single filopodia proximally, which is initially very dynamic but later stabilizes and expands in the new layer, forming the new R8 terminal. In contrast, R7 terminal elongates along the axon shaft, but no directed extension activity is observed on the growth cone.

Movie 6: N-Cadherin functions in growth cone stabilization. All photoreceptors are labeled with myr-mRFP and approximately 10% of R7 photoreceptors were made mutant for *CadN* and labeled with CD4-tdGFP using GMR-FLP through MARCM. Three live imaging sessions are shown. (1) Starting at P+24% (17h). R7 axons arrive correctly to their target layer but they gradually retract from it, preceded by growth cone collapse. (2) Starting at P+53% (20h). Retractions continue despite the wild-type photoreceptors reached their final layer configurations. (3) Starting at P+42% (11h). Some of the R7 axons that retracted at the earlier stages re-extend back into the distal medulla. Note that the growth cones are streamlined during active movement but show expansion while the axons attempt to re-innervate various medulla layers.

Movie 7: Loss of N-Cadherin leads to reduced filopodial dynamics. Representative wild type and *cadN* mutant R7 growth cones are shown at P+28%. Extraction of individual filopodia reveals reduced dynamics over the same time period (1 hour with 1 minute time lapse) as shown in the quantifications in Figure 7.

CHAPTER THREE

Co-regulation of axon filopodial dynamics and synapse formation by presynaptic early active zone components

M. Neset Özel[1,2,3], Abhishek Kulkarni[1,2], Josephine Schallau[4], Vincent J. Dercksen[4], Isa Daumann[1,2], Heike Wolfenberg[1,2], Steffen Prohaska[4], P. Robin Hiesinger[1,2]

1: Division of Neurobiology, Institute for Biology, Freie Universität Berlin, 14195 Berlin, Germany.

2: NeuroCure Cluster of Excellence, Charite Universitätsmedizin Berlin, 10117 Berlin, Germany.

3: Neuroscience Graduate Program, UT Southwestern Medical Center, Dallas, TX 75390, USA.

4: Department of Visual Data Analysis, Zuse Institute Berlin, 14195 Berlin, Germany.

3.1 Abstract

Axonal growth cones in dense brain regions must transform structures with stochastic filopodial dynamics into synapse-specific contact sites. The synaptotropic model describes directional axonal and dendritic branch formation through stabilization and growth stimulation of random filopodial dynamics in regions with more synaptic partners. However, many mature axon terminals are unbranched and the relationship between filopodial dynamics, synaptogenesis and synaptotropic growth remains largely untested in dense brain regions. Here we show that early presynaptic active zone components stabilize axonal filopodia of R7 photoreceptor neurons in intact *Drosophila* brains. Using long-term and high resolution live imaging of developing *Drosophila* brains, we show that loss of the presynaptic assembly factors Liprin-α or Syd-1 does not affect axonal dynamics throughout pathfinding and correct layer targeting, but

destabilizes filopodia dynamics only at the time of synapse formation. The destabilization of filopodia leads to probabilistic destabilization and retraction of axons. In addition, loss of *syd-1*, but not *liprin-α*, causes filopodial overexploration due to increased filopodial extention and retraction speeds. This additional phenotype is independent of its RhoGAP domain, but shared with loss of the RhoGEF Trio and links presynaptic active zone assembly to cytoskeletal dynamics. In contrast to the transient and stabilizing role of early active zone assembly factors in filopodia, mature synapses marked by Brp only form after retraction of filopodia back to the axon trunk and remain stable once formed. We therefore hypothesize that stochastic filopodial dynamics serve a temporary role during the identification of postsynaptic partners in a dense brain region. Consequently, time-restricted inhibition of membrane dynamics reduces the number of synapses and leads to probabilistic destabilization and retraction of axons. Our findings support a model in which stochastic filopodia are captured during synaptic partner finding and stabilized through early active zone components that provide feedback to cytoskeletal dynamics.

3.2 Introduction

Synaptic connections are the fundamental units of information flow in all nervous systems and the study of their function and development is one the largest parts of modern neuroscience. One of the key challenges in the field is to understand the so-called synaptic specificity. Especially in complex nervous systems comprised of hundreds of different cell types populating the same vicinity, a particular cell must have the ability to reach, recognize and form synapses with a specific subset (Sanes and Yamagata, 2009; Yogev and Shen, 2014). Over three decades of research has identified strategies ranging from strict molecular matchmaking between synaptic partners (Hong et al., 2012) to developmental algorithms that ensure the vicinity of correct partners at the right place and time (Langen et al., 2015). Regardless of how a neuron identifies its correct synaptic partners, one basic requirement is to establish physical contacts, in sometimes extremely crowded neuropils, which eventually become synapses. This, perhaps, is the reason why neurons are the most structurally complex cells known to exist (Bullock et al., 2005), with dendritic and axonal compartments forming large and diverse arborizations.

The development of complex arborizations and their relation to synapse formation has been of great interest for over 30 years. One of the most influential ideas has been the synaptotropic hypothesis (Vaughn, 1989), which essentially states that growing neuronal branches or filopodia can be stabilized by nascent synapses, resulting in a directed growth towards potential synaptic partners. An interesting corollary is that neurons must initially employ a stochastic exploration program which eventually leads to a robust specificity towards correct partners. Live imaging experiments, particularly in

the zebrafish system, have indeed shown that deployment of synaptic machinery correlates with stabilization of dynamic filopodia into stable branches in both axons and dendrites (Meyer and Smith, 2006; Niell et al., 2004). However, a direct causal relationship between the two processes during development is yet to be demonstrated and any molecular mechanisms underlying such a relationship remain unknown.

We use *Drosophila* visual system as a model to study distinct steps of synaptic specification during pupal development. The fly eye consists of about 800 ommatidia each containing 8 different type of photoreceptor neurons. While types R1-6 are involved in motion vision and project their axons to the first neuropil, lamina, R7 and R8 cells are required for color vision and their axons terminate in specific layers of the second and largest neuropil, medulla (Bausenwein et al., 1992; Heisenberg and Buchner, 1977). The entire synapse specification program from axon guidance to synapse formation is completed in less than four days and is genetically hardwired (Hiesinger et al., 2006). We recently developed a system which allows fast and long-term live imaging of intact, developing *Drosophila* brains at the resolution of single filopodium and synapse. Using this, we have shown that R7 photoreceptor axons employ a combination of stochastic filopodial exploration and N-Cadherin based adhesion to remain stable at their target layer before the onset of synaptogenesis (Ozel et al., 2015).

In this study, we focus on the distinct filopodial program R7 axons employ during synapse formation to understand the relationship between axonal filopodial dynamics and presynaptic assembly machinery. We found that active zone (AZ) protein Bruchpilot (Brp) is not recruited to filopodia and the mature synapses only form on the axon trunk.

In contrast, earlier factors Liprin-α and Syd-1 can transiently localize to filopodia and are required for AZ assembly. Axons mutant for either gene display late-onset destabilization of filopodia, and eventually the entire axonal terminal. While defects in liprin-α mutant axons appear entirely secondary to AZ assembly function; Syd-1 has an additional role in suppressing cellular filopodial exploration program in later stages. Synapse associated RhoGEF Trio is important for this function independent of AZ formation. Inhibition of membrane dynamics during synaptogenesis results in reduced number of synaptic puncta as well as axonal destabilization. Our results provide a direct molecular link between two major cellular processes of developing neurons as well as a unified understanding of the functions of crucial factors, which were previously only independently studied in the context of synapse formation or growth cone morphology, based on filopodial dynamics.

3.3 Results

3.3.1 R7 axonal filopodia and synapse formation

Mature *Drosophila* R7 axon terminals do not exhibit any branches or other extensions beyond their target layer and column in the adult stage (**Fig. 1A**). However, we had previously described a distinct type of R7 filopodia which are morphologically and dynamically distinct and whose generation coincides with the onset of synaptogenesis (Ozel et al., 2015) (**Fig. 1A**). Given that during the second half of pupal development almost all axon guidance and layer-specific targeting are complete (Fischbach and Hiesinger, 2008), we hypothesized those filopodia which are initiated after P+50% but eliminated before eclosion are involved in synapse formation. To study synapses in conjunction with growth cone dynamics in live settings, we utilized GFP or mKate2 tagged constructs of BrpD3 (or Brp^{short}). This fragment has been shown to localize specifically to sites of intrinsic Brp without affecting synapse function or causing overexpression artefacts seen with other genetically encoded synaptic markers including full-length Brp-GFP (Schmid et al., 2008).

First, we characterized the formation of synaptic puncta through pupal development in fixed preparations (**Fig. 1B**). R7 terminals have virtually no Brp-marked synapses at P+40% and majority of synaptic puncta form between P+50-70% (**Fig. 1C**). This timeline and the number of puncta we observed are consistent with other synaptic marking techniques such as STaR (Chen et al., 2014). Next, we imaged live dynamics of synaptic puncta at 10 min resolution around P+70% (**Movie 1**). We observed that Brp puncta are never localized to filopodia and form by gradual accumulation on the axon

trunk. Furthermore, tracking individual puncta for over 5 hours revealed that vast majority of synapses are stable once formed (**Fig. 1D**). Those with shorter lifetimes most likely reflect difficulty tracking smaller puncta with weak signal in a crowded situation rather than genuinely transient synapses.

3.3.2 Early active zone assembly components may function in filopodia

Previous studies in neuromuscular junction (NMJ) showed that Brp is recruited late to nascent synapses and represent a point of no return for active zone assembly (Owald et al., 2010), while assembly factors including Syd-1 and Liprins act earlier (Owald et al., 2012). Since BrpD3 only marks fully matured and highly stable synapses on the axon trunk, we asked whether earlier steps in synapse formation may occur in filopodial extensions. We hypothesized that filopodia may function in establishing the initial contacts and certain earlier events (e.g. reversal complex) may take place there. These contacts could then be brought back to the main body where the final maturation takes place.

We therefore investigated proteins that are recruited earlier to presynaptic sites. Syd-1 and Liprin-α (Syd-2) have been well studied in the context of active zone development and have been shown to play a role in synapse formation in all systems studied (Dai et al., 2006; Hallam et al., 2002; Owald et al., 2010; Wentzel et al., 2013). We found that unlike Brp, GFP-tagged constructs of Liprin-α and Syd-1 can localize onto filopodia (**Fig. 2A-B**). It was not possible to reliably track individual puncta due to

density of labeling but we observed in the case of Liprinα-GFP that filopodial puncta are generally transient (**Movie 2**).

Finally, even though the roles of Liprin-α and Syd-1 during synapse formation in NMJ and other systems are well-established, they have not been shown in *Drosophila* photoreceptors so far. We checked BrpD3 marked synapses in *liprin-α*^{E} (Choe et al., 2006) and *syd-1*^{w46} (Holbrook et al., 2012) mutants. As both alleles are lethal, we generated MARCM clones (Lee and Luo, 1999) of sparsely labeled R7 cells in an otherwise heterozygous background, allowing us to assess cell-autonomous effects. There was a dramatic reduction in the number of synaptic puncta for both mutants (**Fig. 2C-D, F-G**). Even though *liprin-α* axons appeared to maintain about 40% of puncta based on fixed counts; live imaging has revealed that, unlike wild-type, those puncta were mostly unstable or mobile (**Movie 3, Fig. 2I**), most likely representing vesicular accumulations in the absence of proper active zones. On the other hand, loss of Trio (a synapse-associated RhoGEF) in *trio*^{3} (Newsome et al., 2000) MARCM clones had synaptic puncta indistinguishable from the controls (**Fig. 2E,H**).

3.3.3 Active zone assembly defects lead to late-stage loss of growth cone stability

In addition to their well-established roles in presynaptic assembly, Liprin-α and Syd-1 have previously been implicated in terminal morphology and layer-specific targeting of R7 axons. In the absence of Liprin-α, R7 axons terminate in M3 layer instead of M6 (Choe et al., 2006; Hofmeyer et al., 2006); this was interpreted as a function in target layer recognition (Astigarraga et al., 2010) whereby mutants either fail

to reach the target layer, or retract back to the R7 temporary layer. However, we have recently shown that R7 axons do not employ a temporary layer and target directly to their final location (Ozel et al., 2015), making the late-stage destabilization in target layer far more likely. Similarly, R7 axons lacking *syd-1* also have 'premature stops' in M3 but also what appear to be overextensions beyond the M6 layer (Holbrook et al., 2012); these defects also start to manifest only after P+40%. Given their known roles in synapse formation and the late onset of mutant phenotypes, it was hypothesized by the respective groups that these defects could be associated with presynaptic assembly function. Nevertheless, it remains unclear how the axonal phenotypes develop with respect to growth cone dynamics and a direct link to synaptic functions is yet to be established.

Consistent with previous reports, terminals of R7 *liprin-α*^{E} and *syd-1*^{w46} clones are in their correct target layer at P+40% (i.e. before the onset of synapse formation) and appear morphologically normal (**Fig. 3A-B**). Live imaging has revealed that *liprin-α* axons gradually lose their stability at the target layer starting around P+45% (**Fig. 4F**, **Movie 4**) retracting to M3, and continue to do so throughout the late pupal development; retraction rate reaching to around 50% at P+70% (**Fig. 4D**). Once retracted, *liprin-α* mutants cannot fully extend back to M6. Similarly, *syd-1* R7s also retract from their layer after P+40% (**Fig. 4B,G**). The defects start slightly earlier than *liprin-α*, and a few that retract before P+45% may do so all the way up to M0; however these quickly re-extend back to M3 after P+45%. Unlike *liprin-α*, retracted *syd-1* axons remain fully capable of re-extension back to M6 and even beyond (**Fig. 4G**, **Movie 5**). This behavior compensates for the retraction of *syd-1* axons and results in a much lower rate of

retracted axons when measured from fixed preparations (**Fig. 4D**); even though synaptic defects in *syd-1* mutants are at least as severe as *liprin-α*. Enhanced dynamics of *syd-1* mutant axons are not limited to those that have retracted. R7 axons that remain in M6 also display 'overexploration', forming frequent and long (but transient) processes towards all directions, including beyond M6 (**Fig. 4B,G**) thus presumably underlying the "overextension" defects reported previously. Finally, we compared the number of synaptic puncta in terminals that still remain in M6 at P+70% to the overall mutant population and found no difference (data not shown), confirming that synaptic defects are primary and not due to loss of contact with postsynaptic partners upon retraction.

Loss of *trio* in R7 axons has previously reported to result in very similar defects to *syd-1*, including about 13% of axons having retracted to M3 in adults; leading to the hypothesis that Trio might mediate almost all effects of Syd-1 as a downstream target (Holbrook et al., 2012). However, we did not observe any R7 axons in M3 (or any layer other than M6) at P+70% or P+90% in $trio^{3}$ mutant clones (**Fig. 4C-D**) and live imaging revealed no retractions during development (**Fig. 4H**). This is consistent with *trio* mutants' lack of a synaptic defect as reported above and further supports that retractions observed in $liprin\text{-}\alpha^{E}$ and $syd\text{-}1^{w46}$ axons are secondary to a failure in forming mature synapses. On the other hand, we do observe an overexploration phenotype similar to *syd-1* (albeit milder) and consequent 'overextensions' at P+90% (**Fig. 4C-D**). These suggest that Trio might function in modulating the secondary function of Syd-1 in suppressing growth cone exploration during (but independent from) synapse formation.

Why do retracted R7 axons stop at the M3 layer? This has been repeatedly observed in all mutants that disrupt R7 layer specificity, including N-Cadherin (Lee et

al., 2001; Ting et al., 2005), DLar (Clandinin et al., 2001) and those discussed here; fueling the previous interpretations that M3 functions as a temporary layer for R7s and these proteins are required for this 'second step' of layer targeting. An interesting insight we gained by live imaging previously *CadN* mutants (Ozel et al., 2015) and now *syd-1* is that destabilized R7 axons can retract back to M0 before R8 axons relocate to M3 around P+45% (Akin and Zipursky, 2016; Ting et al., 2005). After this, retracted R7 axons re-extend to M3 and all the subsequent retractions are only up to M3, suggesting that R8 axons might directly provide a secondary attachment to destabilized R7 axons. We tested this by using a GMR-Gogo construct, which forces R8 terminals to M0 layer but does not normally affect R7s (Kulkarni et al., 2016; Tomasi et al., 2008). We observed that *liprin-α*^{E} R7 clones in the background of GMR-Gogo can indeed retract back to M0 and remain there (**Suppl. Fig. 1**), providing a definitive explanation for this long elusive phenomenon.

3.3.4 Synapse formation regulates fast filopodial dynamics

We next sought to understand the changes in fast filopodial dynamics in these mutant axons which could potentially underlie the defects in terminal stabilization. We previously characterized fast filopodial dynamics of wild-type R7 axons at various stages of pupal development (Ozel et al., 2015). These were analyzed with fully manual tracing and tracking of hundreds of individual filopodia. Due to much higher volume of data in this study, we developed a semi-automatic 4D filopodia tracing and tracking toolbox based on Amira filament module. This new tool utilizes a similarity based sequential propagation algorithm, reducing the need to re-trace the same filopodia in

multiple timesteps; as well as built-in automatic tracking of filopodia identity based on the vicinity of their starting points.

Using this tool, we tracked individual filopodia on wild-type and mutant R7 axons, in datasets that were acquired with 1 minute resolution for 1 hour sessions. We performed the analysis in two different developmental stages (before and during synapse formation): immediately at the beginning of culture at P+40% and after 20-22h in culture (approximately P+60%) of the same axons. We considered any changes in filopodial length less than 0.1 μm between two timesteps as technical noise, therefore considered it 'inactive' for those timepoints. We then calculated the rate of inactivity, average length and extension/retraction speeds for each filopodium. We grouped the observed filopodia based on their lifetimes: very transient (<8 mins), transient (8-30 mins) and stable (>30 min).

As we had previously reported, the vast majority of filopodia are very transient (**Fig. 4A, E**). As predicted from their normal morphology, at P+40% we did not observe any significant changes in filopodial dynamics between *liprin-α*^{E} axons and wild-type controls (*syd-1* data is pending) based on any of our parameters (**Fig. A-D**). In contrast, at P+60% both mutants had reduced numbers of very transient filopodia and more importantly reduced rates of inactivity (i.e. stability) of stable filopodia (**Fig. 4F, Movies 6-7**). In addition *syd-1*, but not *liprin-α*, mutant axons had filopodia with significantly increased extension/retraction speeds as well as average lengths, particularly of the filopodia with longer lifetimes (**Fig. 4G-H**).

These changes in fast filopodial dynamics mirror the changes in slow dynamics reported for each mutant above and reveal the underlying cellular defects. Both *syd-1*

and *liprin-α* axons have a deficiency in stabilizing their filopodia, presumably due to a failure in forming proper early synaptic contacts on these structures which may then lead to the retractions observed in both mutants. Additionally, syd-1 mutants have a specific defect with enhanced extension/retraction speeds that result in significantly longer filopodia. These defects appear to underlie the overexploration phenotype observed in slow dynamics and result in 'overextensions' seen in fixed preparations. These data further support the notion that in addition to its shared role with Liprin-α in synapse formation (which is required for stabilization of the filopodia and eventually the entire terminal), Syd-1 has a secondary role in suppressing filopodial cytoskeletal machinery to prevent exuberant filopodial exploration.

3.3.5 Syd-1 RhoGAP function is dispensable for all presynaptic activity

Syd-1 is a putative RhoGAP protein with fully conserved catalytic residues from *C. elegans* to mammals (Wentzel et al., 2013). However, whether it actually functions as a RhoGAP *in vivo*, or the potential importance of that function remained controversial. Mammalian SYD1A GAP domain has been shown to have activity towards RhoA, but both mSYD1a and *C. elegans* Syd-1 GAP domains were at least partially dispensable for most functions (Hallam et al., 2002; Wentzel et al., 2013). Given our finding that Syd-1 has two apparently independent cellular functions, we aimed to test whether the two functions could be structurally dissected; particularly considering that Rho proteins can directly regulate the cytoskeleton and thus, filopodial dynamics.

We created a deletion in *syd-1* locus that eliminated the putative RhoGAP domain completely and specifically, leaving rest of the coding sequence intact on both sides using CRISPR/Cas9 system. The resulting allele *syd-1*$^{\Delta RhoGAP}$ was homozygous viable (unlike any *syd-1* null alleles). Within sparsely generated clones, *syd-1*$^{\Delta RhoGAP}$ R7 axons appeared completely normal (**Suppl. Fig. 2**), suggesting that RhoGAP activity is not required for either presynaptic function of Syd-1. Only partial rescues found in other studies may be attributed to either the overexpression of transgenic fragments (Wentzel et al., 2013) or point mutations (Hallam et al., 2002) rather than deletion of the entire domain of the intrinsic protein. Indeed, when we attempted to rescue *syd-1*^{w46} mutant R7s with overexpression of a transgenic fragment lacking the RhoGAP domain (S. Sigrist), we only saw a partial amelioration (data not shown).

3.3.6 R7 axonal filopodia are important for synapse formation

Our findings in this study provided detailed insight into how synapse formation regulates filopodial and growth cone dynamics. But is the opposite true, i.e. is filopodial exploration required for normal synapse formation on R7 axons?

In order to manipulate filopodial dynamics during synapse formation, we co-expressed Shibire^{ts} with our membrane and synaptic markers in sparsely generated R7 clones. Shi^{ts} is a dominant negative version of *Drosophila* Dynamin and induces rapid and reversible block of most membrane dynamics in restrictive temperatures, while behaving wild-type at 25°C (Gonzalez-Bellido et al., 2009). This allowed us specifically test the requirement of filopodial dynamics during synapse formation by rearing the

pupae at 25°C until P+45%, then shifting them to 31°C for 21h and assessing the terminal morphology and number of synapses right after. We found that Shi^{ts} leads to a clear reduction of R7 axonal processes (**Fig. 5A**) as well as an approximately 40% decrease in the number of synaptic puncta (**Fig. 5C**) compared to controls. There was no difference between Shi^{ts} and control axons at P+70% when reared at 25°C the entire time (**Fig. 5B-C**). As the majority of presynaptic sites can still form, it is unlikely that Shibire block has a direct effect on AZ formation. Further, our results suggest that filopodial exploration may not be absolutely required for formation of synapses, but greatly increases its efficiency.

Interestingly, we saw a few Shi^{ts} axons (less than 10%) having completely retracted to M3 layer after 21h in restrictive temperature (**Fig. 5D**), suggesting a requirement of synapse formation in axon terminal stabilization but this could also originate from a loss of general adhesion based stabilization which also relies on filopodial exploration (Ozel et al., 2015). More prevalent then full retractions, we often observed R7 axons whose terminal structure were mostly collapsed in M6, but still maintained a thin process with a Brp puncta at its tip (**Fig. 5E**). This is reminiscent of observations in support of synaptotropic hypothesis in other systems where a destabilized branch would only retract back till the next synaptic structure (Niell et al., 2004).

3.4 Discussion

The idea that dynamic growth of axonal and dendritic extensions and the process of synapse formation might be interlinked is a very old one (Berry and Bradley, 1976; Vaughn et al., 1974). And it was formulated and tested in the context of synaptotropic hypothesis, where synapse formation leads to directed growth of axonal and dendritic arbors towards correct synaptic partners by selective stabilization of branches (Meyer and Smith, 2006; Niell et al., 2004). From this point of view, *Drosophila* photoreceptors (one of the few neuronal types known in the brain whose adult terminals have no branches) might appear as a counterintuitive model system to study these mechanisms. Indeed, this specific morphological feature makes functional and evolutionary sense. Retinotopy is a common feature of all visual systems which allows the spatial information acquired in the eye to be reflected in the brain (Roskies et al., 1995; Sanes and Zipursky, 2010). Even though retinotopy gradually degrades in higher processing centers, keeping the individual ‘pixel’s separate at the first synaptic level is likely to be advantageous. This would not have been possible if photoreceptor axons formed branches that invaded neighboring columns. Nevertheless, they do employ prevalent filopodial exploration during development; and here we show that this is important for proper connectivity. Just as branching neurons, these are probably used to increase the contact area to find correct synaptic partners; but as the filopodial growth is suppressed in late pupal stages, these contacts must then be brought back to the main body of the axon where mature synapses are located. This appears to be a specific modification to the synaptotropic model (in circumstances where having stabilized branches may be disadvantageous), which we dub: *synaptic capture*.

The exact mechanisms that synapses might regulate filopodia/branch dynamics have remained elusive and virtually no molecular factors have been defined. A number of studies indicated that neurotransmission itself might control part of the process (Rajan et al., 1999; Ruthazer et al., 2006), but *Drosophila* visual system can develop normally in the absence of synaptic activity (Hiesinger et al., 2006) making it unlikely in our model. More importantly, R7 axons present a unique condition where functional synapses are not even localized to filopodia but are exclusively in the main body; and only the earlier factors in active zone formation function in filopodia. Indeed, our live analysis revealed very specific and distinct modulation of filopodial dynamics by those factors.

Our findings represent the first causal requirement of synapse formation machinery (independent of activity) in filopodial or growth cone dynamics beyond correlative studies. We show that formation of early synaptic complexes restricts the dynamics of filopodia, as revealed by reduced inactivity with the loss of *syd-1* or *liprin-α*. This could be achieved by signaling to cytoskeletal regulators from these complexes, or simply by physical restriction by virtue of being attached to another cell. Eventually, forming proper active zones is required for stabilization of not only the filopodia, but the entire axonal terminal. Before the onset of synapse formation, R7 axons are stabilized in their target layer with N-Cadherin based adhesion; however, the wide filopodial arbor that presumably functions as the substrate of this synapse-independent adhesion is largely pruned by P+50% (Ozel et al., 2015). This suggests that synaptic adhesions take over the function of terminal stabilization to preserve layer specificity in later stages.

In addition to its shared role with Liprin-α, we found that Syd-1 has a secondary function, namely the suppression of exuberant filopodial exploration; revealed by increased extension/retraction speeds, and as a result, longer filopodia in its absence. A similar defect was observed in *trio* mutants, which have normal presynaptic puncta, suggesting the existence of a discrete molecular pathway (**Fig. 6**). Previous studies in NMJ have reported that Syd-1 is recruited first to nascent synapses and subsequent deployment of Liprin-α is dependent on that (while vice versa is not true) (Owald et al., 2010). This is consistent with our model such that even in the absence of Liprin-α, Syd-1 can still localize to presumptive synaptic contacts; and even though these contacts will fail to mature, Syd-1 would still be able to suppress filopodial exploration in *liprin-α* mutants.

Surprisingly, RhoGAP domain of Syd-1 was not necessary for any of its presynaptic functions in R7 axons. Mammalian homolog of Syd-1 has been shown to have GAP activity on RhoA but functional or developmental significance of this activity remained less clear (Wentzel et al., 2013). Further, it has been suggested that structural variations in the invertebrate protein might make render it less active. It would thus be of interest to investigate the effects of specific RhoGAP deletion of the intrinsic protein in other systems. Nevertheless, Syd-1 (with or without RhoGAP function) is able to regulate two distinct processes in axonal terminals. Further research into downstream effectors could shed a light onto exact mechanisms.

Despite being uncoupled from active zone maturation *per se*, embodiment of the two functions in a single synaptic protein hints at a novel regulatory mechanism. In a wild-type condition, Syd-1 can act as a coordinator between synaptic partner finding and

filopodial exploration. It can drive the axon to increase filopodial exploration to find more partners if the synapse number is insufficient. Conversely, it can contribute to the full suppression of filopodial exploration before eclosion when synaptic connections have saturated. The finding that these long filopodial extensions persist in *syd-1* and *trio* mutants at P+90% and beyond, when wild-type axons are largely flat, is in support of this model. It would be of great interest to investigate the differential effects of *syd-1* and *liprin-α* mutants in other neurons, particularly those with extensive axonal branches and develop according to conventional synaptotropic models. The straightforward prediction is that while loss of *liprin-α* should lead to reduced arbor sizes due to loss branch stabilization, *syd-1* mutants might have expanded arbors despite the loss of synapses because of disinhibited filopodial exploration.

3.5 Materials and Methods

3.5.1 Genetics

All experiments were performed with Drosophila pupae collected at P+0% (white pupae) and aged in 25°C unless otherwise specified. The genotypes of all stocks used are listed below.

GMR-FLP; GMR-Gal4; FRT80B, UAS-CD4-tdGFP

; GMR-myr-tdTomato; FRT80B, tub-Gal80 / Tm6B

GMR-FLP; FRT42D, GMR-Gal80; GMR-Gal4, UAS-CD4-tdTomato

; FRT42D; UAS-BrpD3-GFP

; FRT42D; UAS-BrpD3-GFP, UAS-Shi^{ts}

GMR-FLP; GMR-Gal4; FRT80B, UAS-CD4-tdTomato

; UAS-Liprinα-GFP; FRT80B, tub-Gal80/ Tm3

; UAS-GFP-Syd1; FRT80B, tub-Gal80/ Tm3

GMR-FLP; FRT40A, tub-Gal80; GMR-Gal4, UAS-CD4-tdTomato

; FRT40A; UAS-BrpD3-GFP

; FRT40A, *liprin-α*^{E}/ CyO-GFP; UAS-BrpD3-GFP

GMR-FLP; GMR-Gal4, UAS-CD4-tdGFP; FRT82B, tub-Gal80

; UAS-BrpD3-mKate2; FRT82B

; UAS-BrpD3-mKate2; FRT82B, *syd-1*^{w46}/ Tm6B

; GMR-myr-tdTomato; FRT82B, *syd-1*^{w46}/ Tm6B

; Sp/CyO; FRT82B, *syd-1*^{dRhoGAP}

GMR-FLP; GMR-Gal4, UAS-CD4-tdGFP; FRT2A, tub-Gal80

; UAS-BrpD3-mKate2; FRT2A

; UAS-BrpD3-mKate2; FRT2A, *trio*^{3}/ Tm6B

; GMR-myr-tdTomato; FRT2A, *trio*^{3}/ Tm6B

GMR-FLP; FRT40A, tub-Gal80; GMR-Gal4, UAS-CD4-tdGFP, GMR-myr-tdTomato

; FRT40A, *liprin-α*^{E}/ CyO::Tm6B ;

3.5.2 Syd1 RhoGAP deletion

syd-1^{dRhoGAP} allele was generated using CRISPR/Cas9 technology by Well Genetics (Taiwan) and verified by genomic PCR and sequencing. Full design details are available in Supplementary Experimental Procedures accessible from:

https://www.dropbox.com/sh/fzrfy553s37po62/AAArJ-zXgw9B_pPAKsL-NJsJa?dl=0

3.5.3 Histology and Fixed Imaging

Eye-brain complexes were dissected in PBS, fixed in 3.7% paraformaldehyde (PFA) in PBS for 40 minutes, washed in PBST (0.4% Triton-X) and mounted in Vectashield (Vector Laboratories, CA). Images were collected using a Leica TCS SP8-X white light laser confocal microscope with a 63X glycerol objective (NA=1.3).

3.5.4 Brain Culture and Live Imaging

Ex vivo eye-brain complexes were prepared as described before (Ozel et al., 2015). For filopodial imaging, brains were dissected at P+40% and 1 µg/ml 20-Hydroxyecdysone was included in the culture media. For synaptic imaging, brains were dissected at P+50% and no ecdysone was included.

Live imaging was performed using a Leica SP8 MP microscope with a 40X IRAPO water objective (NA=1.1) with a Chameleon Ti:Sapphire laser and Optical Parametric Oscillator (Coherent). We used a single excitation laser at 950 nm for two-color GFP/Tomato imaging. For GFP/mKate2 imaging lasers were set to 890 nm (pump) and 1150 nm (OPO).

3.5.5 Data Analysis

Imaging data were analyzed and presented with Imaris (Bitplane). All live imaging data as well as all data involving synaptic markers were deconvolved (10 iterations) using Microvolution Fiji Extension.

Filopodial dynamics were analyzed with a custom new ‘Filopodia’ toolbox based on the Filament module of Amira ZIB Edition. The toolbox provides a full workflow from segmentation of growth cones, tracking and tracing of the filopodia as well as calculation of dynamics parameters for individually tracked filopodia. Further details on the development and functionality of this module is available in Supplementary Materials and Methods.

Further analysis regarding the quantified data and generation of corresponding graphs were done using Prism 7 (GraphPad). Where needed statistical differences were calculated with unpaired, parametric t-tests.

3.6 Chapter Three Figures

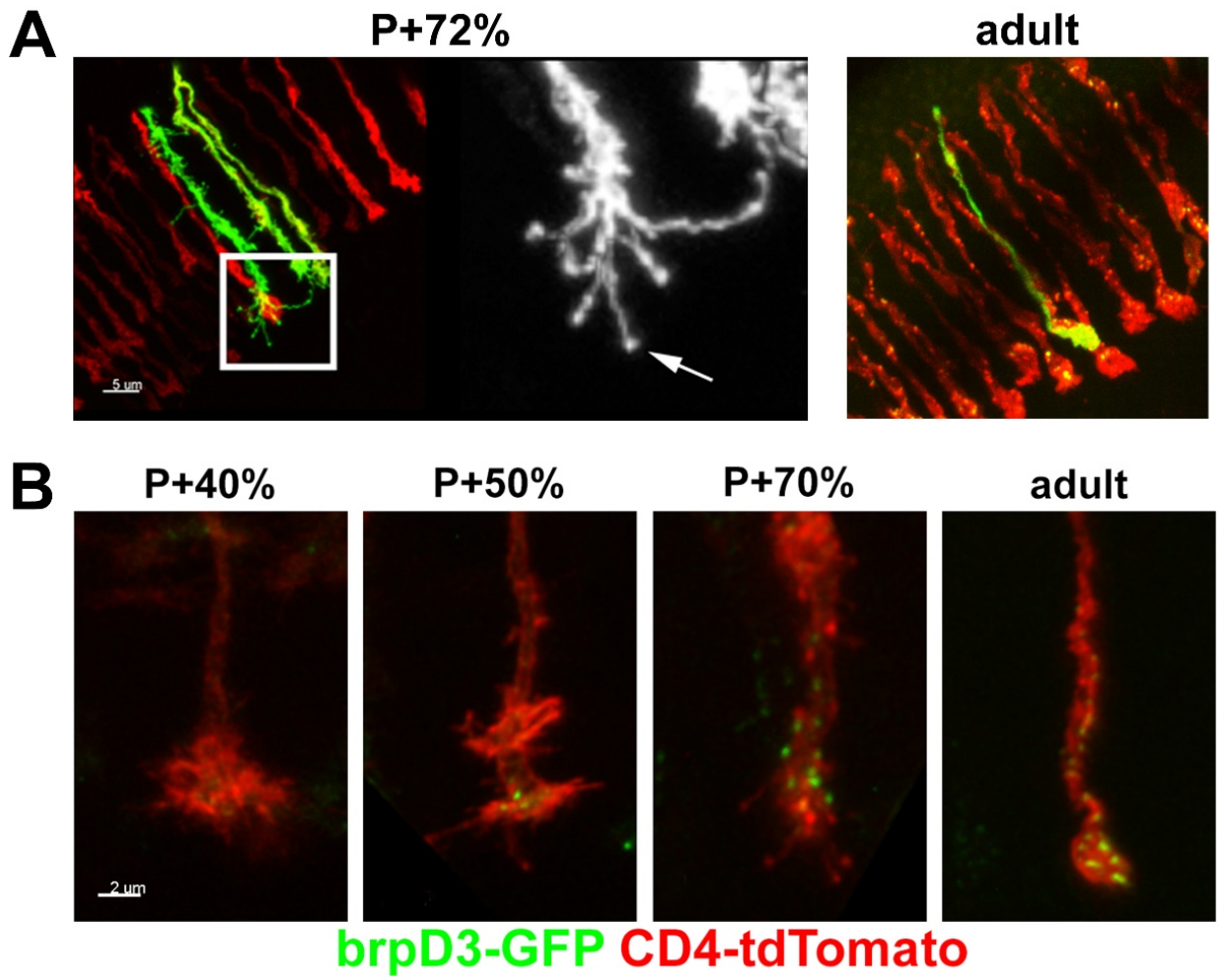

Figure 1: Synapse formation on R7 axonal terminals. A) Sparsely labeled R7 axons labeled with CD4-tdGFP and all photoreceptor terminals are labeled with myr-tdTomato at P+72% and adult stages. Inset shows bulbous filopodia that form in the second half of pupal development, while the adult terminals are devoid of any extensions. **B)** Presynaptic terminals marked with BrpD3-GFP during development and adults in sparsely labeled R7 terminals with CD4-tdTomato. **C)** Quantification of the number of presynaptic puncta per R7 terminal through development (n = 19 (P+40%), 22 (P+50%), 23 (P+70%), 13 (adult)). **D)** Number of presynaptic puncta per R7 terminal binned according to their lifetimes. R7 terminals were live imaged at 10 min resolution starting at P+50% + 22h in culture. Individual puncta were tracked for 5,5h to determine individual lifetimes (n = 5 terminals). Scale bars: 5 µm (A) and 2 µm (B). Error bars denote SEM.

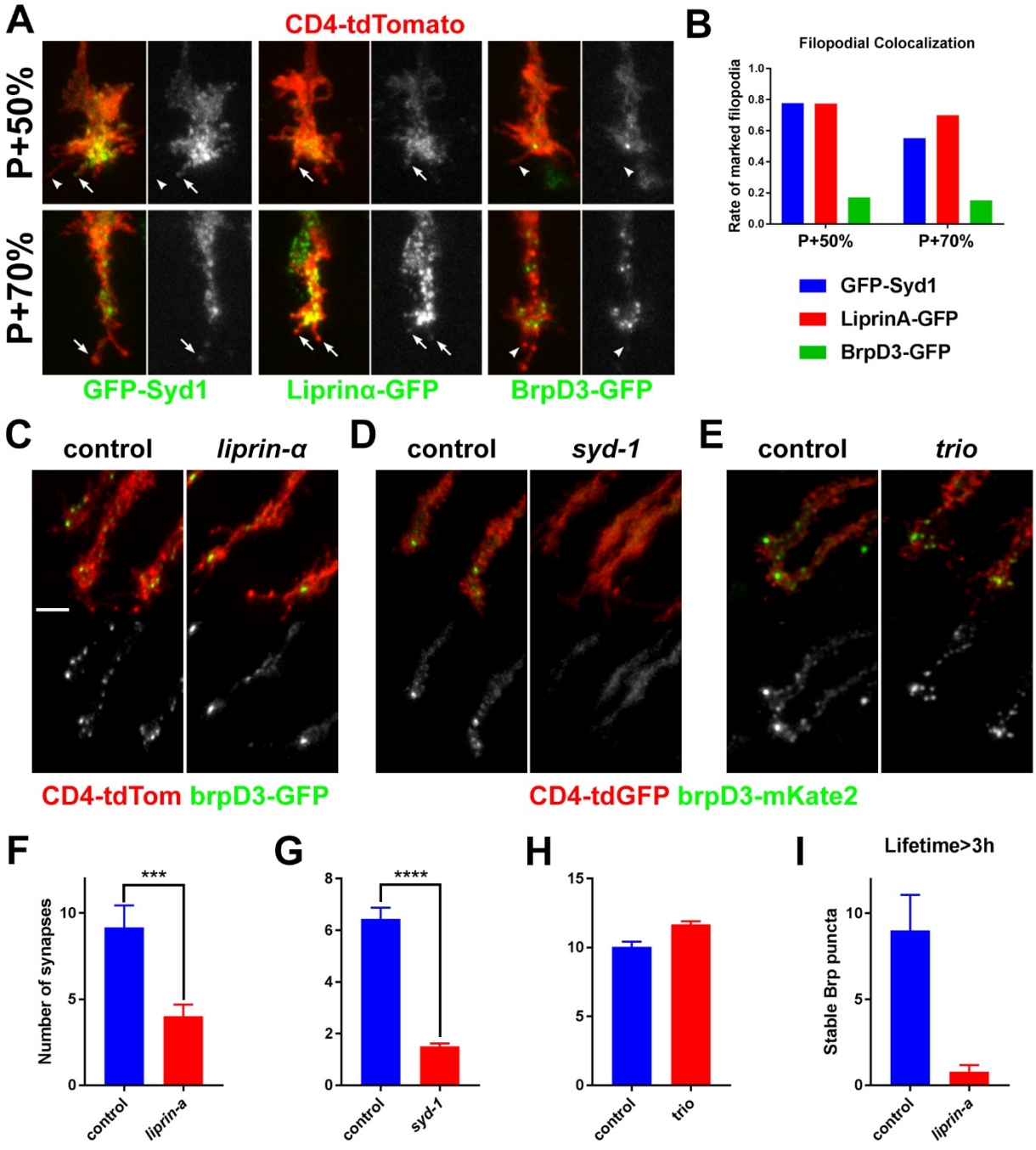
A
CD4-tdTomato
P+50%
P+70%
GFP-Syd1
Liprinα-GFP
BrpD3-GFP
B
Filopodial Colocalization
Rate of marked filopodia
1.0
0.8
0.6
0.4
0.2
0.0
P+50%
P+70%
GFP-Syd1
LiprinA-GFP
BrpD3-GFP
C
control
liprin-α
D
control
syd-1
E
control
trio
CD4-tdTom brpD3-GFP
CD4-tdGFP brpD3-mKate2
F
***
Number of synapses
10
5
0
control
liprin-a
G
****
8
6
4
2
0
control
syd-1
H
15
10
5
0
control
trio
I
Lifetime>3h
Stable Brp puncta
10
5
0
control
liprin-a

Figure 2: Liprin-α and Syd-1 can localize to filopodia and are required for active zone formation in R7 axons. A) Sparsely labeled R7 axons were marked with CD4-tdTomato and GFP tagged synaptic proteins at P+50 and 70%. Arrows indicate filopodia with marker localization while arrowheads indicate those without. **B)** Filopodial colocalization of each protein calculated as: Number of filopodia with marker / Total number of filopodia counted. n = (from left to right) 36, 31, 29, 38, 20, 33 filopodia. **C-E)** Presynaptic puncta at P+70% in sparsely generated R7 clones using **C)** FRT40A and FRT40A, *liprin-α*^{E} **D)** FRT82B and FRT82B, *syd-1*^{w46} **E)** FRT2A and FRT2A, *trio*^{3}. **F-H)** Quantification of Brp puncta per terminal from C-E. **F)** n = 18 and 44 ($p = 0.0003$) **G)** n = 45 and 65 ($p < 0.0001$) **H)** n = 43 and 65. **I)** Number of BrpD3 puncta per terminal with lifetimes greater than 3h in R7 axons live imaged for 4h at P+70% in wild-type (n =5) and *liprin-α*^{E} mutants (n=5). Scale bars: 2 µm. Error bars denote SEM.

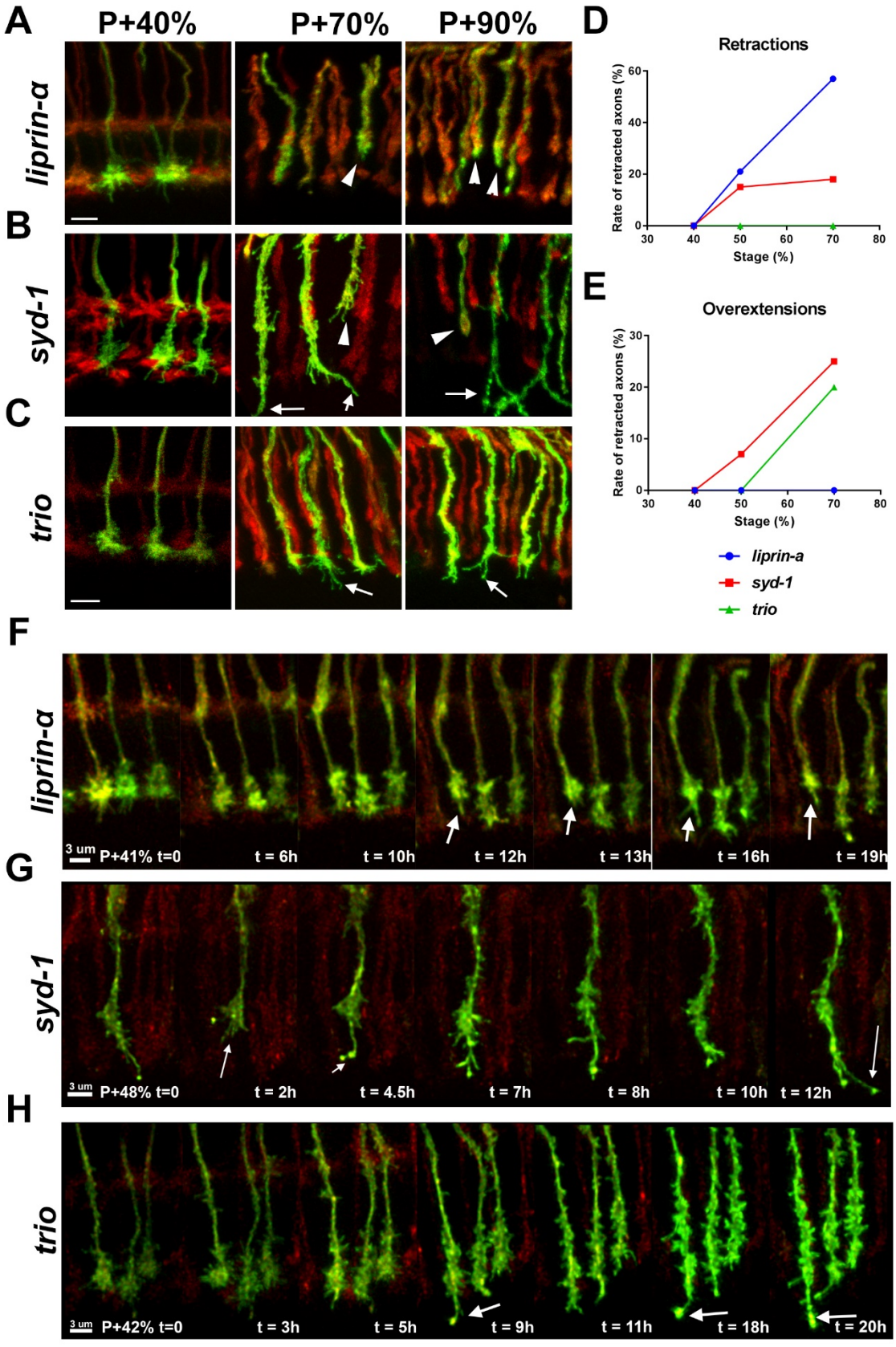
A
P+40%
P+70%
P+90%
liprin-α
B
syd-1
C
trio
D
Retractions
Rate of retracted axons (%)
Stage (%)
E
Overextensions
Rate of retracted axons (%)
Stage (%)
liprin-a
syd-1
trio
F
liprin-α
3 um
P+41% t=0
t = 6h
t = 10h
t = 12h
t = 13h
t = 16h
t = 19h
G
syd-1
3 um
P+48% t=0
t = 2h
t = 4.5h
t = 7h
t = 8h
t = 10h
t = 12h
H
trio
3 um
P+42% t=0
t = 3h
t = 5h
t = 9h
t = 11h
t = 18h
t = 20h

Figure 3: Presynaptic active zone components are required for R7 terminal stability during synapse formation. Sparsely generated **A)** *liprin-α*^{E} **B)** *syd-1*^{w46} **C)** *trio*^{3} mutant R7 axons labeled with CD4-tdGFP while all photoreceptors are marked with myr-tdTomato in fixed preparations during development. Arrowheads indicate retracted axons while arrows show aberrant overextensions. Ratio of mutant R7 axons that show **D)** Retractions **E)** Overextensions through pupal development in fixed preparations. **F-G)** Time series from the live imaging of corresponding genotypes from A-C; arrows demonstrating **F)** a retraction **G)** a retraction, re-extension and overextension **H)** an overextension. Scale bars: 5 µm (A-C) and 3 µm (F-G).

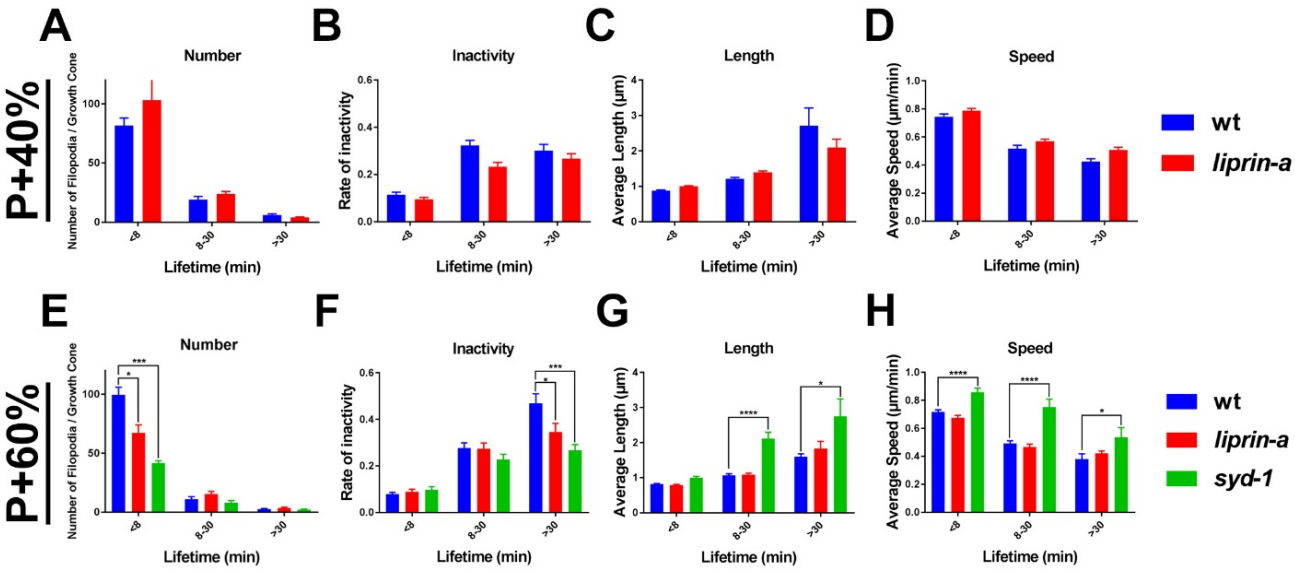

Figure 4: Early active zone components regulate fast filopodial dynamics of R7 axons during synapse formation. Fast filopodial dynamics calculated from wild-type and mutant R7 axons imaged at 1 min resolution for 1h, before **(A-D)** and during **(E-H)** synaptogenesis. Filopodia were placed in three separate classes based on their individual lifetimes (<8 min, 8-30 min and >30 min). **A,E)** Total number of each class of filopodia per terminal. **B,F)** Average ratio of inactivity (timepoints with less than 0.1 µm extension/retraction) of each class. **C,G)** Average length of individual filopodia in each class. **D,H)** Average extension/retraction speed of individual filopodia in each class during active timesteps. Error bars denote SEM.

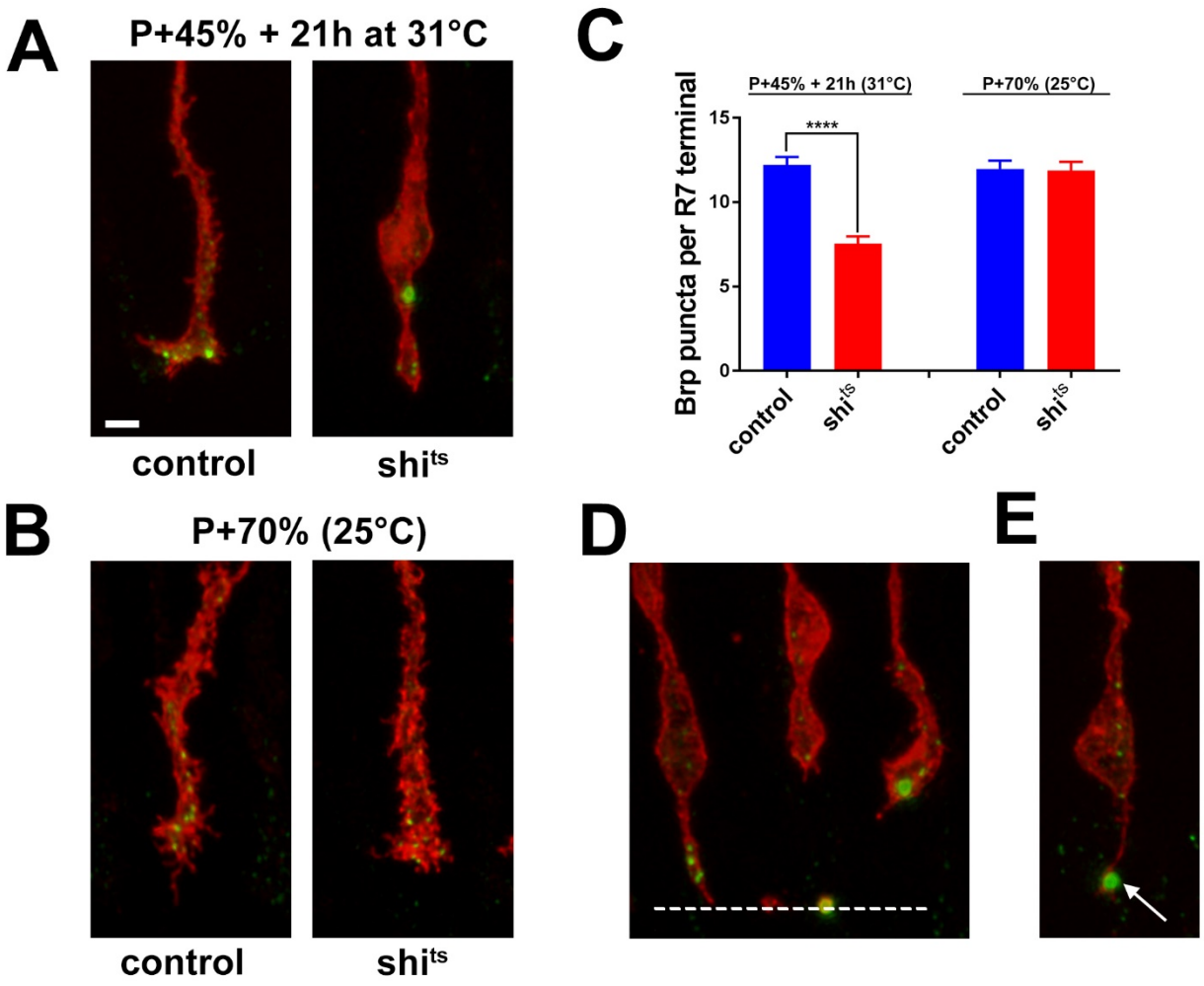

Figure 5: Blockage of membrane dynamics during synapse formation reduces the number presynaptic puncta. R7 axons sparsely labeled with CD4-tdTomato and BrpD3-GFP and express Shibire^{ts}. Pupae were grown till **A)** P+45% in permissive temperature, then placed in restrictive temperature for 21h **B)** P+70% in permissive temperature. **C)** Number of BrpD3 puncta specifically reduced in Shi^{ts} placed in restrictive temperature; unchanged in genetic and permissive temperature controls. n = 34, 33 ($p<0.0001$), 40, 26. **D)** A few Shi^{ts} axons retract to M3 in restrictive temperature. Dotted line marks the M6 layer. **E)** Collapsed Shi^{ts} axons may remain attached to M6 layer at the position of a Brp puncta (arrow). Scale bar: 2 µm. Error bars denote SEM.

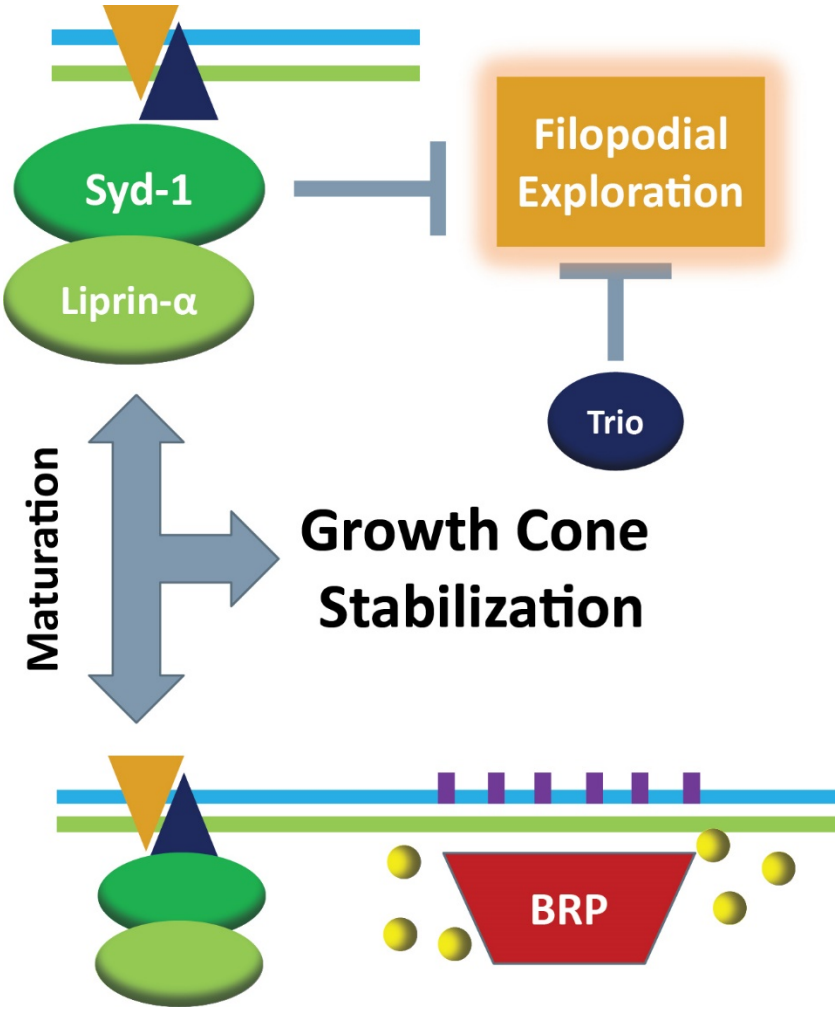

Figure 6: Working model of growth cone dynamics regulation by presynaptic proteins. Syd-1 is among the first proteins to be recruited to the nascent presynaptic contacts and recruits Liprin-α. Together, they are required for maturation of the active zone and, in concert, stability of the axon terminal at the target layer. In addition, Syd-1 is required to suppress axonal filopodial exploration upon synapse formation. Trio is not required for active zone formation but regulates filopodial activity.

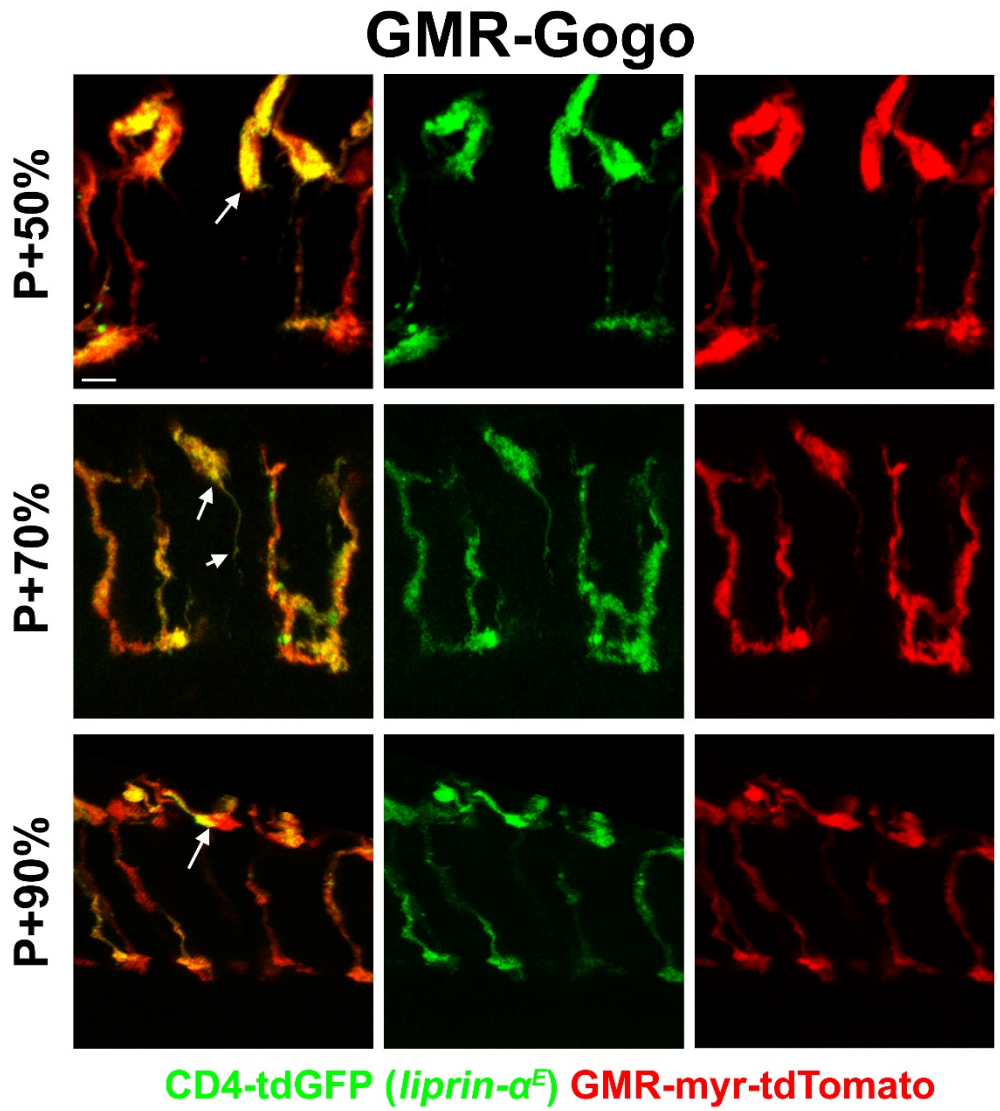

Supplementary Figure 1: R8 axons stabilize retracted R7 axons at M3. Fixed preparations of sparsely generated *liprin-α*^{E} R7 axons marked with CD4-tdGFP and all photoreceptors labeled with myr-tdTomato during pupal development. GMR-Gogo repositions R8 axons to the superficial medulla (M0) which allows *liprin-α* R7 axons to also retract to M0 (arrows). Scale bar: 5 µm.

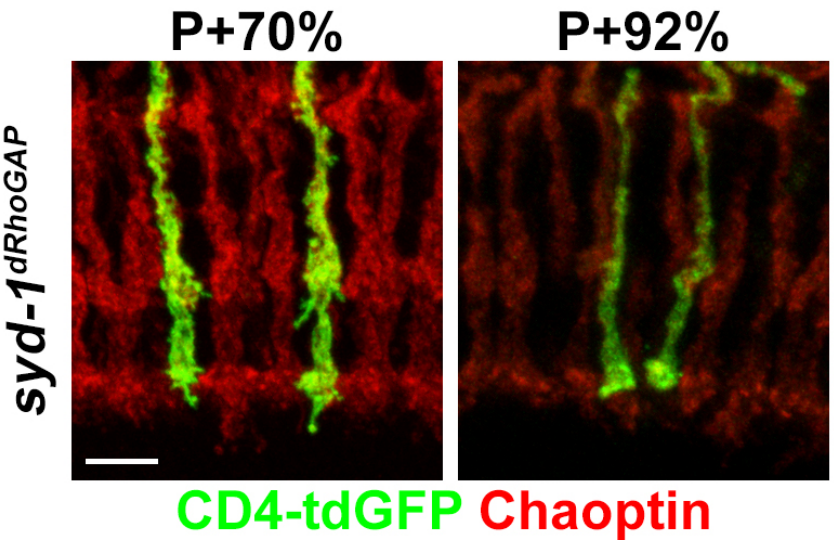

Supplementary Figure 2: RhoGAP domain of Syd-1 is not required in R7 axons. Sparsely generated *syd-1*^{dRhoGAP} R7 clones were marked with CD4-tdGFP and stained with 24B10-Cy3. Mutant axons appear normal at both P+70% and 90%. Scale bar: 5 µm.

3.7 Chapter Three Movies

All movies can be downloaded from:

https://www.dropbox.com/sh/fzrfy553s37po62/AAArJ-zXgw9B_pPAKsL-NJsJa?dl=0

CHAPTER FOUR

Concluding Remarks and Future Directions

The findings of my dissertation research have first of all reinforced the power and importance of live imaging and the level of additional insight we can gain into the various processes that ensure synaptic specificity when one includes the time dimension into the equation. The *ex vivo* imaging technique I developed makes it now straightforward for all *Drosophila* neurobiologists, studying any area of the developing brain, to have access to the fast dynamics of development at the resolution of an individual synapse over long periods. For the specific case of R7 photoreceptors, my research has significantly expanded our understanding of how these axons behave during synapse specification, from targeting to synapse formation, and put the various molecules that were known to be important for different steps of this program into the dynamic context of development.

First, my live analysis of the wild-type development has revealed that, contrary to the previous assumptions, R7 axons do not employ a temporary layer during targeting and appear to reach directly to their final synaptic layer early in the development. This raised the question: What are all of the factors that are known to be required for R7 layer specificity actually important for? Interestingly, we found that none of those mutations actually disrupt the initial targeting of the axons; but their functions are unified under one overarching concept that was only accessible by live imaging: *stabilization*. Early in the development, N-Cadherin mediated adhesions ensure that R7 terminals remain in their target layer while other layers intercalate and the entire structure greatly expands around them. Later, after the onset of synaptogenesis, synaptic connections

appear to take over that role; i.e. failure to form proper active zones leads to a late onset loss of terminal stability. Finally, axon-axon interactions between R7 and R8 cells provide yet another source of stabilization; causing the destabilized R7 axons to stop at M3 layer rather than fully retracting from the medulla.

Second, my findings revealed the importance of filopodial dynamics at all stages of synapse specification. It was long known that R7 axons utilized these thin membrane extensions; but their roles, and even existence, were largely overlooked; perhaps because adult/functional terminals do not have them. I have found that R7 axons employ their widest filopodial arbor early in the development when the structures around them are most dynamic and the need for stabilization is highest (and also when there are no synaptic connections to reinforce that stabilization). If this arbor simply functions as a surface substrate for N-Cadherin mediated adhesion, what is the importance of stochastic dynamics? This is an intriguing question and the answer may again lie in dynamicity of environment. As the other neuronal process which R7 axons attach to continuously shift positions, it may be advantageous to continuously change the adhesion surface to avoid being dragged by the adhesion partners.

By the mid-pupal stages, stochastic exploration of R7 filopodia is largely pruned yet it still continues through the end of pupal development. My results suggest that axons may then utilize this same cytoskeletal program for an entirely different purpose: finding synaptic partners. During synapse formation, a small subset of R7 filopodia display enhanced stabilization, presumably as the sites of contact with postsynaptic partners as the disruption of early active zone assembly interferes with that stabilization. The concept of filopodial stabilization by virtue of synaptic adhesion had already been

established for the neuronal arbors that form stable branches, in the context of synaptotropic hypothesis. However, in the case of R7 axons whose terminal structure is unbranched in adults and mature synapses only exist on the main body, our results suggest the existence of a novel paradigm which we refer to as *synaptic capture*. In cases where axons or dendrites are precluded from having elaborate arbors, yet still have a need to establish contacts with specific synaptic partners in dense brain regions, transient filopodial extensions could serve as searching agents.

Furthermore, I found that filopodial exploration to find synaptic partners does not simply exists as a default cellular program but could be actively regulated by the very process it mediates, synapse formation. Syd-1 emerges as the central co-coordinator of these processes. It is not only one of the first proteins to be recruited to the nascent presynaptic contacts and essential for their maturation, but it can also regulate the level of filopodial exploration. This is an elegant mechanism that could allow an axon to control the aggressiveness of its filopodial exploration depending on the (un)availability of synaptic partners in its vicinity.

In the future it will be important to look at these events in the context of filopodial dynamics in other systems where both pre- and postsynaptic sides are accessible by genetic tools. Co-imaging of both sides of a synaptic connection would provide valuable insights into the mechanisms that control filopodial exploration and stabilization upon contact. Further, it would be of interest to see if Syd-1 mediated suppression of filopodial exploration upon synapse formation is also utilized in neurons with elaborate arbors that grow and stabilize through development.

After all of these new findings, one question, perhaps the oldest one concerning the synaptic specificity of R7 cells, still lingers: How do R7 axons target to their synaptic layer in the first place? I find that no molecule, that has previously been suggested to play a role in this, is actually required for initial targeting. The answer can be simpler than one might imagine. R7 axons' targeting to the medulla is strictly tied to their relationship with R8 axons. Therefore, they could follow a simple development rule: Reach past the R8 terminals and stabilize in the first layer encountered, without a need to recognize this layer as the correct synaptic layer using some kind of molecular code.

The idea that simple timing and arrival order may be sufficient to determine synaptic layers of different axons is an interesting one to test. Lamina monopolar cell axons also target to medulla and intercalate between R7 and R8 layers during early pupal development (Ting et al., 2005) may perhaps be the best model study this hypothesis. N-Cadherin, similarly to R7, have been shown to be important for the layer specificity of these axons (Nern et al., 2008); but in the light of my findings here it is unlikely to play a deterministic role in the initial recognition. Would simply manipulating the arrival order of these axons be enough to cause a switch their target layer? For example, one could eliminate the R7 axons and try to see whether if the first-arriving L-cell axons instead take their place in the M6 layer.

BIBLIOGRAPHY

Agi, E., Langen, M., Altschuler, S.J., Wu, L.F., Zimmermann, T., and Hiesinger, P.R. (2014). The evolution and development of neural superposition. J Neurogenet *28*, 216-232.

Ahmari, S.E., Buchanan, J., and Smith, S.J. (2000). Assembly of presynaptic active zones from cytoplasmic transport packets. Nat Neurosci *3*, 445-451.

Akin, O., and Zipursky, S.L. (2016). Frazzled promotes growth cone attachment at the source of a Netrin gradient in the Drosophila visual system. Elife *5*.

Astigarraga, S., Hofmeyer, K., Farajian, R., and Treisman, J.E. (2010). Three Drosophila liprins interact to control synapse formation. The Journal of neuroscience : the official journal of the Society for Neuroscience *30*, 15358-15368.

Ayaz, D., Leyssen, M., Koch, M., Yan, J., Srahna, M., Sheeba, V., Fogle, K.J., Holmes, T.C., and Hassan, B.A. (2008). Axonal injury and regeneration in the adult brain of Drosophila. The Journal of neuroscience : the official journal of the Society for Neuroscience *28*, 6010-6021.

Bard, L., Boscher, C., Lambert, M., Mege, R.M., Choquet, D., and Thoumine, O. (2008). A molecular clutch between the actin flow and N-cadherin adhesions drives growth cone migration. J Neurosci *28*, 5879-5890.

Bausenwein, B., Dittrich, A.P., and Fischbach, K.F. (1992). The optic lobe of Drosophila melanogaster. II. Sorting of retinotopic pathways in the medulla. Cell and tissue research *267*, 17-28.

Berger-Muller, S., Sugie, A., Takahashi, F., Tavosanis, G., Hakeda-Suzuki, S., and Suzuki, T. (2013). Assessing the role of cell-surface molecules in central synaptogenesis in the Drosophila visual system. PLoS One *8*, e83732.

Berry, M., and Bradley, P. (1976). The growth of the dendritic trees of Purkinje cells in irradiated agranular cerebellar cortex. Brain Res *116*, 361-387.

Braitenberg, V., and Schüz, A. (1991). Peters' Rule and White's Exceptions. In Anatomy of the Cortex: Statistics and Geometry (Berlin, Heidelberg: Springer Berlin Heidelberg), pp. 109-112.

Bullock, T.H., Bennett, M.V., Johnston, D., Josephson, R., Marder, E., and Fields, R.D. (2005). Neuroscience. The neuron doctrine, redux. Science *310*, 791-793.

Cajal, S.R.y. (1890). A quelle epoque apparaissent les expansions des cellule nerveuses de la moelle epinere du poulet. Anat Anzerger *5*, 609–613.

Carrillo, R.A., Ozkan, E., Menon, K.P., Nagarkar-Jaiswal, S., Lee, P.T., Jeon, M., Birnbaum, M.E., Bellen, H.J., Garcia, K.C., and Zinn, K. (2015). Control of Synaptic Connectivity by a Network of Drosophila IgSF Cell Surface Proteins. Cell *163*, 1770-1782.

Chan, C.E., and Odde, D.J. (2008). Traction dynamics of filopodia on compliant substrates. Science *322*, 1687-1691.

Chen, Y., Akin, O., Nern, A., Tsui, C.Y., Pecot, M.Y., and Zipursky, S.L. (2014). Cell-type-specific labeling of synapses in vivo through synaptic tagging with recombination. Neuron *81*, 280-293.

Choe, K.M., Prakash, S., Bright, A., and Clandinin, T.R. (2006). Liprin-alpha is required for photoreceptor target selection in Drosophila. Proceedings of the National Academy of Sciences of the United States of America *103*, 11601-11606.

Clandinin, T.R., and Feldheim, D.A. (2009). Making a visual map: mechanisms and molecules. Current opinion in neurobiology *19*, 174-180.

Clandinin, T.R., Lee, C.H., Herman, T., Lee, R.C., Yang, A.Y., Ovasapyan, S., and Zipursky, S.L. (2001). Drosophila LAR regulates R1-R6 and R7 target specificity in the visual system. Neuron *32*, 237-248.

Dai, Y., Taru, H., Deken, S.L., Grill, B., Ackley, B., Nonet, M.L., and Jin, Y. (2006). SYD-2 Liprin-alpha organizes presynaptic active zone formation through ELKS. Nature neuroscience *9*, 1479-1487.

Duan, X., Krishnaswamy, A., De la Huerta, I., and Sanes, J.R. (2014). Type II cadherins guide assembly of a direction-selective retinal circuit. Cell *158*, 793-807.

Dwivedy, A., Gertler, F.B., Miller, J., Holt, C.E., and Lebrand, C. (2007). Ena/VASP function in retinal axons is required for terminal arborization but not pathway navigation. Development *134*, 2137-2146.

Fernandes, V.M., Chen, Z., Rossi, A.M., Zipfel, J., and Desplan, C. (2017). Glia relay differentiation cues to coordinate neuronal development in Drosophila. Science *357*, 886-891.

Fischbach, K.-F., and Hiesinger, P.R. (2008). Optic Lobe Development. In Brain Development in Drosophila melanogaster, G.M. Technau, ed. (New York, NY: Springer New York), pp. 115-136.

Fischbach, K.F., and Dittrich, A.P.M. (1989). The optic lobe of Drosophila melanogaster. I. A Golgi analysis of wild-type structure. Cell and tissue research *258*, 441-475.

Gallo, G. (2011). The cytoskeletal and signaling mechanisms of axon collateral branching. Developmental neurobiology *71*, 201-220.

Gallo, G., and Letourneau, P.C. (2004). Regulation of growth cone actin filaments by guidance cues. Journal of neurobiology *58*, 92-102.

Gibbs, S.M., and Truman, J.W. (1998). Nitric oxide and cyclic GMP regulate retinal patterning in the optic lobe of Drosophila. Neuron *20*, 83-93.

Godement, P., Wang, L.C., and Mason, C.A. (1994). Retinal axon divergence in the optic chiasm: dynamics of growth cone behavior at the midline. The Journal of neuroscience : the official journal of the Society for Neuroscience *14*, 7024-7039.

Gonzalez-Bellido, P.T., Wardill, T.J., Kostyleva, R., Meinertzhagen, I.A., and Juusola, M. (2009). Overexpressing temperature-sensitive dynamin decelerates phototransduction and bundles microtubules in Drosophila photoreceptors. The Journal of neuroscience : the official journal of the Society for Neuroscience *29*, 14199-14210.

Hadjieconomou, D., Timofeev, K., and Salecker, I. (2011). A step-by-step guide to visual circuit assembly in Drosophila. Current opinion in neurobiology *21*, 76-84.

Hallam, S.J., Goncharov, A., McEwen, J., Baran, R., and Jin, Y. (2002). SYD-1, a presynaptic protein with PDZ, C2 and rhoGAP-like domains, specifies axon identity in C. elegans. Nature neuroscience *5*, 1137-1146.

Han, C., Jan, L.Y., and Jan, Y.N. (2011). Enhancer-driven membrane markers for analysis of nonautonomous mechanisms reveal neuron-glia interactions in Drosophila. Proceedings of the National Academy of Sciences of the United States of America *108*, 9673-9678.

Hassan, B.A., and Hiesinger, P.R. (2015). Beyond Molecular Codes: Simple Rules to Wire Complex Brains. Cell *163*, 285-291.

Hatta, K., Okada, T.S., and Takeichi, M. (1985). A monoclonal antibody disrupting calcium-dependent cell-cell adhesion of brain tissues: possible role of its target antigen in animal pattern formation. Proceedings of the National Academy of Sciences of the United States of America *82*, 2789-2793.

Heidemann, S.R., Lamoureux, P., and Buxbaum, R.E. (1990). Growth cone behavior and production of traction force. J Cell Biol *111*, 1949-1957.

Heisenberg, M., and Buchner, E. (1977). The rôle of retinula cell types in visual behavior ofDrosophila melanogaster. Journal of comparative physiology *117*, 127-162.

Hiesinger, P.R., Zhai, R.G., Zhou, Y., Koh, T.W., Mehta, S.Q., Schulze, K.L., Cao, Y., Verstreken, P., Clandinin, T.R., Fischbach, K.F.*, et al.* (2006). Activity-independent prespecification of synaptic partners in the visual map of Drosophila. Current biology : CB *16*, 1835-1843.

Hofmeyer, K., Maurel-Zaffran, C., Sink, H., and Treisman, J.E. (2006). Liprin-alpha has LAR-independent functions in R7 photoreceptor axon targeting. Proceedings of the National Academy of Sciences of the United States of America *103*, 11595-11600.

Hofmeyer, K., and Treisman, J.E. (2009). The receptor protein tyrosine phosphatase LAR promotes R7 photoreceptor axon targeting by a phosphatase-independent signaling mechanism. Proceedings of the National Academy of Sciences of the United States of America *106*, 19399-19404.

Holbrook, S., Finley, J.K., Lyons, E.L., and Herman, T.G. (2012). Loss of syd-1 from R7 neurons disrupts two distinct phases of presynaptic development. The Journal of neuroscience : the official journal of the Society for Neuroscience *32*, 18101-18111.

Hong, W., Mosca, T.J., and Luo, L. (2012). Teneurins instruct synaptic partner matching in an olfactory map. Nature *484*, 201-207.

Huang, Z., and Kunes, S. (1996). Hedgehog, transmitted along retinal axons, triggers neurogenesis in the developing visual centers of the Drosophila brain. Cell *86*, 411-422.

Jontes, J.D., Buchanan, J., and Smith, S.J. (2000). Growth cone and dendrite dynamics in zebrafish embryos: early events in synaptogenesis imaged in vivo. Nature neuroscience *3*, 231-237.

Kaethner, R.J., and Stuermer, C.A. (1992). Dynamics of terminal arbor formation and target approach of retinotectal axons in living zebrafish embryos: a time-lapse study of single axons. J Neurosci *12*, 3257-3271.

Kaethner, R.J., and Stuermer, C.A. (1994). Growth behavior of retinotectal axons in live zebrafish embryos under TTX-induced neural impulse blockade. J Neurobiol *25*, 781-796.

Kise, Y., and Schmucker, D. (2013). Role of self-avoidance in neuronal wiring. Current opinion in neurobiology *23*, 983-989.

Kolodkin, A.L., and Tessier-Lavigne, M. (2011). Mechanisms and molecules of neuronal wiring: a primer. Cold Spring Harb Perspect Biol *3*.

Kulkarni, A., Ertekin, D., Lee, C.H., and Hummel, T. (2016). Birth order dependent growth cone segregation determines synaptic layer identity in the Drosophila visual system. Elife *5*, e13715.

Langen, M., Agi, E., Altschuler, D.J., Wu, L.F., Altschuler, S.J., and Hiesinger, P.R. (2015). The Developmental Rules of Neural Superposition in Drosophila. Cell *162*, 120-133.

Lee, C.H., Herman, T., Clandinin, T.R., Lee, R., and Zipursky, S.L. (2001). N-cadherin regulates target specificity in the Drosophila visual system. Neuron *30*, 437-450.

Lee, T., and Luo, L. (1999). Mosaic analysis with a repressible cell marker for studies of gene function in neuronal morphogenesis. Neuron *22*, 451-461.

Lerit, D.A., Plevock, K.M., and Rusan, N.M. (2014). Live imaging of Drosophila larval neuroblasts. J Vis Exp.

Lichtman, J.W., and Fraser, S.E. (2001). The neuronal naturalist: watching neurons in their native habitat. Nature neuroscience *4 Suppl*, 1215-1220.

Mason, C., and Erskine, L. (2000). Growth cone form, behavior, and interactions in vivo: retinal axon pathfinding as a model. J Neurobiol *44*, 260-270.

Mason, C.A., and Wang, L.C. (1997). Growth cone form is behavior-specific and, consequently, position-specific along the retinal axon pathway. J Neurosci *17*, 1086-1100.

Mast, J.D., Prakash, S., Chen, P.L., and Clandinin, T.R. (2006). The mechanisms and molecules that connect photoreceptor axons to their targets in Drosophila. Seminars in cell & developmental biology *17*, 42-49.

Matsunaga, M., Hatta, K., Nagafuchi, A., and Takeichi, M. (1988). Guidance of optic nerve fibres by N-cadherin adhesion molecules. Nature *334*, 62-64.

Medioni, C., Ephrussi, A., and Besse, F. (2015). Live imaging of axonal transport in Drosophila pupal brain explants. Nat Protoc *10*, 574-584.

Meinertzhagen, I.A., and Hanson, T.E. (1993). The development of the optic lobe, pp. 1363-1491.

Melnattur, K.V., and Lee, C.H. (2011). Visual circuit assembly in Drosophila. Developmental neurobiology *71*, 1286-1296.

Meyer, M.P., and Smith, S.J. (2006). Evidence from in vivo imaging that synaptogenesis guides the growth and branching of axonal arbors by two distinct mechanisms. The Journal of neuroscience : the official journal of the Society for Neuroscience *26*, 3604-3614.

Morante, J., Desplan, C., and Celik, A. (2007). Generating patterned arrays of photoreceptors. Curr Opin Genet Dev *17*, 314-319.

Murray, M.J., Merritt, D.J., Brand, A.H., and Whitington, P.M. (1998). In vivo dynamics of axon pathfinding in the Drosophilia CNS: a time-lapse study of an identified motorneuron. J Neurobiol *37*, 607-621.

Nern, A., Nguyen, L.V., Herman, T., Prakash, S., Clandinin, T.R., and Zipursky, S.L. (2005). An isoform-specific allele of Drosophila N-cadherin disrupts a late step of R7 targeting. Proceedings of the National Academy of Sciences of the United States of America *102*, 12944-12949.

Nern, A., Zhu, Y., and Zipursky, S.L. (2008). Local N-cadherin interactions mediate distinct steps in the targeting of lamina neurons. Neuron *58*, 34-41.

Newsome, T.P., Schmidt, S., Dietzl, G., Keleman, K., Asling, B., Debant, A., and Dickson, B.J. (2000). Trio combines with dock to regulate Pak activity during photoreceptor axon pathfinding in Drosophila. Cell *101*, 283-294.

Niell, C.M., Meyer, M.P., and Smith, S.J. (2004). In vivo imaging of synapse formation on a growing dendritic arbor. Nature neuroscience *7*, 254-260.

O'Connor, T.P., Duerr, J.S., and Bentley, D. (1990). Pioneer growth cone steering decisions mediated by single filopodial contacts in situ. The Journal of neuroscience : the official journal of the Society for Neuroscience *10*, 3935-3946.

Ortega, F., and Costa, M.R. (2016). Live Imaging of Adult Neural Stem Cells in Rodents. Front Neurosci *10*, 78.

Owald, D., Fouquet, W., Schmidt, M., Wichmann, C., Mertel, S., Depner, H., Christiansen, F., Zube, C., Quentin, C., Korner, J.*, et al.* (2010). A Syd-1 homologue regulates pre- and postsynaptic maturation in Drosophila. J Cell Biol *188*, 565-579.

Owald, D., Khorramshahi, O., Gupta, V.K., Banovic, D., Depner, H., Fouquet, W., Wichmann, C., Mertel, S., Eimer, S., Reynolds, E.*, et al.* (2012). Cooperation of Syd-1 with Neurexin synchronizes pre- with postsynaptic assembly. Nature neuroscience *15*, 1219-1226.

Ozel, M.N., Langen, M., Hassan, B.A., and Hiesinger, P.R. (2015). Filopodial dynamics and growth cone stabilization in Drosophila visual circuit development. Elife *4*.

Paul Bainbridge, S., and Bownes, M. (1988). Ecdysteroid titers during Drosophila metamorphosis. Insect Biochemistry *18*, 185-197.

Petrovic, M., and Hummel, T. (2008). Temporal identity in axonal target layer recognition. Nature *456*, 800-803.

Petrovic, M., and Schmucker, D. (2015). Neural development: Target-independent mechanisms help to establish precision and complexity in axonal wiring. BioEssays *in press*.

Poeck, B., Fischer, S., Gunning, D., Zipursky, S.L., and Salecker, I. (2001). Glial cells mediate target layer selection of retinal axons in the developing visual system of Drosophila. Neuron *29*, 99-113.

Prakash, S., McLendon, H.M., Dubreuil, C.I., Ghose, A., Hwa, J., Dennehy, K.A., Tomalty, K.M., Clark, K.L., Van Vactor, D., and Clandinin, T.R. (2009). Complex interactions amongst N-cadherin, DLAR, and Liprin-alpha regulate Drosophila photoreceptor axon targeting. Developmental biology *336*, 10-19.

Rabinovich, D., Mayseless, O., and Schuldiner, O. (2015). Long term ex vivo culturing of Drosophila brain as a method to live image pupal brains: insights into the cellular mechanisms of neuronal remodeling. Front Cell Neurosci *9*, 327.

Rajan, I., Witte, S., and Cline, H.T. (1999). NMDA receptor activity stabilizes presynaptic retinotectal axons and postsynaptic optic tectal cell dendrites in vivo. Journal of Neurobiology *38*, 357-368.

Rajnicek, A.M., Foubister, L.E., and McCaig, C.D. (2006). Growth cone steering by a physiological electric field requires dynamic microtubules, microfilaments and Rac-mediated filopodial asymmetry. J Cell Sci *119*, 1736-1745.

Raper, J., and Mason, C. (2010). Cellular strategies of axonal pathfinding. Cold Spring Harb Perspect Biol *2*, a001933.

Roskies, A., Friedman, G.C., and O'Leary, D.D. (1995). Mechanisms and molecules controlling the development of retinal maps. Perspect Dev Neurobiol *3*, 63-75.

Ruthazer, E.S., Li, J.L., and Cline, H.T. (2006). Stabilization of axon branch dynamics by synaptic maturation. Journal of Neuroscience *26*, 3594-3603.

Sanes, J.R., and Yamagata, M. (2009). Many paths to synaptic specificity. Annu Rev Cell Dev Biol *25*, 161-195.

Sanes, J.R., and Zipursky, S.L. (2010). Design principles of insect and vertebrate visual systems. Neuron *66*, 15-36.

Schmid, A., Hallermann, S., Kittel, R.J., Khorramshahi, O., Frolich, A.M., Quentin, C., Rasse, T.M., Mertel, S., Heckmann, M., and Sigrist, S.J. (2008). Activity-dependent site-specific changes of glutamate receptor composition in vivo. Nature neuroscience *11*, 659-666.

Schwabe, T., Borycz, J.A., Meinertzhagen, I.A., and Clandinin, T.R. (2014). Differential adhesion determines the organization of synaptic fascicles in the Drosophila visual system. Current biology : CB *24*, 1304-1313.

Schwabe, T., Neuert, H., and Clandinin, T.R. (2013). A network of cadherin-mediated interactions polarizes growth cones to determine targeting specificity. Cell *154*, 351-364.

Sekino, Y., Kojima, N., and Shirao, T. (2007). Role of actin cytoskeleton in dendritic spine morphogenesis. Neurochem Int *51*, 92-104.

Senti, K.A., Usui, T., Boucke, K., Greber, U., Uemura, T., and Dickson, B.J. (2003). Flamingo regulates R8 axon-axon and axon-target interactions in the Drosophila visual system. Current biology : CB *13*, 828-832.

Shinza-Kameda, M., Takasu, E., Sakurai, K., Hayashi, S., and Nose, A. (2006). Regulation of layer-specific targeting by reciprocal expression of a cell adhesion molecule, capricious. Neuron *49*, 205-213.

Sperry, R.W. (1943). Effect of 180 degree rotation of the retinal field on visuomotor coordination. Journal of Experimental Zoology *92*, 263-279.

Spillane, M., Ketschek, A., Donnelly, C.J., Pacheco, A., Twiss, J.L., and Gallo, G. (2012). Nerve growth factor-induced formation of axonal filopodia and collateral branches involves the intra-axonal synthesis of regulators of the actin-nucleating Arp2/3 complex. J Neurosci *32*, 17671-17689.

Spillane, M., Ketschek, A., Jones, S.L., Korobova, F., Marsick, B., Lanier, L., Svitkina, T., and Gallo, G. (2011). The actin nucleating Arp2/3 complex contributes to the formation of axonal filopodia and branches through the regulation of actin patch precursors to filopodia. Developmental neurobiology *71*, 747-758.

Takemura, S.Y., Bharioke, A., Lu, Z., Nern, A., Vitaladevuni, S., Rivlin, P.K., Katz, W.T., Olbris, D.J., Plaza, S.M., Winston, P.*, et al.* (2013). A visual motion detection circuit suggested by Drosophila connectomics. Nature *500*, 175-181.

Takemura, S.Y., Xu, C.S., Lu, Z., Rivlin, P.K., Parag, T., Olbris, D.J., Plaza, S., Zhao, T., Katz, W.T., Umayam, L.*, et al.* (2015). Synaptic circuits and their variations within different columns in the visual system of Drosophila. Proceedings of the National Academy of Sciences of the United States of America *112*, 13711-13716.

Tan, L., Zhang, K.X., Pecot, M.Y., Nagarkar-Jaiswal, S., Lee, P.T., Takemura, S.Y., McEwen, J.M., Nern, A., Xu, S., Tadros, W.*, et al.* (2015). Ig Superfamily Ligand and Receptor Pairs Expressed in Synaptic Partners in Drosophila. Cell *163*, 1756-1769.

Timofeev, K., Joly, W., Hadjieconomou, D., and Salecker, I. (2012). Localized netrins act as positional cues to control layer-specific targeting of photoreceptor axons in Drosophila. Neuron *75*, 80-93.

Ting, C.Y., Herman, T., Yonekura, S., Gao, S., Wang, J., Serpe, M., O'Connor, M.B., Zipursky, S.L., and Lee, C.H. (2007). Tiling of r7 axons in the Drosophila visual system is mediated both by transduction of an activin signal to the nucleus and by mutual repulsion. Neuron *56*, 793-806.

Ting, C.Y., and Lee, C.H. (2007). Visual circuit development in Drosophila. Current opinion in neurobiology *17*, 65-72.

Ting, C.Y., McQueen, P.G., Pandya, N., Lin, T.Y., Yang, M., Reddy, O.V., O'Connor, M.B., McAuliffe, M., and Lee, C.H. (2014). Photoreceptor-derived activin promotes dendritic termination and restricts the receptive fields of first-order interneurons in Drosophila. Neuron *81*, 830-846.

Ting, C.Y., Yonekura, S., Chung, P., Hsu, S.N., Robertson, H.M., Chiba, A., and Lee, C.H. (2005). Drosophila N-cadherin functions in the first stage of the two-stage layer-selection process of R7 photoreceptor afferents. Development *132*, 953-963.

Tomasi, T., Hakeda-Suzuki, S., Ohler, S., Schleiffer, A., and Suzuki, T. (2008). The transmembrane protein Golden goal regulates R8 photoreceptor axon-axon and axon-target interactions. Neuron *57*, 691-704.

Vaughn, J.E. (1989). Fine structure of synaptogenesis in the vertebrate central nervous system. Synapse *3*, 255-285.

Vaughn, J.E., Henrikson, C.K., and Grieshaber, J.A. (1974). A quantitative study of synapses on motor neuron dendritic growth cones in developing mouse spinal cord. J Cell Biol *60*, 664-672.

Vitriol, E.A., and Zheng, J.Q. (2012). Growth cone travel in space and time: the cellular ensemble of cytoskeleton, adhesion, and membrane. Neuron *73*, 1068-1081.

Wentzel, C., Sommer, J.E., Nair, R., Stiefvater, A., Sibarita, J.B., and Scheiffele, P. (2013). mSYD1A, a mammalian synapse-defective-1 protein, regulates synaptogenic signaling and vesicle docking. Neuron *78*, 1012-1023.

Williamson, W.R., and Hiesinger, P.R. (2010). Preparation of developing and adult Drosophila brains and retinae for live imaging. J Vis Exp.

Yogev, S., and Shen, K. (2014). Cellular and molecular mechanisms of synaptic specificity. Annu Rev Cell Dev Biol *30*, 417-437.

Yonekura, S., Xu, L., Ting, C.Y., and Lee, C.H. (2007). Adhesive but not signaling activity of Drosophila N-cadherin is essential for target selection of photoreceptor afferents. Developmental biology *304*, 759-770.

Zheng, J.Q., Wan, J.J., and Poo, M.M. (1996). Essential role of filopodia in chemotropic turning of nerve growth cone induced by a glutamate gradient. The Journal of neuroscience : the official journal of the Society for Neuroscience *16*, 1140-1149.

Zschatzsch, M., Oliva, C., Langen, M., De Geest, N., Ozel, M.N., Williamson, W.R., Lemon, W.C., Soldano, A., Munck, S., Hiesinger, P.R.*, et al.* (2014). Regulation of branching dynamics by axon-intrinsic asymmetries in Tyrosine Kinase Receptor signaling. Elife *3*, e01699.